Proteomic studies of human placentas reveal partnerships associated with preeclampsia, diabetes, gravidity, and labor

Shannon J. Ho[1,10], Dale Chaput[2,10], Rachel G. Sinkey[1], Amanda H. Garces[3], Erika P. New[1], Maja Okuka[1], Peng Sang[4], Sefa Arlier[1], Nihan Semerci[1], Thora S. Steffensen[5], Thomas J. Rutherford[1,6], Angel E. Alsina[7], Jianfeng Cai[4], Matthew L. Anderson[1,6], Ronald R. Magness[1], Vladimir N. Uversky[8], Derek A. T. Cummings[9] & John C. M. Tsibris[1,8] ✉

[1]Department of Obstetrics and Gynecology, University of South Florida, Tampa, Florida, USA. [2]Department of Cell Biology, Microbiology and Molecular Biology, University of South Florida, Tampa, Florida, USA. [3]Lisa Muma Weitz Microscopy Laboratory, University of South Florida, USA. [4]Department of Chemistry, University of South Florida, Tampa, Florida, USA. [5]Department of Pathology, Tampa General Hospital, Tampa, Florida, USA. [6]Cancer Center, Tampa General Hospital, Tampa, Florida, USA. [7]Transplant Surgery Center, Tampa General Hospital, Tampa, Florida, USA. [8]Department of Molecular Medicine, University of South Florida, Tampa, Florida, USA. [9]Department of Biology and Emerging Pathogens Institute, University of Florida, Gainesville, FL, USA. [10]These authors contributed equally. ✉e-mail: tsibris@usf.edu

Abstract

VEGFR2 is a central regulator of placental angiogenesis. The study of the VEGFR2 proteome of chorionic villi at term revealed its partners MDMX and PICALM. The oxytocin receptor (OT-R) and vasopressin V1aR receptor were detected in MDMX and PICALM immunoprecipitations. Immunogold electron microscopy showed VEGFR2 on endothelial cell (EC) nuclei, mitochondria, and Hofbauer cells (HC), the tissue-resident macrophages. MDMX, PICALM, and V1aR were on EC plasma membranes, nuclei, and HC nuclei. Unexpectedly, PICALM and OT-R were detected on EC projections into the fetal lumen and OT-R on 20-150 nm clusters therein, prompting the hypothesis that placental exosomes transport OT-R to the fetus and across the blood-brain barrier. Insights on gestational complications were gained by univariable and multivariable regression analyses associating preeclampsia with lower MDMX protein levels in membrane extracts of chorionic villi, and lower MDMX, PICALM, OT-R, and V1aR with spontaneous vaginal deliveries compared to cesarean deliveries before labor. We found select associations between higher MDMX, PICALM, OT-R and either gravidity, diabetes, BMI, maternal age, or neonatal weight, and correlations between PICALM-OT-R ($p<2.7x10^{-8}$), PICALM-V1aR ($p<0.006$), and OT-R-V1aR ($p<0.001$). These results offer for exploration new partnerships in metabolic networks, tissue-resident immunity, and labor, notably for HC that predominantly express MDMX.

The placenta is a transient organ that performs the functions of major organs of the fetus, such as lungs, liver, and kidney[1], supplies the fetus and in particular the fetal brain with oxygen and nutrients, and facilitates waste disposal and provides immune protection[2,3]. The genomes of placenta and fetus are identical except in cases of confined placental mosaicism. The vascular endothelial growth factor A (VEGF-A) is a key regulator of vasculogenesis, angiogenesis and placental growth that acts mainly through VEGFR1 and VEGFR2, two tyrosine kinase single-pass transmembrane receptors[4-6].

Preeclampsia is a serious complication of human pregnancy occurring in 5-7% of all gestations with newly-onset hypertension and proteinuria as its primary clinical characteristics[2,7]. Preeclampsia is a multisystemic syndrome of different subtypes associated with serious health problems to mother and child even after pregnancy[8]. Lipid bilayer-enclosed extracellular vehicles (EV) transport extracellular nucleic acids, proteins, lipids, and metabolites[9-12]. Cancer cells deploy EV to activate VEGF signaling in endothelial cells[12]. Exosomes are EV measuring 20–150 nm in diameter. Placental-derived exosomes released in the maternal circulation are associated with pregnancy disorders and parturition[11].

Tissue-based maps of the human proteome of many organs, including placentas, have been published,[13-16] but great challenges remain to discover which among the hundreds of detected proteins regulate key metabolic networks, specifically, during normal and complicated pregnancies and labor. To obtain such information, we chose to immunoprecipitate VEGFR2, an ideal target as an extensively documented regulator of placental angiogenesis. To deploy a wide net for the membrane partners of VEGFR2, we analyzed the pellets obtained after high-speed centrifugation of chorionic villi homogenates. Uterine blood in the maternal intervillous space exchanges substances with fetal blood at the villous tree. Although the villi are physically separated from uterine blood[1,3], the pellets contain cells and EV from it. To preserve protein complexes, we extracted the pellets with ASB-14 (amidosulfobetaine-14), an efficient non-denaturing detergent. The extracts were immunoprecipitated with the bait antibody (Ab) charged on magnetic beads knowing that extraction of membrane proteins from their native environment could alter their structure and protein links. Mass spectrometry identified proteins immunoprecipitated with VEGFR2, especially its newly discovered placental

partners, the multifunctional MDMX (Double minute 4 protein) and PICALM (Phosphatidylinositol-binding clathrin assembly protein).

MDMX, also known as MDM4 and HDMX, is a zinc-binding protein and a p53 inhibitor acting in coordination with MDM2, a zinc-dependent E3 ubiquitin ligase[17]. MDMX and MDM2 have numerous p53-independent activities. In preeclampsia, p53 is upregulated in villous trophoblasts[18]. PICALM is a nuclear and plasma membrane protein that interacts with phosphatidylinositol to recruit clathrin and adaptor protein-2, initiates endocytosis of clathrin-coated vesicles, internalizes ligand-receptor complexes, and participates in iron and cholesterol homeostasis[19,20]. PICALM is a genetic risk factor for late-onset Alzheimer's disease that participates in amyloid-β transcytosis and processing of amyloid precursor protein (APP). Human placentas express APP and APP-processing enzymes which are increased in preeclampsia[21]. Oxytocin is a hydrophilic neuropeptide and Pitocin, a synthetic oxytocin, is prescribed in the USA to induce labor and decrease postpartum hemorrhage. The oxytocin receptor (OT-R, *OXTR*) is a magnesium-dependent G protein-coupled receptor[22] that activates a phosphatidylinositol-calcium second messenger system[23]. OT-R participates in numerous activities ranging from parturition to lactation and mother-child bonding[22,23]. OT-R functions as a homodimer and in heterocomplexes with vasopressin receptors V1aR (*AVPR1A)*[24], V2R, and other receptors. V1aR is the most abundant among vasoactive receptors in human arteries[25].

Here, among the newly detected partners of VEGFR2 we focused on MDMX and PICLAM based on their documented biochemical functions, and their partners OT-R and V1aR. Finding OT-R in exosome-size clusters in the fetal lumen led to the hypothesis that placental OT-R is carried to the fetus in exosomes, potential transporters of future therapeutic agents. MDMX, PICALM, OT-R, and V1aR protein levels, estimated by western blots and relative to an internal control sample, were associated with clinical characteristics of the 44 patients we studied. Potential insights on the molecular mechanisms of placental MDMX and PICALM were gained, respectively, from the cancer and Alzheimer's disease literature.

Results

Immunoprecipitations (IP). Key prerequisite for this study was that VEGFR2 protein complexes withstood tissue freezing and extraction by ASB-14. Since Blue-Native electrophoresis (BN) resolves protein mixtures under non-denaturing conditions, we fractionated placental extracts by BN followed by VEGFR2 immunostaining which revealed streaks extending up to 800 kDa. VEGFR2 monomers appear at 220 kDa in western blots. Apparently, ASB-14 stabilized the extracted protein complexes of VEGFR2. Several proteins described in this study were efficiently extracted by ASB-14 (see Methods). New VEGFR2 partners, MDMX and PICALM, were also selected for IP.

Fig. 1 shows western blots of the fractions eluted from the magnetic beads and used to select the fraction for mass spectrometric analysis. Representative fractions are identified by the patient's assigned letter-number code shown on Table 1. Magnetic beads retained all of the applied VEGFR2 (**A**) as none was detected in the flow-through fraction, but the MDMX and PICALM antibodies charged on the beads retained only a fraction of their target protein as shown, respectively, in **E** and **F**. All target proteins were greatly enriched in the eluted fraction-E relative to the applied placental extract, fraction-X. OT-R co-immunoprecipitated with MDMX (**G**, right side) and with PICALM (**G**, left side), but not with VEGFR2 (**D**). V1aR co-immunoprecipitated with MDMX (**H**, left side) and with PICALM (**H**, right side), but not with VEGFR2 (**C**). Eluted MDMX appeared smaller in the VEGFR2 IP (**B**) and MDMX IP (**E**), whereas PICALM (**F**), OT-R (**G**) and V1aR (**H**) appeared larger. The size of eluted VEGFR2 was the same as in the extracts (**A**).

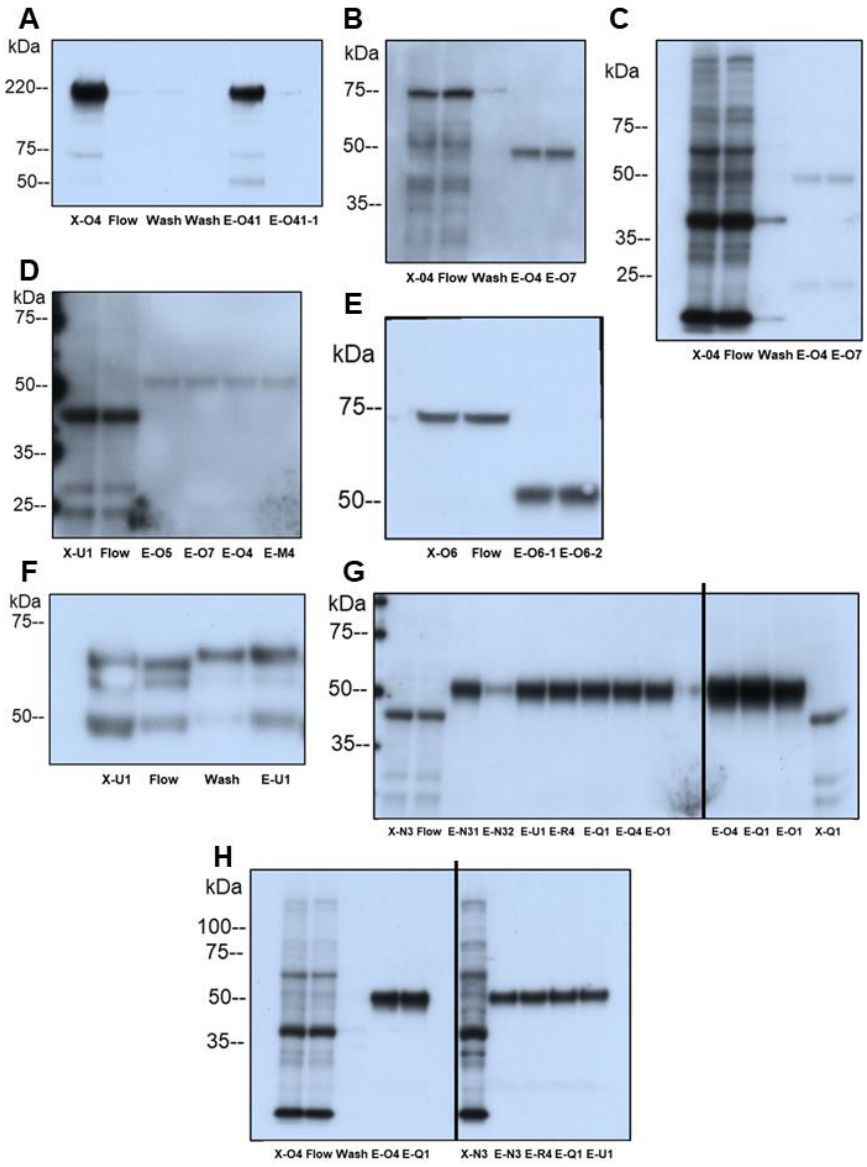

Fig. 1. Protein elution profiles in VEGFR2, MDMX and PICALM IP. Detergent-extracted villous sample X was incubated with magnetic bead suspension charged with the target Ab (see Methods). E denotes eluted protein fractions. Western blots detected the target proteins eluted in the uniformly performed IP experiments. **A.** VEGFR2 in VEGFR2-IP. **B.** MDMX in VEGFR2-IP. **C.** V1aR in VEGFR2-IP. **D.** OT-R in VEGFR2-IP. **E.** MDMX in MDMX-IP. **F.** PICALM in PICALM-IP. **G.** Left-side, OT-R in samples from PICALM-IP, and right-side OT-R in samples from MDMX-IP. **H.** Left-side, V1aR in samples from MDMX-IP, and right-side samples from PICALM-IP. Panel **C** shows the membrane in **B** reprobed for V1aR without stripping.

Proteomic analysis. Results of the immunoprecipitations of VEGFR2 (samples O4, O5, O7, U1), MDMX (samples O1, O4, O6, Q1, Q4, R4), and PICALM (samples N3, O1, R4, Q1, Q4, U1) are listed in Tables 2-4. The peptide coverage was not consistent among the placental extracts in each immunoprecipitation group due to different clinical characteristics of the patients whose tissues we tested, and potential differences in post-translational modifications, such as acetylation, and ubiquitination. Soluble proteins in villous homogenates having an affinity for membrane proteins would be retained on the pellets obtained after centrifugation at 100,000*g* for 1h.

Select proteins that co-immunoprecipitated with VEGFR2 (Table 2). VEGFR2 was retained on the beads by an Ab raised to the cytoplasmic tail of VEGFR2 exposing extracted proteins to its extracellular, VEGF-binding, domain (see Methods). Therefore, most VEGFR2 partners must have interacted, even after VEGFR2 internalization, with its extracellular rather than its intracellular tyrosine kinase domain, and in binary associations while fewer would bind via some intermediate protein partners. In principle, VEGFR2, MDMX, and PICALM isoforms post-translationally modified at the target sequence of the immunoprecipitating antibodies, are unlikely to be retained on the beads. Our experimental design provided only an estimate of peptide levels in each placental sample. Very basic proteins, such as VEGF-A (pI=9.2), were not detected due to excessive trypsin digestion of these mostly intrinsically disordered proteins prior to mass spectrometric analysis. For example, more than 65% of the VEGF-A residues are expected to be disordered. Nevertheless, western blot analysis showed that VEGF-A co-immunoprecipitated in VEGFR2 IP, and that OT-R (pI=9.6) and V1aR (pI=9.5) co-immunoprecipitated in MDMX and PICALM IP. p53 and MDM2 were detected in IP eluates only by western blots. Under our protocol, proteins larger than 220 kDa were, most likely, identified by peptides from their smaller forms in the placenta.

The E3 ubiquitin ligase TRIM21 (tripartite motif-containing protein 21) co-immunoprecipitated with VEGFR2 and in MDMX and PICALM IP (Tables 2-4). TRIM21, a member of the large TRIM family, contains a zinc-binding as well as other motifs. TRIM21 is found in the cytosol and nucleus and is unique among all proteins as the highest-affinity Fc receptor in humans[26]. TRIM21 does not distinguish free from bound antibodies. Another VEGFR2 partner was PDC-E2 (*DLAT*), the E2 component of pyruvate dehydrogenase

(Table 2). The association of PDC-E2 with VEGFR2 probably occurs in the nuclei[27] and mitochondria, as discussed later, and is shown in the vasculature of the villi (video). Other VEGFR2 partners were complement components (Table 2) revealing complement activation known to occur in placental dysfunctions[28]. Immunoglobulin heavy constant alpha 1 (*IGHA1*), an autoantibody antigen and signature protein of plasma cells[29], was among the large amounts of immunoglobulins detected that are carried by placental endothelial cells[30] and maternal blood cells. A smaller than 220 kDa form of the giant protein titin was also detected in VEGFR2 and PICALM IP (Tables 2, 4).

Select proteins that co-immunoprecipitated with MDMX and PICALM (Tables 3, 4). VEGFR2 was not detected in MDMX and PICALM IP, probably because of the limited binding capacity of the MDMX and PICALM antibody charged on the beads. Among the proteins that co-immunoprecipitated with MDMX were PICALM, annexins, arginase-1, RNA-binding protein HNPNPA2B1[31] and others that immunoprecipitated also in VEGFR2 and PICALM IP (Tables 2, 4). Protein-glutamine gamma-glutamyltransferase 2 *(TGM2)*, which co-immunoprecipitated with MDMX and PICALM (Tables 3, 4), catalyzes protein cross-linking, is considered a bridge between inflammation and hypertension, and is upregulated in preeclampsia[32]. We indicated in Table 3 the few proteins common in VEGFR2, MDMX and PICALM immunoprecipitations, and many more that co-immunoprecipitated only with MDMX, likely members of the HC proteome. After an initial statistical analysis associated MDMX with the mode of delivery, we were prompted to study the OT-R, which is activated in the myometrium causing uterine contractions[22], and its partner V1aR, after validating two commercial antibodies (Figure 10).

Immunohistochemistry and whole mount immunofluorescence. VEGFR2 strongly stained the endothelium of the villous capillaries (Fig. 2A). TRIM21 staining is seen in the cytoplasm of villous trophoblasts and stronger staining in intervillous maternal leukocytes (Fig. 2B, arrows). MDMX is predominantly expressed (Fig. 2, C and D) on Hofbauer cells (HC)[33-37] that are targets of Zika and other viruses[38]. Strong MDMX staining was limited to the cytoplasm of HC, easily identified within the villous stroma, some within stromal channels (Fig. 2C). CD163[33,39], a marker for placental macrophages[40], stained the

cytoplasm of the HC (Fig. 2D). PICALM showed strong staining of trophoblasts and syncytiotrophoblasts (Fig. 2E) and on higher power images (Fig. 2F) positive cytoplasmic staining of the villous capillary endothelial cells was also seen.

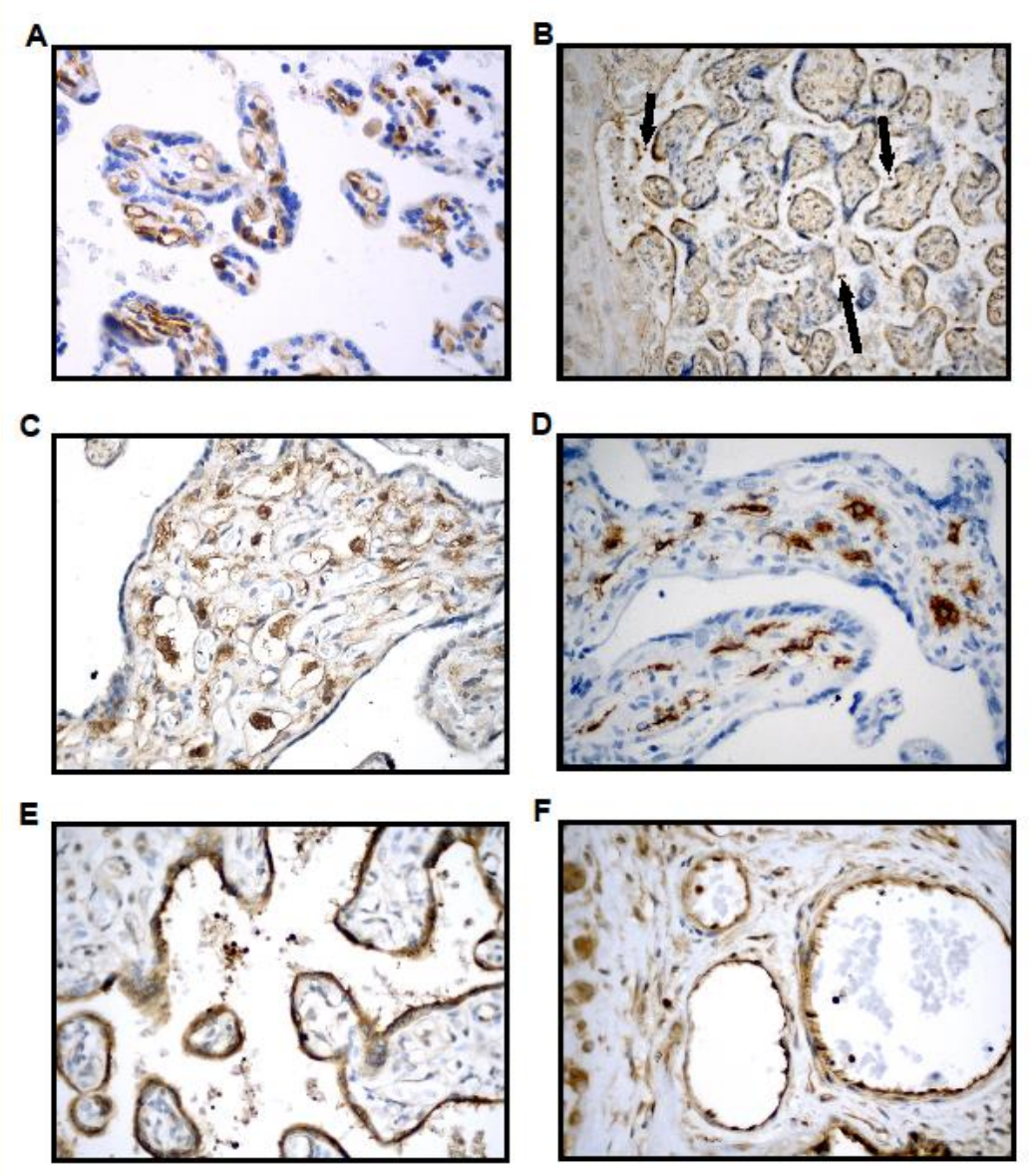

Fig. 2. Immunohistochemical staining of placental sections. A. VEGFR2 immunostaining is strongly positive in villous endothelial cells (patient Q3). **B**. TRIM21 is uniformly positive in villous trophoblast (patient N4). Very strong staining is seen of maternal leukocytes (arrows). **C.** MDMX is strongly positive in the cytoplasm of HC and moderately positive in endothelial cells (patient W2). **D.** CD163 is strongly positive in the cytoplasm of the HC (patient U1). **E.** PICALM is strongly positive in the trophoblast (patient R4). **F.** PICALM positivity seen in the villous endothelial cells and fetal blood leukocytes (patient R4). Magnifications in A-F were 10x, 20x and 40x.

The co-localization of VEGFR2 (red) and PDC-E2 (green) in endothelial cells of the villous vasculature of a normotensive patient is shown on the video obtained from reconstructed stacked images of whole mount immunofluorescence. Nuclei were stained blue with DAPI.

Immunogold electron microscopy (IGEM). VEGFR2 was localized along segments of endoplasmic reticulum, and in mitochondria (Fig. 3). MDMX was localized diffusely within the cytoplasm of an HC and was seen clustering in the nucleus and cytosol. Clusters ran along the nuclear membrane and appeared associated with mitochondrial and endoplasmic reticulum membranes (Fig. 4). PICALM was localized to endothelial cell junctions, along endothelial cell plasma membrane, in cytoplasmic projection into the lumen and adjacent stroma and fetal blood (Fig. 5). OT-R was detected in endoplasmic reticulum and cytoplasmic “peninsulas” of endothelial cells extending into the lumen and on clusters (Fig. 6). V1aR was localized to endothelial cell membrane, nucleus, and stroma. V1aR was also seen on a fetal RBC (Fig. 7). Details are seen in Figures 3-7.

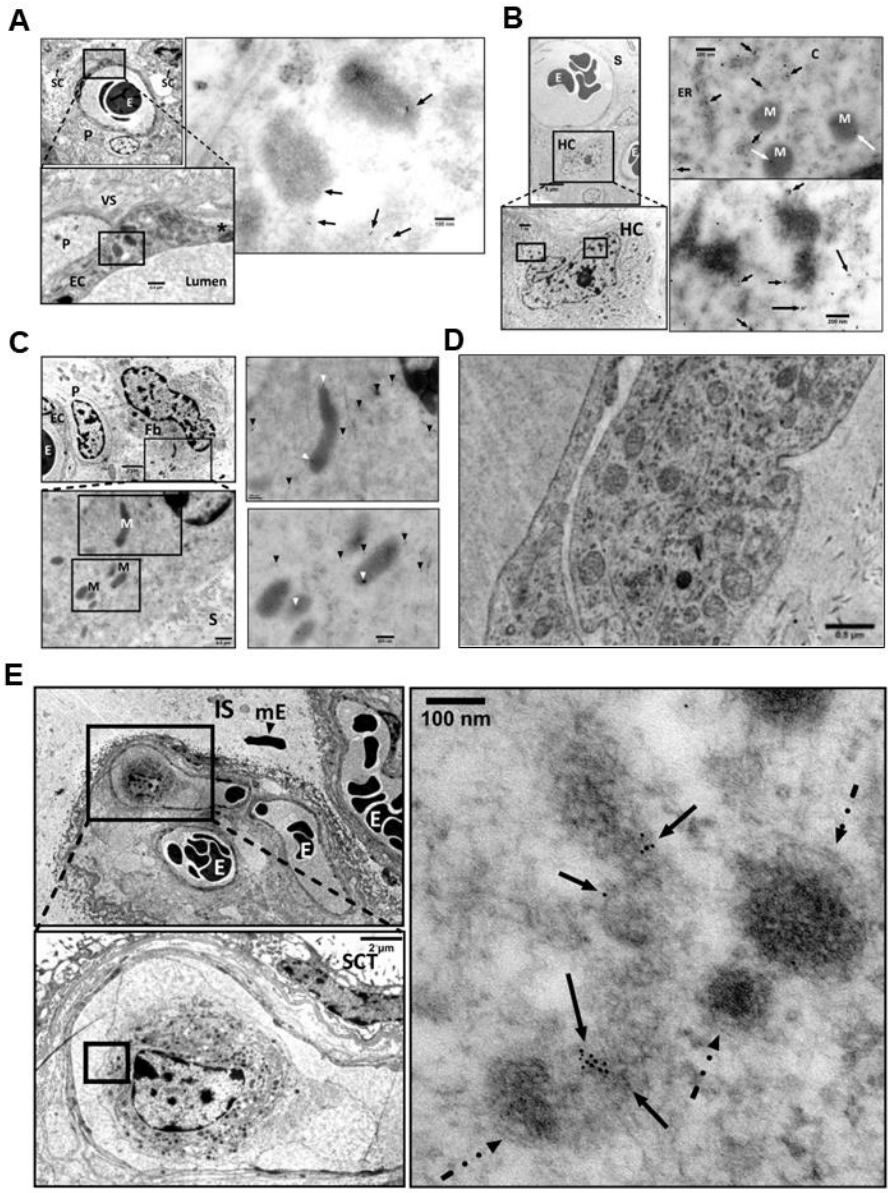

Fig. 3. Detection of VEGFR2 by IGEM in chorionic villi of placenta Ho-73 (preeclamptic). A. Top left micrograph shows a villous capillary. P: pericyte, E: RBC, SC: stromal cells. Bottom image details area outlined on the top micrograph and shows endothelial cell (EC) cytoplasm, pericyte (P), tight junction (*), collagen fibers in villous stroma (VS), and capillary lumen (L). Image at right: Enlargement of area outlined on the bottom left shows VEGFR2 in mitochondria (arrows). **B.** Micrograph on top left shows villous capillary, stroma (S), luminal RBC (E), and Hofbauer cell (HC). Enlargement of rectangle at bottom shows prominent nucleolus, mitochondria, and endoplasmic reticulum of HC. Micrographs on the right show enlargement of areas outlined on the bottom left

245 micrograph that detail clusters of VEGFR2 (arrows) in the cytosol (C), along segments of
246 endoplasmic reticulum (ER), and mitochondria (M). Enlargement of image at bottom right
247 shows diffuse localization of VEGFR2 clusters throughout the nucleoplasm (arrows). **C.**
248 Top left micrograph: Villus stroma depicting a fibroblast (Fb), and a pericyte (P) associated
249 with fetal capillary in partial profile, RBC (E), and EC cytoplasm. Bottom left is enlargement
250 of area outlined on the top graph and shows fibroblast cytosol, mitochondria (M), and
251 villous stroma (S). To the right, enlargement of two areas show VEGFR2 in cytoplasm and
252 in partial profiles of mitochondrial matrix (white arrow heads). **D.** A TEM micrograph after
253 osmication provided a better outline of mitochondria in an EC, compared to **A, B** and **C**
254 panels**. E.** Fetal capillaries with luminal RBC (E) are shown in the top left image, IS:
255 intervillous space; mE: maternal RBC. Bottom: enlargement of outlined area shows a fetal
256 macrophage in greater detail; a syncytiotrophoblast (SCT) is also present. Right
257 micrograph: enlargement of area in bottom left micrograph, points to VEGFR2 labelling in
258 an incomplete profile of a mitochondrion. Dashed arrows outline the outer double
259 membrane of the labeled and unlabeled mitochondria. The gold particle diameter is 6 nm.

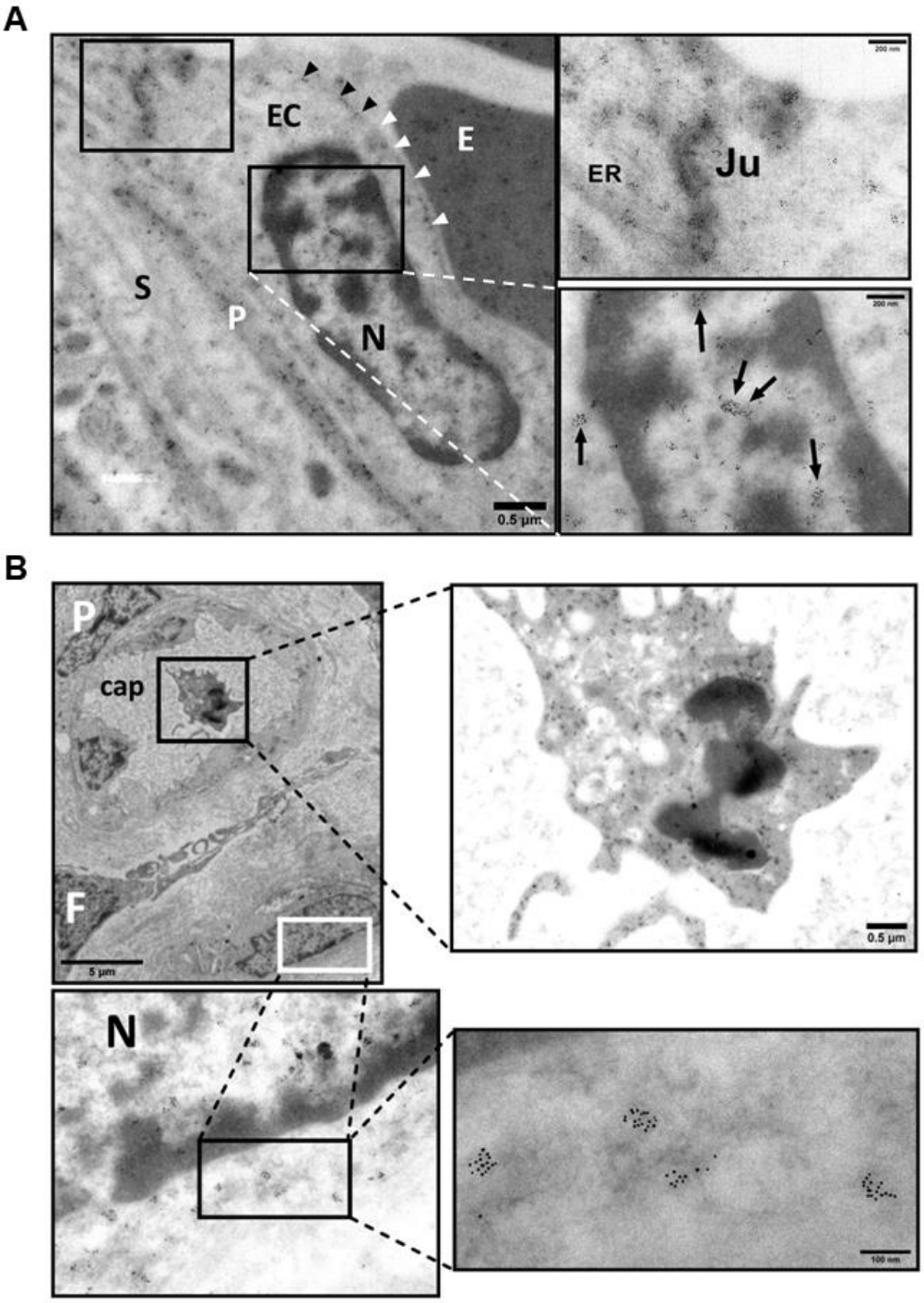

Fig. 4. Detection of MDMX by IGEM in chorionic villi of placentas Ho-71 (normotensive) and Ho-73 (preeclamptic). A. Left micrograph: Nucleus (N) of endothelial cell (EC) from Ho-73. Arrow heads point to small MDMX clusters, parallel to the inner aspect of the EC plasma membrane. Area outlined, top left: EC junction; P: pericyte process; E: RBC in capillary lumen, S: stroma. This area is enlarged on the top right graph and shows MDMX clusters along the junction (Ju), and endoplasmic reticulum

(ER). Bottom right: enlargement of outlined area shows diffuse pattern of MDMX clusters throughout the nucleoplasm. **B.** Top left micrograph shows an outline of apoptotic macrophage in the lumen of fetal capillary (cap) from Ho-71. P: pericyte, F: partial profile of fibroblast (F) and HC partially marked by a white outline. Enlargement on the top right image shows diffuse MDMX localization in the vacuolated cytoplasm of luminal macrophage. Image at bottom left is enlargement of area outlined in white and shows MDMX clustering in the nucleus (N) and cytosol of the HC. Clusters, averaging 50-100 nm in diameter, run along the nuclear membrane and appear to be associated with mitochondrial and endoplasmic reticulum membranes. Bottom right: enlarged area shows MDMX clusters of approximately 100 nm. The gold particle diameter is 6 nm.

277

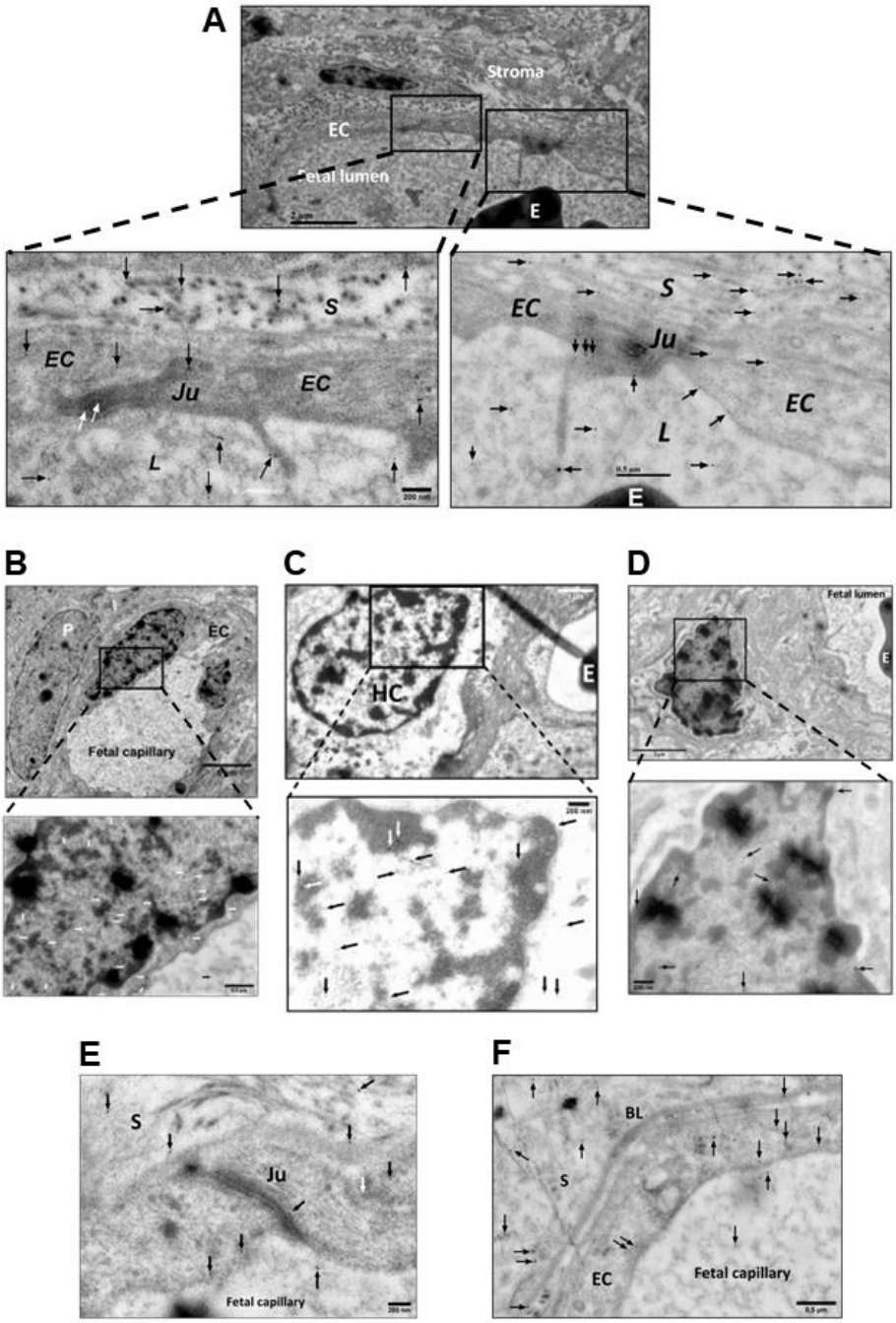

278 **Fig. 5. Detection of PICALM in chorionic villi of placentas Ho-71 (normotensive) and**
279 **Ho-73 (preeclamptic). A.** Top IGEM micrograph: partial profile of villus capillary from Ho-
280 71. EC: endothelial cells; E: RBC; stroma. Bottom images: enlargement of two selected
281 areas of endothelium show PICALM localization (arrows) at EC junctions (Ju), along EC
282 plasma membrane, in cytoplasmic projections into lumen (L) and adjacent stroma (S). **B.**
283 Top micrograph: the nuclei of endothelium of a villus capillary from Ho-71, and the adjacent
284 pericyte (P) are patent. Bottom image: enlargement of nucleus, shows PICALM in

nucleoplasm near chromatin, on EC cytoplasmic membrane (white arrows) and in luminal space (black arrow). **C.** Top micrograph: HC in stroma of Ho-73. E: RBC in capillary. At bottom: enlargement shows PICALM in HC nucleus (arrows). **D.** Top micrograph: HC cell in the stroma of placenta Ho-71. Bottom image: enlargement shows PICALM in nucleoplasm in association with chromatin. **E.** PICALM is shown (arrows) at the junction (Ju), and plasma membrane of EC and in adjacent stroma (S) of fetal capillary from Ho-73. **F.** PICALM is shown (arrows) in cytoplasm and plasma membrane of EC of capillary from Ho-71, and in basal lamina (BL), stroma (S) and capillary lumen. The gold particle diameter is 10 nm.

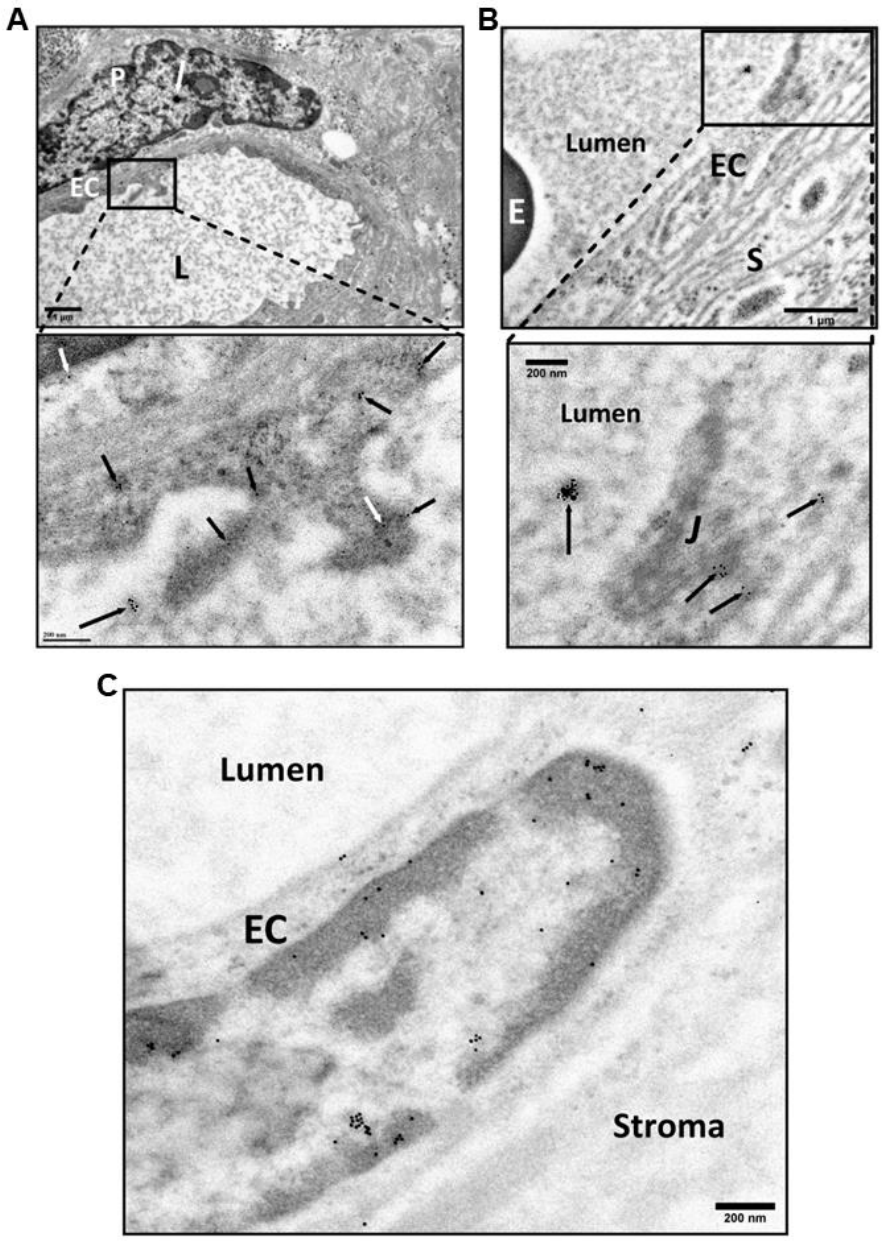

Fig. 6. Detection of Oxytocin Receptor (OT-R) in chorionic villi of placentas of normotensive Ho-71, and preeclamptic Ho-73 patients. A. Top IGEM micrograph: Villus capillary from Ho-71. P: pericyte adjacent to the endothelial cell (EC); L: lumen. White arrow shows cluster of PICALM on P. Bottom: enlargement shows OT-R in endoplasmic reticulum (ER) and cytoplasm projections of EC into the lumen. (arrows). **B.** Top micrograph: Partial view of villus capillary from Ho73, E: RBC; S: stroma. Bottom graph shows EC junction (J) and OT-R clusters on J, EC cytoplasm, and lumen (arrow). **C.** OT-R is seen in the nucleus of an EC from Ho-73.The gold particle diameter is 10 nm.

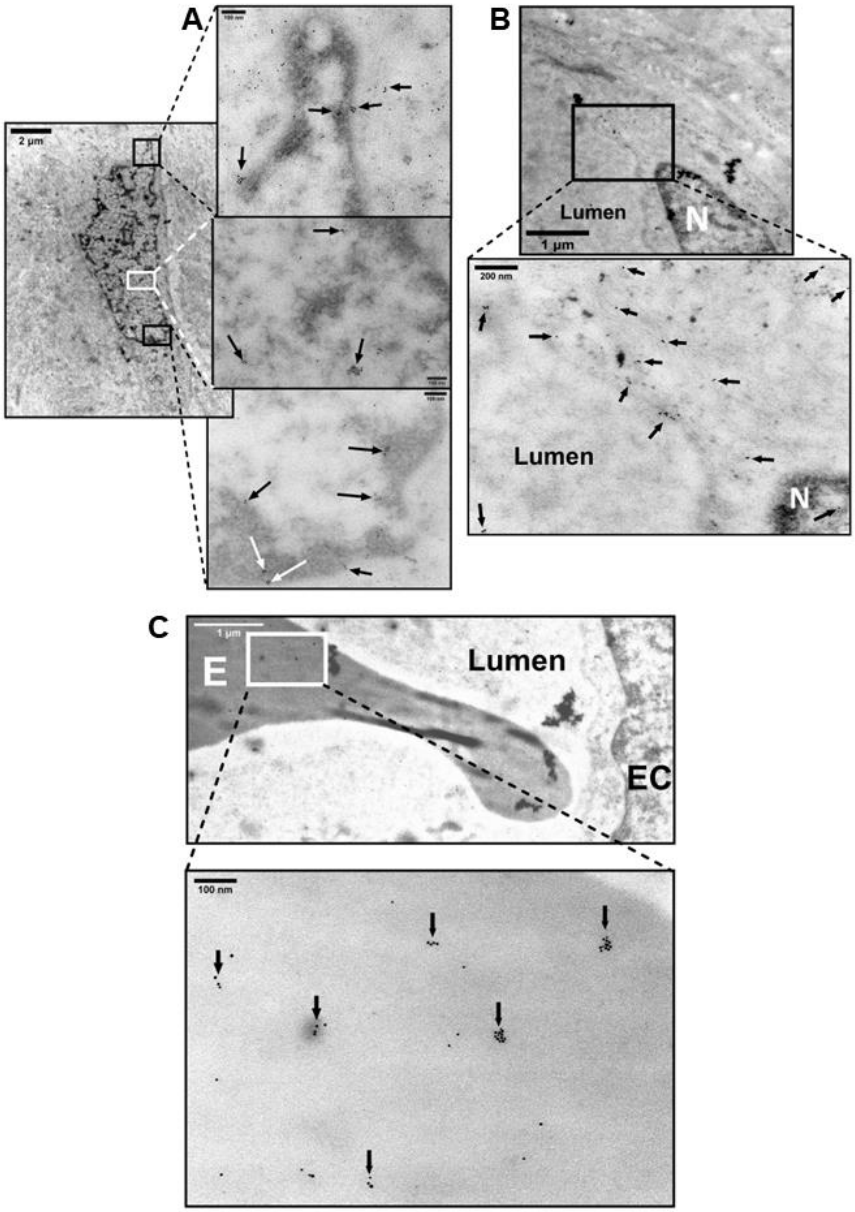

305

306 **Fig. 7. Detection of Vasopressin Receptor V1aR in chorionic villus of placenta Ho-**
307 **72 (diabetic). A.** Composite IGEM image shows nucleus of HC in stroma on the left and
308 enlargements of three demarcated regions of its nucleus on the right. V1aR clusters, 20-
309 100 nm, in the nucleus are indicated by arrows. **B.** Top micrograph shows EC aspect of a
310 villus capillary. Bottom image is enlargement that shows V1aR on EC membrane, nucleus,
311 and stroma (arrows). **C.** Top micrograph shows aspect of EC of villus capillary; an RBC is
312 seen in the lumen. Bottom image is enlargement that shows several 20-100 nm clusters
313 of V1aR on surface of the RBC (arrows). The gold particle diameter is 10 nm.

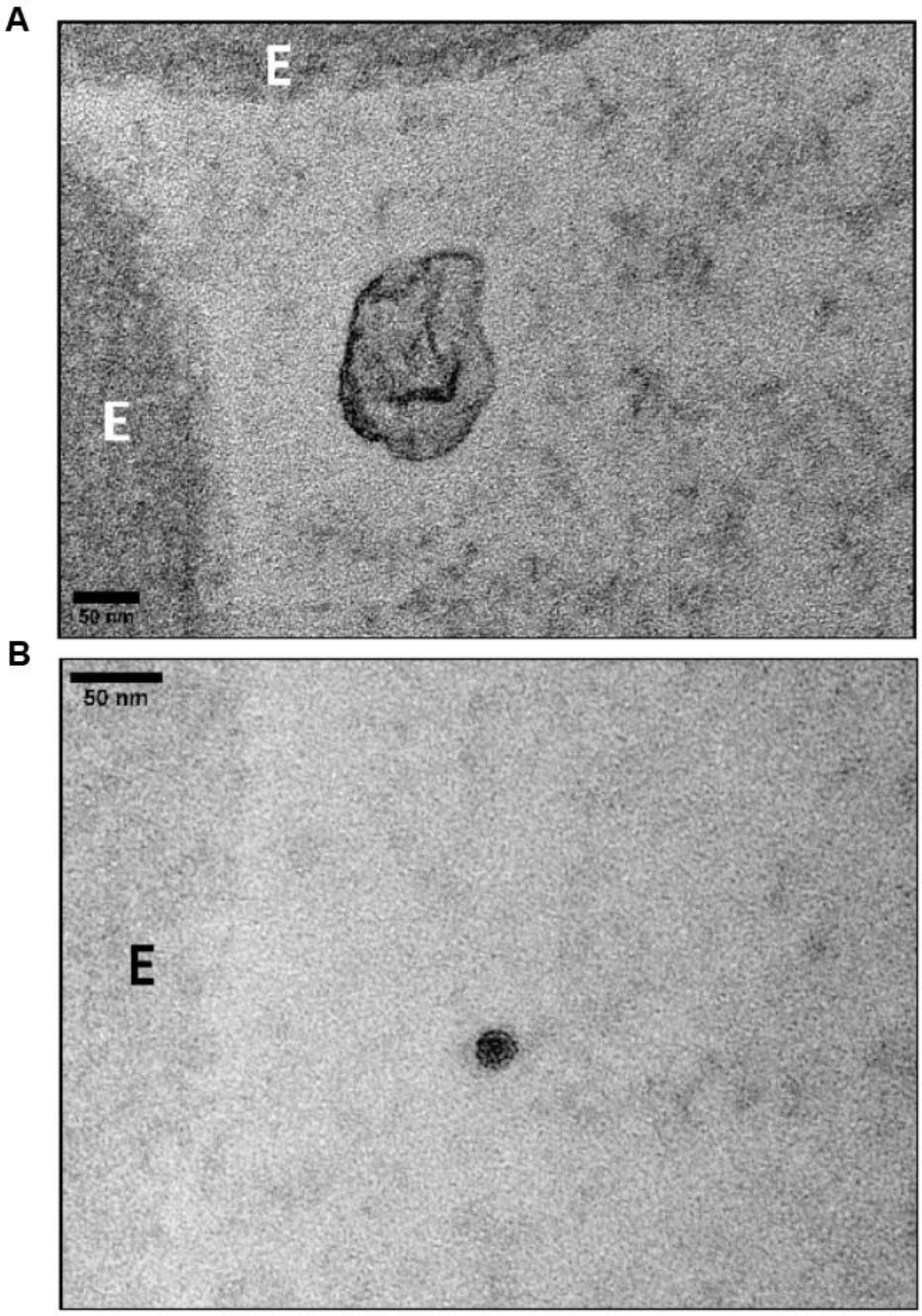

Fig. 8. Transmission electron microscopy of osmicated chorionic villus from placenta Ho-73 (preeclamptic). A. An exosome[9] is shown in the lumen with the characteristic lipid bilayer adjacent to RBC (E). **B.** A dense particle with a lipid bilayer, perhaps an exomere[12], is shown in the lumen next to an RBC (E). Scale in A and B is 50 μm.

Statistical analysis of protein levels in placental extracts. To estimate the protein levels of MDMX, PICALM, OT-R and V1aR, we analyzed by western blots 25 µg protein from each of the 44 placental extracts (Table 1). The intensity of the native-protein band, shown at the top of the representative western blots in Fig. 9, is relative to an internal control sample (Q1 or V1) taken as 100% (Table 5). Violin plots show the analysis of the mean protein levels (Fig. 9) among different clinical conditions. Precluded from the statistical analysis were VEGFR2, since its protein levels did not differ significantly among the 44 placentas analyzed in this study, and TRIM21 due to extensive degradation of its native 50-kDa form in our placental extracts.

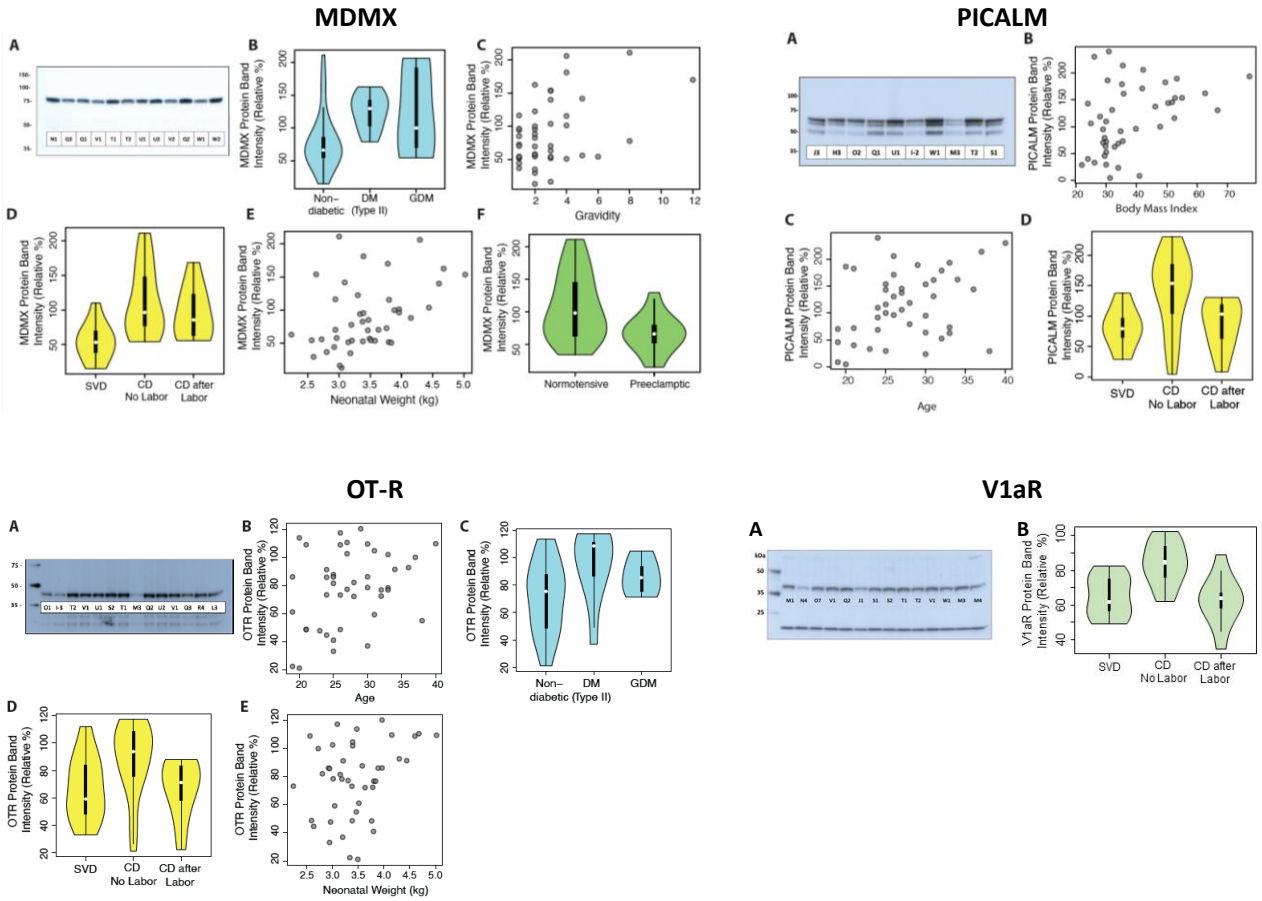

Fig. 9. Representative western blots (A) of MDMX, PICALM, OT-R, and V1aR, and violin plots of their relative protein levels associated with diabetes, gravidity, labor, neonatal weight, preeclampsia, BMI, or maternal age, as indicated in B-E. Western blots show the molecular mass (kDa) and the placental extracts identified by a letter-number code shown in Table 1. Internal control for MDMX and PICALM was sample Q1, and sample V1 for OT-R and V1aR.

Next, we performed univariable and multivariable analyses, shown in Tables 6-12, to test whether the mean protein levels of MDMX, PICALM, OT-R and V1aR, represented by western blot band intensity of placental extracts and relative to an internal reference sample Q1 or T1, varied as a function of maternal age, gravidity, gestational age, body mass index, race, preeclampsia, diabetic status, delivery mode, neonatal sex, and neonatal weight. Preeclamptic patients were compared to non-preeclamptic, and diabetic to non-diabetic patients.

Univariable analysis of protein levels. Protein expression units are the percent values relative to an internal control sample taken as 100% (Table 5).

MDMX protein levels were associated with diabetes with an increase of 47.63 units (95% CI 14.27, 90.00) among those with Type II diabetes and 47.91 (95% CI 5.51, 90.32) among those with gestational diabetes mellitus (GDM) compared to those without diabetes, and gravidity with an increase of 9.66 (95% CI 3.59, 15.70) with each unit increase in gravidity, neonatal weight (an increase of 0.03 (95% CI 0.01, 0.06) for each increase in grams), and preeclampsia (-44.13 (95% CI -71.63, -16.64). Regarding the mode of delivery, cesarean delivery, CD, prior to the onset of labor was associated with an increase of 56.16 (95% CI 24.13, 88.18) compared to those with SVD. See Table 6 for full results. Recently, CD163 expression in Hofbauer cells was associated with BMI, gravidity, and fetal birthweight[41].

Increased PICALM levels were associated with maternal age with an increase of 3.68 (95% CI 0.28, 7.08) in intensity for each year increase, and body mass index with an increase of 2.06 (95% CI 0.66, 3.45) for each unit increase. Regarding the mode of delivery, CD prior to the onset of labor had an increase of 59.96 (19.24, 100.68) compared to those with SVD. See Table 7 for full results.

OT-R protein levels were associated with maternal age, an increase of 1.56 (95% CI 0.13, 2.99) for each year of age, and diabetes with an increase of 24.16 (95% CI 5.47, 42.85) among those with Type II diabetes compared to those without diabetes. Neonatal weight was associated with an increase of 0.01 (95% CI 8.36×10^{-4}, 0.03) for each increase in grams. See Table 8 for full results.

V1aR protein levels were statistically significantly associated with mode of delivery, CD prior to onset of labor 20.36 (95% CI 10.58, 30.13) compared to SVD. See Table 9 for

full results. No associations were found for race, neonatal sex, or gestational age between 35-42 weeks for any outcome.

Multivariable analysis of protein levels. A multivariable model considered simultaneously all variables that were statistically significant in univariable analysis. MDMX protein levels showed a statistically significantly association with gravidity 7.19 (95% CI 1.24, 13.14), and preeclampsia -40.61 (95% CI -66.18, -15.04) as shown on Table 10. There were no significant associations for PICALM or OT-R as shown in Tables 11-12. The best fit model for V1aR included only an intercept (no covariate).

To account for the spread in the replicate measurements of MDMX, PICALM, OT- and V1aR (Table 5), we carried out the bootstrapping analysis shown in Tables 14-19. The statistical results were robust to bootstrapped resampling (n=1000) of data points included in the analyses.

We also looked at the correlation of MDMX, PICALM, OT-R and V1aR protein levels with each other and found significant correlations between PICALM and OT-R (0.72 95% CI 0.54, 0.84, $p<2.7x10^{-8}$), PICALM and V1aR (0.41 95% CI 0.12, 0.63, $p<0.006$), and OT-R and V1aR (0.47 95% CI 0.20, 0.67, $p<0.001$). MDMX was not correlated with PICALM, OT-R or V1aR.

Discussion

Mass spectrometry placed VEGFR2, MDMX and PICALM and their partners in the molecular landscape of chorionic villi of placentas at term. The co-immunoprecipitated proteins represent the most prevalent and stable complexes. IGEM provided a detailed map of VEGFR2, MDMX, PICALM, OT-R and V1aR in the villi, and hints about protein traffic, specifically, of placental exosomes transporting OT-R to the fetus. In future studies, IGEM can show if two proteins are within 10-20 Å of each other, with secondary antibodies labeled with gold particles of different size[42], such as 6 nm and 12 nm, even though larger particles may occasionally eclipse the smaller ones.

A comprehensive statistical analysis of 44 placental extracts associated MDMX, PICALM, OT-R and V1aR protein levels with labor at term and a number of clinical parameters and gestational complications. Further studies may assign their binary protein

interactions into networks of signaling partnerships among patient groups with normal gestation and gestational complications.[43] The predominant expression of MDMX on fetal macrophages (HC)[37] and the association of MDMX levels in the villi with most of the clinical characteristics we tested, suggest that MDMX has a central role in comorbidities, that originate from deficient trophoblast proliferation,[44] and are linked to pre-existing conditions and environmental exposures.[45]

MDMX immunoprecipitations. We were puzzled that the immunoprecipitated MDMX had a molecular mass of 50 kDa, instead of 75 kDa in the placental extracts (Fig. 1, B and E). A possible explanation was offered by the discovery[46] that MDMX interacts with TRPM7, a bi-functional cation channel protein fused with a kinase domain. TRPM7 is a master regulator of the cellular balance of divalent cations, that mediates the uptake of Zn^{2+}, Mg^{2+} and Ca^{2+},[47] and senses oxidative stress to release Zn^{2+} from intracellular vesicles[48]. TRPM7 regulates MDMX levels by modulating Zn^{2+} concentration, and induces the formation of faster moving forms of MDMX on SDS-PAGE gels[46]. These forms depend on the channel function of TRPM7 and proteasomal degradation. We hypothesize that placental TRPM7, which is downregulated in preeclampsia,[49] interacted with MDMX during the overnight incubation with the immunoprecipitation beads stripping MDMX of Zn^{2+}. Proteasomal degradation was prevented by including MG-132 in our tissue-extraction and IP buffer. We missed detecting TRPM7 because it did not enter the top section of the 4-12% Bis-Tris NuPAGE gels we used to fractionate the IP proteins with and submit the 25-220 kDa strips for proteomic analysis (see Methods). TRPM7 has a theoretical mass of 213 kDa and pI 8.1, but on SDS-PAGE gels it is shown at 230 kDa and was reported at 245 kDa in BN electrophoresis.

Autoantibody antigens and TRIM21. Although our patients did not show symptoms of autoimmune diseases, a few of the immunoprecipitated proteins listed on Table 20 were also among the autoantigens detected by Neiman *et al*. in healthy adults[50], such as the extensively studied autoantigens TRIM21/Ro(SS-A) and PDC-E2, also an autoantigen in primary biliary cholangitis and other autoimmune diseases. PDC-E2 would be held on the beads as a partner of VEGFR2. TRIM21 is also extracted from intervillous maternal

leucocytes based on their staining with TRIM21 (Fig. 2B). Maternal autoantigen-autoantibody complexes, with an affinity for proteins in the villous membrane fraction, would be trapped on the beads by Fc-receptor TRIM21 based on its high affinity for IgG[26]. Since TRIM21 has broad species specificity, it could bind to the sheep anti-rabbit Ab on the Dynabeads and the IP-bait, the anti-rabbit Ab the beads were charged with. If TRIM21 clusters on the beads remain catalytically active, they could, in principle, retain VEGFR2, MDMX and PICALM, as substrates of ubiquitin ligases, along with other proteins, many not *in vivo* TRIM21 substrates, detected by mass spectrometry. Consequently, TRIM21 can confound immunoprecipitations, performed according to our protocol, by retaining proteins unrelated to the bait-Ab. Based on the extensive TRIM21 literature, placental TRIM21 could participate in metabolic pathways as an E3 ubiquitin ligase,[51,52] and as Fc receptor defending against infections.

Immunohistochemistry and immunogold electron microscopy. The distribution of VEGFR2, MDMX and PICALM in the villi was shown by IHC (Fig. 2) and by IGEM which also showed the distribution of OT-R and V1aR (Figures 3-7). VEGFR2 was detected in the nucleus, as previously reported[27,53], and in mitochondria, a novel observation to the best of our knowledge (Fig. 3, panels A, B and C). Translocation in the other direction, mitochondria to the nucleus, was shown for the entire pyruvate dehydrogenase complex to supply acetyl-CoA for histone acetylation[54]. VEGFR2 is distributed through relay networks in lipid rafts and endosomal trafficking[55] and SUMOylation holds VEGFR2 at the traffic control Golgi apparatus[56]. Gradients in receptor concentration may exist along the placental vascular tree, as was shown for the purinergic $P2Y_2$ receptor (pI=9.7)[57]. Distortion of receptor gradients in preeclampsia and diabetes could affect protein traffic and even expose proteins to degradation. Regarding the latter, it may be pertinent to consider the mechanism of action of estrogen receptor antagonists that decreased the estrogen receptor intra-nuclear mobility and subsequently induced its turnover[58].

MDMX appeared in nuclear clusters (Fig. 4, A and B). PICALM was detected in nuclei (Fig. 5, B and C). The very basic OT-R and V1aR were also detected (Figures 6 and 7). Surprisingly, clusters of V1aR became clearly visible on a fetal RBC after increasing gamma (Fig. 7, C). Since vasopressin receptors participate in erythropoiesis[59]

their presence on RBC was not very surprising. We hypothesize that in addition to non-traditional functions, such as critical immune sensors,[60] RBC transport V1aR to the endothelial cells of the villi[25].

PICALM and OT-R were detected on endothelial cell projections into the fetal lumen (Figures 5A, 6A) where OT-R clusters were also observed (Fig. 6, A and B) matching the dimensions of microvesicles-exosomes[10,11]. Although we cannot prove that OT-R clusters are inside exosomes with the characteristic bi-lipid membranes, as seen in standard EM cellular morphology, we propose that fetal exosomes carry to the fetus the OT-R and other proteins produced in the placenta. A limitation of IGEM, from the exosome perspective, is that bi-lipid layers are greatly impaired during the processing of tissues because OsO_4 is omitted in a post-fixation step used to increase the visualization of such membranes. OsO_4 reacts strongly with lipid complexes, and while it enhances contrast for standard EM cell morphological imaging, it can oxidize many antigen epitopes in IGEM. Fig. 8 shows representative intraluminal vesicles[9] seen in the fetal capillary of the placenta sample that was processed with the OsO_4 post-fixational step included. Membranes are more clearly defined here, compared to the IGEM sample, representing exosomes or microvesicles[9] in the fetal lumen (Fig. 8, A and B). We noticed similarities between our IGEM Figures 5 and 6 and transmission electron microscopy images in a study at two polluted cities in Mexico showing that environmental nanoparticles of Fe, Ti, Cu, Hg and Sn accumulated in HC and endothelial cells of chorionic villi sampled at term[61].

Statistical analysis of protein levels and clinical presentations. Our search for the function of the newly detected placental membrane proteins MDMX, PICALM, and of OT-R and V1aR, was accelerated by a statistical analysis of their protein levels, which revealed numerous associations with clinical characteristics of the 44 patients. MDMX, located predominantly in HC (Fig. 2C), took center stage based on its association with most of the clinical characteristics we tested. Although many of our statistical associations from 44 placentas are highly unlikely to be observed by chance, our conclusions could change by testing a larger number of placenta samples and integrating, after further research, protein isoforms and post-translational modifications of the newly detected proteins. But to what extent did proteins from intervillous blood, reflecting also the maternal

493 immune system,[45] contribute to the observed clinical associations? An initial answer was
494 provided for MDMX by the statistical analyses showing that tissue-resident HC contributed
495 most extensively since they predominantly express MDMX (Fig. 2).
496
497 **Diabetes.** In diabetic patients, higher MDMX levels (Table 6) seem to correspond to the
498 higher number of cells stained with CD163[62], a marker of HC[39]. It is not known if MDMX
499 upregulation and higher HC numbers mark a metabolic shift towards diabetes. A diabetic
500 atherosclerosis rat model showed upregulation of MDMX mRNA and protein levels[63].
501 MDMX was shown in cell cultures to serve as a nutrient sensor by inhibiting mTORC1[64].
502 HC could facilitate nutrient transportation in the villous stroma[34] linking placental MDMX to
503 nutrient levels and metabolic networks. OT-R levels are higher in Type 2 diabetes (Table
504 8), and there is an association of *OXTR* variants with insulin sensitivity and Type 2
505 diabetes[65].
506
507 **Preeclampsia.** Villous trophoblasts in pregnancies complicated by preeclampsia had
508 higher p53 and lower MDM2 levels [18]. Although MDMX was not measured, we believe it
509 would have been decreased also. Lower MDMX levels (Tables 6, 10) could reflect the
510 decreased numbers of HC in preeclampsia[40,41]. What can cause the decrease of HC? In
511 cancer, abnormal vascularity disrupts the penetration of immune cells,[66] and their function
512 is hindered by the tumor microenvironment[67,68]. Here, defective placental vascularity and
513 increased placental stiffness[69], both changing the architecture of the villi, could have an
514 adverse effect on HC levels. In preeclampsia, placental stiffness could be increased by
515 higher levels of tissue transglutaminase/*TGM2* (Tables 3, 4) which catalyzes protein
516 crosslinking[32]. MDMX could be involved in the reprogramming of fetal macrophages (HC)
517 during preeclampsia and other gestational complications and labor. Drawing from the
518 breast cancer literature[70], downregulation of placental MDMX in preeclampsia could be
519 linked to estrogen receptor-α[71] and lower estrogen levels[72,73].
520 In preeclampsia large quantities of magnesium sulfate are prescribed to prevent
521 seizures. A potentially relevant study of a blood-brain barrier (BBB) model of primary
522 endothelial cells from human brain[74], showed that TRPM7 mediated the entry of
523 extracellular Mg^{2+} into cells and that high Mg^{2+} levels speeded up the clearance of Aβ to

the blood side via BBB transcytosis and upregulation of PICALM and LRP-1 that is also expressed in HC[75]. It was shown recently that TRPM7 kinase activity induces amyloid-β degradation and clearance[76]. Among other mechanisms, the accumulation of placental Aβ[21] could be related to TRPM7 and limiting PICALM-dependent transcytosis.

Gravidity. Univariable and multivariable regression analysis found a significant association of gravidity with MDMX levels (Tables 6, 10). Gravidity was recently associated with HC levels determined by CD163 immunostaining[41]. While multigravida women have shorter telomeres and increased DNA methylation age,[77] a role of p53 and MDMX on telomere length is not established in normal human tissues, to the best of our knowledge. DNA methylation age is associated with MDMX and prenatal smoke exposure[78]. The gravidity-MDMX association, which registers in the villi, could reflect the cost of multiple pregnancies to the mother[79].

PICALM, OT-R and V1aR. The association of placental PICALM levels with BMI (Table 7) is intriguing because the placenta functions in the absence of adipocytes. A potential precedent for such association was provided by a study on gastric bypass surgery where PICALM mRNA levels in the blood were decreased after a significant drop of BMI[80]. Furthermore, among the Alzheimer's risk nucleotide polymorphisms (SNP), a PICALM SNP is associated with obesity[81].

The strong correlation of protein levels of PICALM with OT-R ($p<2.7x10^{-8}$), PICALM with V1aR ($p<0.006$), and OT-R with V1aR ($p<0.001$) point to fundamental interactions by yet unknown mechanisms. MDMX was not correlated with PICALM, OT-R or V1aR.

Downregulation of OT-R in spontaneous vaginal deliveries (SVD) relative to CD prior to the onset of labor (Table 8), would be consistent with the higher oxytocin levels in SVD than CD. It is not known to what extend extravillous blood cells and exosomes may have supplied OT-R, and V1aR, detected in placental membrane extracts. Nevertheless, IGEM images of the chorionic villi support the hypothesis that the lipid-covered exosomes carry a cargo of the very basic, magnesium-dependent OT-R across the blood-brain barrier to interact also with fetal microglia[82-84], the resident immune cells of the brain[85]. OT-R protein levels in venous and arterial blood from the umbilical cord may reveal differences

in bi-directional OT-R traffic in normal, preterm and postterm deliveries. In that case, OT-R protein levels and epigenetic modifications[86] may lead to therapeutic interventions with exosomes[87] prepared, ideally, with the transmembrane orientation[12] of OT-R in villous exosomes.

Labor. The decrease of MDMX in the membrane fraction of chorionic villi in SVD vs. CD prior to the onset of labor (Table 6), could be related to the decrease of immune cells in peripheral maternal blood with approaching labor[88], and the molecular signature of the "immune clock".[45,89] Lower MDMX levels could also indicate a molecular switch in late gestation, locally, to energy-preserving measures or other mechanisms involving uterine macrophages[90]. MDMX, PICALM, OT-R and V1aR could be components of the fetal and maternal immune system during pregnancy and as the fetus develops immunity in preparation for birth.[91,92] Concomitant downregulation of MDMX, PICALM, OT-R and V1aR occurred only in SVD compared to CD prior to the onset of labor (Tables 6-9) signifying a potential convergence of metabolic networks to prepare the uterus for the final act in pregnancy, delivery of the fetus.

Materials and methods

Human Subjects. All patients signed consent forms prior to their inclusion in the study according to the protocol approved by the Institutional Review Board of the University of South Florida and Tampa General Hospital. Placental samples were obtained from 44 patients with singleton pregnancies, aged 19-40 and gestational ages ranging from 35-42 weeks based on the dating criteria from the American College of Obstetricians and Gynecologists (ACOG) (https://pubmed.ncbi.nlm.nih.gov/28426621/) for women who delivered vaginally or by cesarean delivery (CD), between 7 AM to 4 PM, based on obstetric indications (Table 1). Patients were excluded if they had active viral infections or fetal growth restriction, defined as estimated fetal weight of <10th% per the Hadlock growth curve. Preeclampsia was diagnosed according to the criteria established in 2013 by ACOG (DOI: 10.1097/01.AOG.0000437382.03963.88). Low risk pregnancy was defined by the absence of maternal co-morbidities including chronic hypertension defined as

hypertension prior to pregnancy or systolic blood pressure ≥140 mm Hg or diastolic blood pressure ≥90 mm Hg prior to 20 weeks' gestation, pregestational or gestational diabetes, smoking, renal disease, and autoimmune disease. Patients with preeclampsia with severe features defined by the 2013 ACOG Guidelines received magnesium sulfate for seizure prophylaxis during induction of labor or CD through 24*h* postpartum. The demographic Table 21 shows that 91% of study participants were 18-34 years old and 75% were multiparous. Most participants (91%) were ≥37 weeks' gestation. There was no risk of bias in the selection of placentas which was at random. Sample/patient IDs (e.g., H-1, J-1, etc.) are not known to anyone outside the research group, and are assigned identifiers not using any personally identifiable information.

Reagents. Most of the reagents were purchased from Thermo Fisher Scientific (Waltham, MA, USA), MMP-200 metalloprotease inhibitor III, proteasome inhibitor MG-132, protease inhibitor cocktail III, marimastat, Hammarsten-grade casein, detergent ASB-14, Novagen S-protein HRP conjugate 69047-3, Novex 4-12% BT SDS-PAGE gels, CL-XPosure film, magnetic Dynabeads M-280 charged with sheep anti-rabbit antibodies, Maxisorp Nunc C-bottom 8-well strips, protein assay Pierce BCA 562 nm kit 23225 (Pierce, Rockford, IL), and Protein Perfect HRP MW markers 69079-3/ Millipore-Calbiochem (Billerica, MA). Additional reagents are provided in the sections below.

Antibodies (Protein target/vendor). VEGFR2 (55B11) no. 2479/Cell Signaling (Danvers, MA), MDMX A300-287A/Bethyl Laboratories (Montgomery, TX), PDC-E2 SC-365276/Santa Cruz Biotechnology (Santa Cruz, CA), PICALM Sigma Prestige HPA019053, OT-R ABN1735/Millipore (Temecula, CA), V1aR MBS176788/MyBiosource (San Diego, CA), CD163 MA5-33091/InVitrogen-Thermo Fisher Scientific, TRIM21 Novus NBP1-33548 (Centennial, CO), Alexa-488 (green) and Alexa-64 (red) goat anti-rabbit/mouse conjugated secondary antibodies/Life Technologies (Eugene, OR), immunogold donkey-anti-rabbit secondary antibodies 25702 (6 nm) and 25705 (10 nm) (Electron Microscopy Sciences (Hatfield, PA).

Placenta tissue collection, homogenization, and protein extraction with ASB-14 Within 15 min of the delivery of the placenta, samples were obtained from the fetal side of the placental bed at 4-5 cm from the umbilical cord and were placed on dry ice and then

stored at -80^{o}C. Tissues were also fixed in formalin for IHC or in paraformaldehyde-tannic acid for IGEM. Frozen tissue samples were finely cut and placed, at 150 mg per mL, in homogenization buffer containing 50 mM sodium phosphate pH 7.6, 50 mM NaCl, 50 µM sodium o-vanadate, 10 mM NaF, 20 µM proteasome inhibitor MG-132, 10 µM marimastat and 6 µL protease inhibitor cocktail-III per mL. After homogenization at 4^{0}C by three 15s bursts of a homogenizer with one-minute cooling in between, the homogenates were centrifuged for 1h at 100,000*g*. On top of the pellets was a thin pink fluffy layer, presumably of RBC membranes, which was included when the pellets were suspended in homogenization buffer containing 1% ASB-14 and then extracted overnight, due to logistical reasons, at 6-8^{0}C by end-over-end rotation. The zwitterionic detergent ASB-14 was superior in solubilizing membrane proteins to CHAPSO or n-octyl β-D-maltoside. After centrifugation at 100,000*g* for 1h, the supernatant solution was used in immunoprecipitations and western blots. We refrained from washing the membrane pellets in order to capture weak protein complexes. Protein levels of the membrane extracts were determined in quadruplicate at two dilutions with the Pierce BCA 562 nm kit. Final yield: 10-15 mg of detergent-extracted proteins per g wet tissue. To determine the efficiency of protein extraction by ASB-14, the post-ASB-14 100,000*g* pellets were solubilized in SDS-DTT at 95^{0}C and then probed in western blots. Extraction yield was 100% for VEGFR2, MDMX and PICALM, 86% for PDC-E2 and 64% for TOMM20, a marker for inner mitochondrial membranes.

Peptide synthesis to validate the OT-R and V1aR antibodies. Fig. 10 shows OT-R peptides EGNRTAGPPRRNEA (within the OT-R immunogen range given for this antibody), AEAPEGAAAGDGGRVA (outside the OT-R immunogen range) and V1aR immunogen peptide HPLKTLQQPARRSRLMIAA to validate the OT-R Millipore ABN1735 (0.5 µg/µL) and V1aR MyBioSourse MBS176788 (0.5 µg/µL) antibodies. The peptides were synthesized on 100 mg Rink Amide-MBHA resin (0.65 mmol/g) at room temperature under air using standard solid phase peptide synthesis protocol.

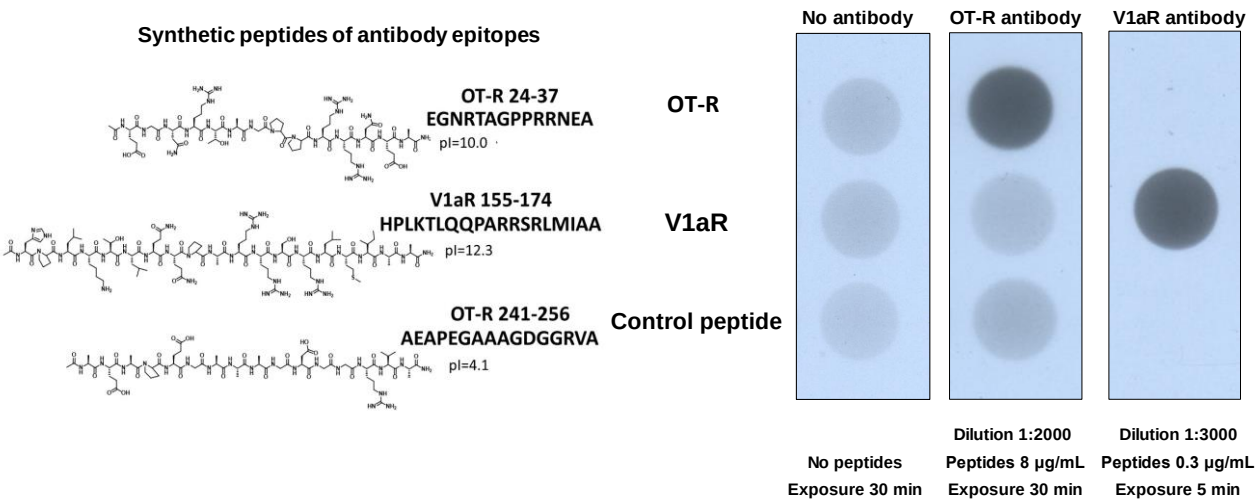

Fig. 10. Validation of OT-R and V1aR antibodies. The synthesized peptides and their pI are shown next to the scans of the coated Nunc C-bottom strips probed with the antibodies being validated.

Validation method for OT-R and V1aR antibodies. Maxisorp Nunc C-bottom strips were coated overnight at 4^0C with the indicated amounts of synthetic peptides (Fig. 10) dissolved in sodium carbonate buffer pH 9.6[93]. After blocking, as in western blot experiments, the OT-R and V1aR antibodies were added for 2h at room temperature at the indicated dilution followed by the secondary anti-rabbit antibody conjugated with horseradish peroxidase. Detection of bound OT-R or V1aR antibodies was conducted by ECL on films exposed for the indicated times. The OT-R and V1aR antibodies bound only to peptide sequences used to raise them.

Immunoprecipitations. Each immunoprecipitation of the 4-6 placental extracts, shown in Table 3-5, was carried out in one batch. Half mL of pellicular support M-280 Dynabeads was washed in homogenization buffer containing 1% ASB-14 and charged separately at room temperature for 2h with 0.9 µg VEGFR2, 15 µg MDMX or 7.5 µg PICALM antibody. Three mg of ASB14-extracted placental membranes from each placenta were mixed separately with the beads, overnight for logistical reasons, at 6-8^0C. Most proteins adhering to the beads were removed by washing four times with homogenization buffer

containing 1% ASB-14 and once with detergent-free buffer. Bound proteins were eluted at 95^0C with 100 mM Tris-HCl pH 7.6, 4% SDS (w/v) and 100 mM DTT. Eluted proteins were fractionated on 4-12% Bis-Tris NuPAGE gels. After Coomassie blue staining, gel strips from 25-220 kDa were submitted for mass spectrometric analysis.

Mass spectrometry. Samples were submitted and analyzed in a double-blinded fashion. Immunoprecipitated proteins were digested with Trypsin/Lys-C overnight at 37^0 C as described[94]. Each group of immunoprecipitated samples was analyzed with a new trap and HPLC column. Peptides were dried in a vacuum concentrator and resuspended in 0.1% formic acid for LC-MS/MS analysis. Peptides were separated with a C18 reversed-phase-HPLC column on an Ultimate3000 UHPLC with a 60-min gradient and analyzed on a Q-Exactive Plus using data-dependent acquisition. Raw data files were processed in MaxQuant (www.maxquant.org) and searched against the UniprotKB human protein sequence database. Search parameters included constant modification of cysteine by carbamidomethylation and the variable modification, methionine oxidation. Proteins were identified using the filtering criteria of 1% protein and peptide false discovery rate.

Western blot analysis. 25 µg of protein from placental extracts were resolved on 4-12% Bis-Tris NuPAGE gels, transferred to PVDF membranes and blocked overnight at room temperature in 1% Hammarsten-grade casein or 5% Difco skimmed milk powder. MDMX, PICALM, OT-R or V1aR primary antibody dilutions ranged from 1:800 to 1:10000. PVDF membranes incubated with ECL reagents were exposed to film for 1-20s. Films were scanned in the transmittance mode (Epson Perfection 3200 Photo, Epson America, Los Alamitos, CA, USA). The intensity of the top band (Fig. 9) was measured with Li-Cor Image Studio Lite software (Lincoln, Nebraska, USA) and chosen from a film exposed at the linear portion of the correlation between band intensity and film exposure time before films were overexposed. In the statistical analyses we used the mean intensity from 3.6 blots, on the average, and relative to an internal control sample Q1 or V1 (Table 5).

Immunohistochemistry. 4 µm formalin-fixed paraffin embedded tissue sections were processed for IHC and stained with VEGFR2 (1:50), MDMX (1:500) or PICALM (1:1000)

antibodies. Slides were exposed with diaminobenzidine tetrahydrochloride dehydrate as a chromogen and counterstained with hematoxylin before permanent mounting.

Immunogold electron microscopy. Tissue samples were promptly fixed in buffered 4% paraformaldehyde and kept overnight at 4^0C and then immersed in 0.75% buffered solution of tannic acid for 2h at room temperature. Samples were rinsed in filtered glass-distilled water, dehydrated through a series of increasing ethanol concentration, infiltrated, and embedded in LRW acrylic resin. Selected blocks were sectioned at 90-100 nm and mounted on formvar coated copper grids. The immunogold reaction was performed by incubating grids in standard blocking solution for 30 min at room temperature and transferring to either 1:100 MDMX rabbit Ab, 1:400 PICALM rabbit Ab, 1:100 VEGFR2 rabbit Ab or 1:600 OT-R or V1aR rabbit Ab for an overnight incubation at 4^0C. After washing in PBS, gold-conjugated donkey anti-rabbit Ab 25703 (Electron Microscopy Sciences, Hatfield, PA), was applied at 1:50 dilution for 90 min at room temperature. The diameter of the gold particles (Electron Microscopy Sciences, Hatfield, PA) was 6 nm in VEGFR2 and MDMX and 10 nm in PICALM and OT-R experiments. Excess secondary antibody was removed by washing with glass-distilled water and the grids were further treated with 2% aqueous uranyl acetate added for contrast. In control experiments excluding the primary antibody, 1-2 gold particles were detected throughout the grids. In morphological analysis by transmission electron microscopy, tissues were fixed in 2% OsO4, after 2.5% glutaraldehyde fixation and prior to the dehydration and resin infiltration steps. Images were obtained with a JEM-1400 transmission electron microscope (JEOL, Peabody, MA) and Orius-832 camera (Gatan Inc., Pleasanton, CA).

Whole mount immunofluorescence (WMIF). Small samples (2x2x2 mm) of placental tissues ,were fixed in 1 mL 90% methanol for 2*h* at 4°C according to Bushway et al.[95] with modifications. After washing with PBS, the samples were blocked for 2h at 4^0C with 1% Hammarsten-grade casein in PBS containing 0.02% Thimerosal. After washing with 0.5% Casein in PBS, antibodies to VEGFR2 and PDC-E2 were added at 1:400 dilution and incubated overnight at 4^0C, followed by washing with 0.5% Casein-PBS containing 0.3% Triton-X and incubation with the secondary antibodies at 1:100 dilutions. WMIF slides were

observed with a Leica TCS SP5 AOBS laser scanning confocal microscope through a 40X/1.3NA Plan Apochromat oil immersion objective lens (Leica Microsystems CMS GmbH, Germany). 405 Diode, Argon 488 and He-Ne 647 laser lines were applied to excite the samples and tunable emissions were used to minimize crosstalk between fluorochromes. Images were captured with photomultiplier detectors and prepared with the LAS AF software version 2.7 (Leica Microsystems CMS GmbH, Germany). A 3D projected image was created by Z-stack of images taken at 1.0-0.5-micron intervals to create a movie by Imaris version 7.6 (Bitplane AG, Switzerland) (video).

Statistical analysis. The protein levels of MDMX, PICALM, OT-R and V1aR were analyzed for univariable and multivariable associations by linear regression using the R statistical program (https://www.r-project.org, 4.1.3). Parsimonious multivariable models were selected using Akaike's Information Criteria with a stepwise selection procedure (StepAIC in the MASS package of R) and were run with covariates that were identified as statistically significant in univariable analysis. A p-value of less than 0.05 was considered statistically significant. Violin plots were made by R statistical program, and data Figures and graphs were assembled using Fiji ImageJ, GraphPad Prism 9.4.0, Adobe Illustrator and Windows Office365 software. To test the robustness of results to the specific datapoints included in the analysis, bootstrapped resampling (with replacement) was used to generate 1000 replicate datasets, upon which regression analyses were redone. Results of bootstrapped resampled analyses were summarized and compared to the full dataset to characterize consistency of point estimates and patterns of statistical significance. Pearson correlation coefficients were used to characterize correlation of protein measurements with each other.

Acknowledgements

This study was supported by the Department of Obstetrics and Gynecology at the University of South Florida and research funds from Tampa General Hospital (AEA) and the Teasley Foundation (TJR). The WMIF images were obtained by the Analytic Microscopy Core Facility at the H. Lee Moffitt Cancer Center & Research Institute, an NCI designated Comprehensive Cancer Center (P30-CA076292). We thank Umit A. Kayisli for

advice on IHC, and Santo V. Nicosia and Greg Arsenis for reading the manuscript and comments.

Author contributions

JCMT conceived the study, performed most wet chemistry experiments, and wrote the first draft of the manuscript in consultation with VNU and RRM. SJH, RGS, and EPN recruited patients, collected, and interpreted clinical data in consultation with TSS, TJR, AEA, and MLA. DC performed proteomic analyses. MO assisted in the analysis of western blot data and confocal and WMIF experiments. SA and NS performed IHC experiments. AG performed and interpreted IGEM. PS and JC synthesized OT-R and V1aR peptides. DATC performed analyses and statistical data presentation. All authors critically read and approved the manuscript.

Competing interests

DATC declares a grant from Merck for research unrelated to this manuscript. The remaining authors declare no competing interests.

Data availability

The video of the chorionic villi is deposited at https://nam04.safelinks.protection.outlook.com/?url=https%3A%2F%2Fzenodo.org%2Frecord%2F8160169%3Ftoken%3DeyJhbGciOiJIUzUxMiIsImV4cCI6MTY5MjMwOTU5OSwiaWF0IjoxNjg5Njk3NDQzfQ.eyJkYXRhIjp7InJlY2lkIjo4MTYwMTY5fSwiaWQiOjM1ODEzLCJybmQiOiJjMTlkOTM2NCJ9.2OSYKMRxBpqO7afBKem_S8HdQJgmbtnahLFTgJ_5hoiK3wxcbB2fvuyqEPJ0PeTtF_r9f9Zuocr6LcfXPs2-gw&data=05%7C01%7Ctsibris%40usf.edu%7C02564875fb61480dab4f08db87ae6fdb%7C741bf7dee2e546df8d6782607df9deaa%7C0%7C0%7C638252955485880125%7CUnknown%7CTWFpbGZsb3d8eyJWIjoiMC4wLjAwMDAiLCJQIjoiV2luMzIiLCJBTiI6Ik1haWwiLCJXVCI6Mn0%3D%7C3000%7C%7C%7C&sdata=iukZjlFOvoIiQAdfd566alnMH33jLMz3TV%2BDqPv5Trk%3D&reserved=0.

All MS raw files and corresponding results files will be deposited to the ProteomeXchange Consortium via the PRIDE partner repository.

REFERENCES

1 Burton, G. J. & Fowden, A. L. The placenta: a multifaceted, transient organ. *Philos Trans R Soc Lond B Biol Sci* **370**, 20140066 (2015). https://doi.org:10.1098/rstb.2014.0066

2 Burton, G. J., Redman, C. W., Roberts, J. M. & Moffett, A. Pre-eclampsia: pathophysiology and clinical implications. *BMJ* **366**, l2381 (2019). https://doi.org:10.1136/bmj.l2381

3 Aplin, J. D., Myers, J. E., Timms, K. & Westwood, M. Tracking placental development in health and disease. *Nat Rev Endocrinol* **16**, 479-494 (2020). https://doi.org:10.1038/s41574-020-0372-6

4 Shibuya, M. VEGFR and type-V RTK activation and signaling. *Cold Spring Harbor perspectives in biology* **5**, a009092 (2013). https://doi.org:10.1101/cshperspect.a009092

5 Peach, C. J. *et al.* Molecular Pharmacology of VEGF-A Isoforms: Binding and Signalling at VEGFR2. *Int J Mol Sci* **19** (2018). https://doi.org:10.3390/ijms19041264

6 Simons, M., Gordon, E. & Claesson-Welsh, L. Mechanisms and regulation of endothelial VEGF receptor signalling. *Nature reviews. Molecular cell biology* **17**, 611-625 (2016). https://doi.org:10.1038/nrm.2016.87

7 Qu, H. & Khalil, R. A. Vascular mechanisms and molecular targets in hypertensive pregnancy and preeclampsia. *Am J Physiol Heart Circ Physiol* **319**, H661-H681 (2020). https://doi.org:10.1152/ajpheart.00202.2020

8 Roberts, J. M. *et al.* Subtypes of Preeclampsia: Recognition and Determining Clinical Usefulness. *Hypertension* **77**, 1430-1441 (2021). https://doi.org:10.1161/HYPERTENSIONAHA.120.14781

9 Mincheva-Nilsson, L. Immunosuppressive Protein Signatures Carried by Syncytiotrophoblast-Derived Exosomes and Their Role in Human Pregnancy. *Front Immunol* **12**, 717884 (2021). https://doi.org:10.3389/fimmu.2021.717884

10 Ormazabal, V., Nair, S., Carrion, F., McIntyre, H. D. & Salomon, C. The link between gestational diabetes and cardiovascular diseases: potential role of extracellular vesicles. *Cardiovasc Diabetol* **21**, 174 (2022). https://doi.org:10.1186/s12933-022-01597-3

11 Morelli, A. E. & Sadovsky, Y. Extracellular vesicles and immune response during pregnancy: A balancing act. *Immunol Rev* (2022). https://doi.org:10.1111/imr.13074

12 Kugeratski, F. G., Santi, A. & Zanivan, S. Extracellular vesicles as central regulators of blood vessel function in cancer. *Science signaling* **15**, eaaz4742 (2022). https://doi.org:10.1126/scisignal.aaz4742

13 Uhlen, M. *et al.* Proteomics. Tissue-based map of the human proteome. *Science* **347**, 1260419 (2015). https://doi.org:10.1126/science.1260419

14 Wang, D. *et al.* A deep proteome and transcriptome abundance atlas of 29 healthy human tissues. *Mol Syst Biol* **15**, e8503 (2019). https://doi.org:10.15252/msb.20188503

15 Di Meo, A. *et al.* Proteomic Profiling of the Human Tissue and Biological Fluid Proteome. *J Proteome Res* **20**, 444-452 (2021). https://doi.org:10.1021/acs.jproteome.0c00502

16 Manna, S. *et al.* A proteomic profile of the healthy human placenta. *Clin Proteomics* **20**, 1 (2023). https://doi.org:10.1186/s12014-022-09388-4

17 Klein, A. M., de Queiroz, R. M., Venkatesh, D. & Prives, C. The roles and regulation of MDM2 and MDMX: it is not just about p53. *Genes Dev* (2021). https://doi.org:10.1101/gad.347872.120

18 Sharp, A. N. *et al.* Preeclampsia is associated with alterations in the p53-pathway in villous trophoblast. *PLoS One* **9**, e87621 (2014). https://doi.org:10.1371/journal.pone.0087621

19 Tebar, F., Bohlander, S. K. & Sorkin, A. Clathrin assembly lymphoid myeloid leukemia (CALM) protein: localization in endocytic-coated pits, interactions with clathrin, and the impact of

overexpression on clathrin-mediated traffic. *Mol Biol Cell* **10**, 2687-2702 (1999). https://doi.org:10.1091/mbc.10.8.2687

20 Ando, K. *et al.* PICALM and Alzheimer's Disease: An Update and Perspectives. *Cells* **11** (2022). https://doi.org:10.3390/cells11243994

21 Buhimschi, I. A. *et al.* Protein misfolding, congophilia, oligomerization, and defective amyloid processing in preeclampsia. *Science translational medicine* **6**, 245ra292 (2014). https://doi.org:10.1126/scitranslmed.3008808

22 Meyerowitz, J. G. *et al.* The oxytocin signaling complex reveals a molecular switch for cation dependence. *Nat Struct Mol Biol* (2022). https://doi.org:10.1038/s41594-022-00728-4

23 Jurek, B. & Neumann, I. D. The Oxytocin Receptor: From Intracellular Signaling to Behavior. *Physiol Rev* **98**, 1805-1908 (2018). https://doi.org:10.1152/physrev.00031.2017

24 Dekan, Z. *et al.* Nature-inspired dimerization as a strategy to modulate neuropeptide pharmacology exemplified with vasopressin and oxytocin. *Chem Sci* **12**, 4057-4062 (2021). https://doi.org:10.1039/d0sc05501h

25 Liu, X., Luo, D., Zhang, J. & Du, L. Distribution and relative expression of vasoactive receptors on arteries. *Sci Rep* **10**, 15383 (2020). https://doi.org:10.1038/s41598-020-72352-5

26 Zeng, J. *et al.* Target-induced clustering activates Trim-Away of pathogens and proteins. *Nat Struct Mol Biol* **28**, 278-289 (2021). https://doi.org:10.1038/s41594-021-00560-2

27 Domingues, I., Rino, J., Demmers, J. A., de Lanerolle, P. & Santos, S. C. VEGFR2 translocates to the nucleus to regulate its own transcription. *PLoS One* **6**, e25668 (2011). https://doi.org:10.1371/journal.pone.0025668

28 Collier, A. Y., Smith, L. A. & Karumanchi, S. A. Review of the immune mechanisms of preeclampsia and the potential of immune modulating therapy. *Hum Immunol* **82**, 362-370 (2021). https://doi.org:10.1016/j.humimm.2021.01.004

29 Streicher, K. *et al.* The plasma cell signature in autoimmune disease. *Arthritis & rheumatology (Hoboken, N.J.)* **66**, 173-184 (2014). https://doi.org:10.1002/art.38194

30 Gafencu, A., Heltianu, C., Burlacu, A., Hunziker, W. & Simionescu, M. Investigation of IgG receptors expressed on the surface of human placental endothelial cells. *Placenta* **24**, 664-676 (2003). https://doi.org:10.1016/s0143-4004(03)00041-9

31 Hu, L. *et al.* Identification of a novel heterogeneous nuclear ribonucleoprotein A2B1 (hnRNPA2B1) ligand that disrupts HnRNPA2B1/nucleic acid interactions to inhibit the MDMX-p53 axis in gastric cancer. *Pharmacol Res* **189**, 106696 (2023). https://doi.org:10.1016/j.phrs.2023.106696

32 Liu, C., Kellems, R. E. & Xia, Y. Inflammation, Autoimmunity, and Hypertension: The Essential Role of Tissue Transglutaminase. *Am J Hypertens* **30**, 756-764 (2017). https://doi.org:10.1093/ajh/hpx027

33 Reyes, L. & Golos, T. G. Hofbauer Cells: Their Role in Healthy and Complicated Pregnancy. *Front Immunol* **9**, 2628 (2018). https://doi.org:10.3389/fimmu.2018.02628

34 Zulu, M. Z., Martinez, F. O., Gordon, S. & Gray, C. M. The Elusive Role of Placental Macrophages: The Hofbauer Cell. *J Innate Immun* **11**, 447-456 (2019). https://doi.org:10.1159/000497416

35 Semmes, E. C. & Coyne, C. B. Innate immune defenses at the maternal-fetal interface. *Curr Opin Immunol* **74**, 60-67 (2021). https://doi.org:10.1016/j.coi.2021.10.007

36 Fakonti, G., Pantazi, P., Bokun, V. & Holder, B. Placental Macrophage (Hofbauer Cell) Responses to Infection During Pregnancy: A Systematic Scoping Review. *Front Immunol* **12**, 756035 (2021). https://doi.org:10.3389/fimmu.2021.756035

37 Ning, J., Zhang, M., Cui, D. & Yang, H. The pathologic changes of human placental macrophages in women with hyperglycemia in pregnancy. *Placenta* **130**, 60-66 (2022). https://doi.org:10.1016/j.placenta.2022.11.004

38 Girsch, J. H. *et al.* Host-Viral Interactions at the Maternal-Fetal Interface. What We Know and What We Need to Know. *Frontiers (Boulder)* **2** (2022). https://doi.org:10.3389/fviro.2022.833106

39 Lasch, M. *et al.* Isolation of Decidual Macrophages and Hofbauer Cells from Term Placenta-Comparison of the Expression of CD163 and CD80. *Int J Mol Sci* **23** (2022). https://doi.org:10.3390/ijms23116113

40 Mercnik, M. H., Schliefsteiner, C., Fluhr, H. & Wadsack, C. Placental macrophages present distinct polarization pattern and effector functions depending on clinical onset of preeclampsia. *Front Immunol* **13**, 1095879 (2022). https://doi.org:10.3389/fimmu.2022.1095879

41 Mittelberger, J. *et al.* The programmed cell death protein 1 (PD1) and the programmed cell death ligand 1 (PD-L1) are significantly downregulated on macrophages and Hofbauer cells in the placenta of preeclampsia patients. *Journal of reproductive immunology* **157**, 103949 (2023). https://doi.org:10.1016/j.jri.2023.103949

42 Zinn, V. Z., Khatri, A., Mednieks, M. I. & Hand, A. R. Localization of cystic fibrosis transmembrane conductance regulator signaling complexes in human salivary gland striated duct cells. *Eur J Oral Sci* **123**, 140-148 (2015). https://doi.org:10.1111/eos.12184

43 Maron, B. A. *et al.* Individualized interactomes for network-based precision medicine in hypertrophic cardiomyopathy with implications for other clinical pathophenotypes. *Nat Commun* **12**, 873 (2021). https://doi.org:10.1038/s41467-021-21146-y

44 Burton, G. J. & Jauniaux, E. The human placenta: new perspectives on its formation and function during early pregnancy. *Proc Biol Sci* **290**, 20230191 (2023). https://doi.org:10.1098/rspb.2023.0191

45 Ozen, M. *et al.* Omics approaches: interactions at the maternal-fetal interface and origins of child health and disease. *Pediatr Res*, 1-10 (2022). https://doi.org:10.1038/s41390-022-02335-x

46 Wang, H. *et al.* The ion channel TRPM7 regulates zinc depletion-induced MDMX degradation. *J Biol Chem*, 101292 (2021). https://doi.org:10.1016/j.jbc.2021.101292

47 Nadezhdin, K. D. *et al.* Structural mechanisms of TRPM7 activation and inhibition. *Nat Commun* **14**, 2639 (2023). https://doi.org:10.1038/s41467-023-38362-3

48 Abiria, S. A. *et al.* TRPM7 senses oxidative stress to release Zn(2+) from unique intracellular vesicles. *Proc Natl Acad Sci U S A* **114**, E6079-E6088 (2017). https://doi.org:10.1073/pnas.1707380114

49 Yang, H., Kim, T. H., Lee, G. S., Hong, E. J. & Jeung, E. B. Comparing the expression patterns of placental magnesium/phosphorus-transporting channels between healthy and preeclamptic pregnancies. *Mol Reprod Dev* **81**, 851-860 (2014). https://doi.org:10.1002/mrd.22353

50 Neiman, M. *et al.* Individual and stable autoantibody repertoires in healthy individuals. *Autoimmunity* **52**, 1-11 (2019). https://doi.org:10.1080/08916934.2019.1581774

51 Cheng, J. *et al.* TRIM21 and PHLDA3 negatively regulate the crosstalk between the PI3K/AKT pathway and PPP metabolism. *Nat Commun* **11**, 1880 (2020). https://doi.org:10.1038/s41467-020-15819-3

52 Park, J. S. *et al.* Mechanical regulation of glycolysis via cytoskeleton architecture. *Nature* **578**, 621-626 (2020). https://doi.org:10.1038/s41586-020-1998-1

53 Silva, J. A. F., Qi, X., Grant, M. B. & Boulton, M. E. Spatial and temporal VEGF receptor intracellular trafficking in microvascular and macrovascular endothelial cells. *Sci Rep* **11**, 17400 (2021). https://doi.org:10.1038/s41598-021-96964-7

54 Sutendra, G. *et al.* A nuclear pyruvate dehydrogenase complex is important for the generation of acetyl-CoA and histone acetylation. *Cell* **158**, 84-97 (2014). https://doi.org:10.1016/j.cell.2014.04.046

55 Kofler, N. *et al.* The Rab-effector protein RABEP2 regulates endosomal trafficking to mediate vascular endothelial growth factor receptor-2 (VEGFR2)-dependent signaling. *J Biol Chem* **293**, 4805-4817 (2018). https://doi.org:10.1074/jbc.M117.812172

56 Zhou, H. J. *et al.* SUMOylation of VEGFR2 regulates its intracellular trafficking and pathological angiogenesis. *Nat Commun* **9**, 3303 (2018). https://doi.org:10.1038/s41467-018-05812-2

57 Buvinic, S. *et al.* P2Y1 and P2Y2 receptor distribution varies along the human placental vascular tree: role of nucleotides in vascular tone regulation. *The Journal of physiology* **573**, 427-443 (2006). https://doi.org:10.1113/jphysiol.2006.105882

58 Guan, J. *et al.* Therapeutic Ligands Antagonize Estrogen Receptor Function by Impairing Its Mobility. *Cell* **178**, 949-963 e918 (2019). https://doi.org:10.1016/j.cell.2019.06.026

59 Mayer, B. *et al.* Vasopressin stimulates the proliferation and differentiation of red blood cell precursors and improves recovery from anemia. *Science translational medicine* **9** (2017). https://doi.org:10.1126/scitranslmed.aao1632

60 Lam, L. K. M. *et al.* DNA binding to TLR9 expressed by red blood cells promotes innate immune activation and anemia. *Science translational medicine* **13**, eabj1008 (2021). https://doi.org:10.1126/scitranslmed.abj1008

61 Calderon-Garciduenas, L. *et al.* Environmental Nanoparticles Reach Human Fetal Brains. *Biomedicines* **10** (2022). https://doi.org:10.3390/biomedicines10020410

62 Kerby, A. *et al.* Placental Morphology and Cellular Characteristics in Stillbirths in Women With Diabetes and Unexplained Stillbirths. *Arch Pathol Lab Med* **145**, 82-89 (2021). https://doi.org:10.5858/arpa.2019-0524-OA

63 Li, Y. *et al.* MicroRNA profiling of diabetic atherosclerosis in a rat model. *Eur J Med Res* **23**, 55 (2018). https://doi.org:10.1186/s40001-018-0354-5

64 Mancini, F. *et al.* MDM4 actively restrains cytoplasmic mTORC1 by sensing nutrient availability. *Mol Cancer* **16**, 55 (2017). https://doi.org:10.1186/s12943-017-0626-7

65 Amin, M., Wu, R. & Gragnoli, C. Novel Risk Variants in the Oxytocin Receptor Gene (OXTR) Possibly Linked to and Associated with Familial Type 2 Diabetes. *Int J Mol Sci* **24** (2023). https://doi.org:10.3390/ijms24076282

66 Huang, Y. *et al.* Improving immune-vascular crosstalk for cancer immunotherapy. *Nat Rev Immunol* **18**, 195-203 (2018). https://doi.org:10.1038/nri.2017.145

67 Kao, K. C., Vilbois, S., Tsai, C. H. & Ho, P. C. Metabolic communication in the tumour-immune microenvironment. *Nat Cell Biol* **24**, 1574-1583 (2022). https://doi.org:10.1038/s41556-022-01002-x

68 Zheng, W. *et al.* Manipulation of the crosstalk between tumor angiogenesis and immunosuppression in the tumor microenvironment: Insight into the combination therapy of anti-angiogenesis and immune checkpoint blockade. *Front Immunol* **13**, 1035323 (2022). https://doi.org:10.3389/fimmu.2022.1035323

69 Spiliopoulos, M. *et al.* Characterizing placental stiffness using ultrasound shear-wave elastography in healthy and preeclamptic pregnancies. *Arch Gynecol Obstet* **302**, 1103-1112 (2020). https://doi.org:10.1007/s00404-020-05697-x

70 Mancini, F., Giorgini, L., Teveroni, E., Pontecorvi, A. & Moretti, F. Role of Sex in the Therapeutic Targeting of p53 Circuitry. *Front Oncol* **11**, 698946 (2021). https://doi.org:10.3389/fonc.2021.698946

71 Swetzig, W. M., Wang, J. & Das, G. M. Estrogen receptor alpha (ERalpha/ESR1) mediates the p53-independent overexpression of MDM4/MDMX and MDM2 in human breast cancer. *Oncotarget* **7**, 16049-16069 (2016). https://doi.org:10.18632/oncotarget.7533

72 Berkane, N. *et al.* From Pregnancy to Preeclampsia: A Key Role for Estrogens. *Endocr Rev* **38**, 123-144 (2017). https://doi.org:10.1210/er.2016-1065

73 Jobe, S. O., Tyler, C. T. & Magness, R. R. Aberrant synthesis, metabolism, and plasma accumulation of circulating estrogens and estrogen metabolites in preeclampsia implications for vascular

dysfunction. *Hypertension* **61**, 480-487 (2013). https://doi.org:10.1161/HYPERTENSIONAHA.111.201624

74 Zhu, D., Su, Y., Fu, B. & Xu, H. Magnesium Reduces Blood-Brain Barrier Permeability and Regulates Amyloid-beta Transcytosis. *Mol Neurobiol* **55**, 7118-7131 (2018). https://doi.org:10.1007/s12035-018-0896-0

75 Hentschke, M. R. *et al.* Is the atherosclerotic phenotype of preeclamptic placentas due to altered lipoprotein concentrations and placental lipoprotein receptors? Role of a small-for-gestational-age phenotype. *J Lipid Res* **54**, 2658-2664 (2013). https://doi.org:10.1194/jlr.M036699

76 Zhang, S., Cao, F., Li, W. & Abumaria, N. TRPM7 kinase activity induces amyloid-beta degradation to reverse synaptic and cognitive deficits in mouse models of Alzheimer's disease. *Science signaling* **16**, eade6325 (2023). https://doi.org:10.1126/scisignal.ade6325

77 Ryan, C. P. *et al.* Reproduction predicts shorter telomeres and epigenetic age acceleration among young adult women. *Sci Rep* **8**, 11100 (2018). https://doi.org:10.1038/s41598-018-29486-4

78 Richmond, R. C., Suderman, M., Langdon, R., Relton, C. L. & Davey Smith, G. DNA methylation as a marker for prenatal smoke exposure in adults. *Int J Epidemiol* **47**, 1120-1130 (2018). https://doi.org:10.1093/ije/dyy091

79 Ryan, C. P. *et al.* Immune cell type and DNA methylation vary with reproductive status in women: possible pathways for costs of reproduction. *Evol Med Public Health* **10**, 47-58 (2022). https://doi.org:10.1093/emph/eoac003

80 Ghanim, H. *et al.* Reduction in inflammation and the expression of amyloid precursor protein and other proteins related to Alzheimer's disease following gastric bypass surgery. *J Clin Endocrinol Metab* **97**, E1197-1201 (2012). https://doi.org:10.1210/jc.2011-3284

81 Hinney, A. *et al.* Genetic variation at the CELF1 (CUGBP, elav-like family member 1 gene) locus is genome-wide associated with Alzheimer's disease and obesity. *Am J Med Genet B Neuropsychiatr Genet* **165B**, 283-293 (2014). https://doi.org:10.1002/ajmg.b.32234

82 Behura, S. K. *et al.* The brain-placental axis: Therapeutic and pharmacological relevancy to pregnancy. *Pharmacol Res* **149**, 104468 (2019). https://doi.org:10.1016/j.phrs.2019.104468

83 Mairesse, J. *et al.* Oxytocin receptor agonist reduces perinatal brain damage by targeting microglia. *Glia* **67**, 345-359 (2019). https://doi.org:10.1002/glia.23546

84 Shook, L. L., Sullivan, E. L., Lo, J. O., Perlis, R. H. & Edlow, A. G. COVID-19 in pregnancy: implications for fetal brain development. *Trends Mol Med* **28**, 319-330 (2022). https://doi.org:10.1016/j.molmed.2022.02.004

85 Lazarov, T., Juarez-Carreno, S., Cox, N. & Geissmann, F. Physiology and diseases of tissue-resident macrophages. *Nature* **618**, 698-707 (2023). https://doi.org:10.1038/s41586-023-06002-x

86 Erickson, E. N., Myatt, L., Danoff, J. S., Krol, K. M. & Connelly, J. J. Oxytocin receptor DNA methylation is associated with exogenous oxytocin needs during parturition and postpartum hemorrhage. *Commun Med (Lond)* **3**, 11 (2023). https://doi.org:10.1038/s43856-023-00244-6

87 Liang, Y., Duan, L., Lu, J. & Xia, J. Engineering exosomes for targeted drug delivery. *Theranostics* **11**, 3183-3195 (2021). https://doi.org:10.7150/thno.52570

88 Stelzer, I. A. *et al.* Integrated trajectories of the maternal metabolome, proteome, and immunome predict labor onset. *Science translational medicine* **13** (2021). https://doi.org:10.1126/scitranslmed.abd9898

89 Aghaeepour, N. *et al.* An immune clock of human pregnancy. *Sci Immunol* **2** (2017). https://doi.org:10.1126/sciimmunol.aan2946

90 Gomez-Lopez, N. *et al.* Macrophages exert homeostatic actions in pregnancy to protect against preterm birth and fetal inflammatory injury. *JCI Insight* **6** (2021). https://doi.org:10.1172/jci.insight.146089

91 Rackaityte, E. & Halkias, J. Mechanisms of Fetal T Cell Tolerance and Immune Regulation. *Front Immunol* **11**, 588 (2020). https://doi.org:10.3389/fimmu.2020.00588

92 Miller, D. *et al.* Single-Cell Immunobiology of the Maternal-Fetal Interface. *J Immunol* **209**, 1450-1464 (2022). https://doi.org:10.4049/jimmunol.2200433

93 Braitbard, O., Glickstein, H., Bishara-Shieban, J., Pace, U. & Stein, W. D. Competition between bound and free peptides in an ELISA-based procedure that assays peptides derived from protein digests. *Proteome Sci* **4**, 12 (2006). https://doi.org:10.1186/1477-5956-4-12

94 Shevchenko, A., Tomas, H., Havlis, J., Olsen, J. V. & Mann, M. In-gel digestion for mass spectrometric characterization of proteins and proteomes. *Nat Protoc* **1**, 2856-2860 (2006). https://doi.org:10.1038/nprot.2006.468

95 Bushway, M. E. *et al.* Morphological and phenotypic analyses of the human placenta using whole mount immunofluorescence. *Biol Reprod* **90**, 110 (2014). https://doi.org:10.1095/biolreprod.113.115915

Table 1.

Clinical characteristics of 47 patients in the study group.

A. Patient samples were labelled with a code consisting of a letter and 1, 2, 5, 6, 7 for non-preeclamptic, 3, 4 for preeclamptic patients or a Ho-number**. B**. Patients Ho-71, Ho-72 and Ho-73 provided placental samples for immunogold electron microscopy.

A

Patient	Age Range	Gravida	Gestational Age (weeks)	BMI in L&D	Race	cHTN	Preeclampsia	DM	Delivery Mode	Pitocin pre-delivery	Sex F=1	Neonatal weight (g)
H1	21-25	1	38.0	30.0	6	0	0	0	1	1	1	2,940
H2	21-25	2	37.0	24.0	8	0	0	0	1	NA	2	2,590
H3	31-35	2	37.0	32.0	8	0	1	0	1	NA	1	3,040
I-1	21-25	3	38.0	34.0	2	0	0	0	3	1	2	2,631
I-2	21-25	1	42.0	30.0	1	0	0	0	1	1	2	3,759
I-3	26-30	8	35.0	34.0	2	0	1	2	2	0	2	3,195
I-4	18-20	1	36.6	41.0	8	0	1	0	3	0	1	3,335
J-1	26-30	2	39.0	25.0	8	0	0	0	3	0	2	3,300
J-2	36-40	2	37.4	22.0	1	0	0	0	1	1	1	3,460
J-3	26-30	3	38.5	28.0	1	0	1	3	3	*1*	2	3,630
L1	21-25	1	39.0	24.0	3	0	0	0	3	0	1	3,147
L2	18-20	1	39.0	29.0	6	0	0	0	1	1	1	2,920
L3	21-25	3	35.0	30.0	2	0	1	0	2	0	2	2,235
L4	26-30	3	40.0	29.0	8	0	1	0	1	NA	1	3,010
M1	21-25	3	40.1	55.0	2	0	0	0	2	0	1	3,795
M3	18-20	2	37.0	31.3	8	0	1	0	2	0	1	3,490
M4	26-30	1	40.1	39.8	8	0	1	0	1	1	2	3,380
N1	31-35	4	39.1	30.0	8	0	0	2	2	0	2	3,800
N2	31-35	2	39.3	32.8	8	0	0	0	2	0	1	3,180
N3	31-35	2	39.0	35.5	8	0	1	0	2	0	2	3,390
N4	18-20	2	36.4	29.5	1	0	1	0	3	1	2	3,510
O1	21-25	2	39.3	26.2	1	0	0	0	4	1	1	2,960
O2	21-25	1	38.4	34.8	1	0	0	0	1	1	1	2,940
O3	26-30	1	37.1	29.5	1	0	1	0	1	1	1	2,800
O4	21-25	3	40.3	52.5	1	0	1	0	3	*1*	2	3,575
O5	36-40	4	39.1	50.4	8	0	0	3	2	0	2	4,295
O7	32-35	12	39.3	35.2	2	0	0	0	2	0	1	3,780
Q1	21-25	2	37.0	47.8	1	0	0	3	2	0	1	3,885
Q2	31-35	4	39.1	35.8	2	0	0	3	2	0	1	3,390
Q3	26-30	2	37.2	66.7	1	1	1	0	3	*1*	2	3,375
Q4	31-35	4	39.1	77.2	2	0	1	3	2	0	2	3,835
R3	21-25	1	37.6	49.5	1	1	1	0	1	1	2	2,560
R4	26-30	4	39.1	29.8	2	0	1	2	3	*1*	1	3,960
R5	21-25	6	39.0	30.9	2	0	0	0	2	0	1	3,205
S1	26-30	2	37.4	46.2	8	0	0	2	2	0	2	4,675
S2	26-30	3	37.5	42.2	1	0	0	2	2	0	1	4,600
T1	26-30	5	38.0	41.9	1	0	0	2	2	0	1	3,090
T2	26-30	1	39.1	53.3	1	0	0	2	2	0	2	3,960
U1	31-35	3	37.1	62.6	2	1	0	2	2	0	2	4,440
U2	26-30	3	37.1	52.7	1	1	0	2	2	0	2	5,020
V1	36-40	5	37.1	35.5	2	1	0	0	2	0	2	2,720
V2	36-40	2	38.4	26.1	1	0	0	0	2	0	2	4,150
W1	18-20	1	39.2	30.5	1	0	0	0	2	0	2	3,470
W2	26-30	8	37.0	51.7	2	1	0	0	2	0	1	3,000

B

Ho-71	31-35	6	37.1	N/A	2	0	0	0	2	0	1	3,195
Ho-72	26-30	1	39.3	29.4	2		0	3	2	NA	1	3,400
Ho-73	26-30	1	37.0	29.1	8	0	1	0	1	1	2	2,780

Abbreviations: *Race*: White 1, Black 2, Asian 3, Hispanic 8, unknown 6. *Chronic hypertension*: cHTN 1. *Preeclampsia* 1. *Diabetes (DM)*: Type-1 1, Type-2 2, Gestational 3. *Delivery mode*: Spontaneous vaginal delivery (SVD) 1, Cesarean delivery (CD) prior to the onset of labor 2, CD after the onset of labor 3, Vaginal birth after CD (VBAC) 4. Pitocin pre-delivery 1. *Fetal sex*: Female 1, Male 2. *L&D*: Labor and delivery suite. *NA*, not available. The number of patients in each category were as follows: Diabetes: 30 no, Type-2 9, Gestational 5. Preeclampsia: 28 no, 16 yes. Delivery Mode: SVD 12; CD prior to the onset of labor 23; CD after the onset of labor 9; VBAC 1.

Table 2

Proteins identified in VEGFR2 immunoprecipitations.

Placental extracts O4, O5, U1, and O7 were immunoprecipitated in one experiment.

Majority Protein ID	Protein	Gene	Total Intensity	Intensity VEGFR2 O4	Intensity VEGFR2 O5	Intensity VEGFR2 U1	Intensity VEGFR2 O7	Peptides
P01857	Ig gamma-1 chain C region	IGHG1	24,993,000,000	8,554,400,000	4,872,000,000	4,017,600,000	7,549,400,000	16
O15151-5	Protein Mdm4	MDM4	14,682,000,000	14,638,000,000	0	21,714,000	22,289,000	14
P01834	Ig kappa chain C region	IGKC	11,450,000,000	1,978,700,000	1,363,300,000	2,438,900,000	5,668,800,000	7
A0A0B4J231	Immunoglobulin lambda-like polypeptide 5;Ig lam	IGLL5	10,336,000,000	1,336,300,000	2,654,400,000	2,053,600,000	4,291,800,000	4
P01871	Ig mu chain C region	IGHM	4,544,300,000	2,132,500,000	923,280,000	706,680,000	781,900,000	16
P20073-2	Annexin A7	ANXA7	3,045,300,000	1,631,900,000	402,390,000	522,590,000	488,400,000	19
P01624	Ig kappa chain V-III region POM	IGKV3D-15	2,885,700,000	707,630,000	775,800,000	20,798,000	1,381,500,000	2
A0A286YES1	Ig gamma-3 chain C region	IGHG3	2,266,900,000	1,322,900,000	493,150,000	239,480,000	211,400,000	14
Q9Y6R7	IgGFc-binding protein	FCGBP	1,815,700,000	1,201,900,000	310,570,000	246,590,000	56,630,000	50
J3KT55	Protein-tyrosine-phosphatase;Receptor-type tyro	PTPRM	1,604,700,000	511,350,000	129,960,000	380,380,000	582,970,000	1
P01701	Ig lambda chain V-I region NEW	IGLV1-51	1,311,400,000	193,890,000	242,130,000	234,850,000	640,570,000	3
P50995-2	Annexin A11	ANXA11	984,170,000	401,780,000	125,800,000	283,580,000	173,010,000	18
P01583	Ig kappa chain V-I region AU	IGKV1D-33	948,420,000	223,440,000	220,510,000	138,140,000	366,330,000	2
P01709	Ig lambda chain V-II region MGC;	IGLV2-8	640,270,000	48,724,000	120,690,000	169,210,000	301,660,000	2
P05783	Keratin, type I cytoskeletal 18	KRT18	610,030,000	342,270,000	114,070,000	75,571,000	78,111,000	19
P35968	Vascular endothelial growth factor receptor 2	KDR	571,130,000	132,550,000	167,190,000	146,080,000	125,310,000	28
A0A286YEY4	Ig gamma-2 chain C region	IGHG2	460,180,000	213,440,000	63,593,000	99,658,000	83,492,000	13
A0A286YEY1	Ig alpha-1 chain C region	IGHA1	403,780,000	211,760,000	52,913,000	85,992,000	53,116,000	6
Q8WZ42	Titin	TTN	396,070,000	215,440,000	31,243,000	97,005,000	52,381,000	2
A0A075B6K4	Ig lambda chain V-IV region Bau	IGLV3-10	353,630,000	0	105,060,000	0	248,570,000	1
P01602	Ig kappa chain V-I region HK102	IGKV1-5	352,740,000	23,518,000	98,394,000	83,336,000	147,490,000	1
P07355	Annexin A2;Annexin;Putative annexin A2-like pro	ANXA2	310,810,000	50,471,000	50,738,000	48,427,000	161,170,000	9
P0DP08	Ig heavy chain V-II region NEWM;Ig heavy chain	IGHV4-61	304,360,000	139,200,000	44,252,000	64,988,000	55,917,000	2
A0A4W8ZXM2	Immunoglobulin heavy variable 3-72	IGHV3-72	293,310,000	149,140,000	29,272,000	50,152,000	64,749,000	3
A0A140T8W4	Ras/Rap GTPase-activating protein SynGAP	SYNGAP1	288,030,000	44,004,000	63,931,000	66,499,000	113,600,000	1
P01619	Ig kappa chain V-III region B6	IGKV3D-20	270,720,000	61,855,000	116,270,000	75,359,000	17,241,000	3
A0A0C4DH42	Ig heavy chain V-III region BUT;Ig heavy chain V	IGHV3-66	262,750,000	165,010,000	39,894,000	44,120,000	13,734,000	3
A0A087WW87	Ig kappa chain V-II region FR;Ig kappa chain V-II	IGKV2-40	253,710,000	36,751,000	64,720,000	43,474,000	108,760,000	3
P59666	Neutrophil defensin 3;HP 3-56;Neutrophil defens	DEFA3	216,520,000	69,150,000	64,470,000	3,576,200	79,326,000	3
P69905	Hemoglobin subunit alpha	HBA1	215,170,000	0	0	7,679,400	207,490,000	3
P68871	Hemoglobin subunit beta;LVV-hemorphin-7;Spin	HBB	212,010,000	31,855,000	0	8,761,200	171,400,000	5
A0A2R8Y804	Catenin beta-1	CTNNB1	209,290,000	166,480,000	20,293,000	22,516,000	0	1
H0Y2X5	Aldehyde dehydrogenase family 1 member A3	ALDH1A3	208,040,000	81,161,000	28,288,000	92,767,000	5,824,900	1
P0DOY3	Ig lambda-6 chain C region;Ig lambda-7 chain C	IGLC6	206,310,000	71,942,000	14,393,000	49,459,000	70,513,000	3
P17931	Galectin-3;Galectin	LGALS3	177,750,000	8,812,900	12,846,000	37,357,000	118,730,000	4
P60709	Actin, cytoplasmic 1;Actin, cytoplasmic 1, N-term	ACTB	169,720,000	77,252,000	11,135,000	41,447,000	39,882,000	7
P0DP03	Ig heavy chain V-III region CAM;Ig heavy chain V	IGHV3-23	161,210,000	84,420,000	37,310,000	16,539,000	22,945,000	3
P08670	Vimentin	VIM	138,160,000	72,126,000	18,191,000	31,138,000	16,707,000	14
A0A0A0MRZ8	Ig kappa chain V-III region VG	IGKV3D-11	111,170,000	34,909,000	76,260,000	0	0	1
A0A075B6K5	Ig lambda chain V-III region LOI	IGLV3-9	96,087,000	25,060,000	23,281,000	14,993,000	32,753,000	1
A0A286YFJ8	Ig gamma-4 chain C region	IGHG4	87,485,000	47,260,000	30,192,000	1,565,900	8,467,600	9
A0A075B6Z5	T cell receptor alpha joining 4	TRAJ4	81,903,000	16,074,000	21,003,000	0	44,826,000	1
Q96Q89-4	Kinesin-like protein KIF20B	KIF20B	80,885,000	35,045,000	8,063,900	37,776,000	0	1
P31942-3	Heterogeneous nuclear ribonucleoprotein H3	HNRNPH3	80,200,000	14,536,000	9,591,700	10,848,000	45,224,000	4
P0DP01	Ig heavy chain V-I region HG3;Ig heavy chain V-I	IGHV1-3	75,366,000	33,904,000	12,319,000	16,686,000	12,457,000	1
C9JA05	Immunoglobulin J chain	JCHAIN	74,956,000	6,239,800	24,681,000	8,971,600	35,063,000	1
A6NJ08	Putative methyl-CpG-binding domain protein 3-lik	MBD3L5	72,585,000	0	0	72,585,000	0	1
O43866	CD5 antigen-like	CD5L	67,251,000	6,765,200	12,049,000	0	48,437,000	3
A0A075B6H9	Immunoglobulin lambda variable 4-69	IGLV4-69	66,271,000	0	23,139,000	15,467,000	27,664,000	1
A0A0C4DH31	Ig heavy chain V-I region V35	IGHV1-18	66,003,000	33,480,000	6,768,000	14,275,000	11,480,000	2
Q8IZ41	Ras and EF-hand domain-containing protein	RASEF	63,614,000	0	0	0	63,614,000	1
Q5JTQ6	Alpha-catulin	CTNNAL1	57,823,000	0	0	0	57,823,000	1
S4R460	Immunoglobulin heavy variable 3/OR16-9	IGHV3OR16-9	55,031,000	38,287,000	3,882,000	8,163,400	4,697,800	3
P31943	Heterogeneous nuclear ribonucleoprotein H;Hete	HNRNPH1	53,003,000	27,450,000	6,928,200	12,581,000	6,044,000	8
P01700	Ig lambda chain V-I region HA	IGLV1-47	52,593,000	4,428,100	9,274,400	10,578,000	28,313,000	2
P69892	Hemoglobin subunit gamma-2;Hemoglobin subur	HBG2	51,210,000	4,832,700	6,432,400	4,039,100	35,906,000	2
Q01469	Fatty acid-binding protein, epidermal	FABP5	49,218,000	9,923,200	8,054,700	6,476,700	24,764,000	1
A0A0C4DH38	Immunoglobulin heavy variable 5-51	IGHV5-51	47,777,000	21,306,000	9,176,600	9,526,200	7,768,200	2
P06312	Ig kappa chain V-IV region	IGKV4-1	45,342,000	3,210,900	8,777,500	9,179,900	24,174,000	2
A0A075B7B8	Immunoglobulin heavy variable 3/OR16-12	IGHV3OR16-12	42,463,000	23,390,000	6,964,700	8,836,000	3,272,300	2
D6RF44	Heterogeneous nuclear ribonucleoprotein D0	HNRNPD	42,167,000	25,423,000	6,531,800	3,981,200	6,231,100	2
P12314	High affinity immunoglobulin gamma Fc receptor	FCGR1A	41,035,000	21,744,000	3,306,900	13,766,000	2,217,200	4
A0A075B6I0	Immunoglobulin lambda variable 8-61	IGLV8-61	36,318,000	0	15,369,000	0	20,949,000	1
P01023	Alpha-2-macroglobulin	A2M	34,428,000	24,712,000	0	5,408,900	4,307,000	9
M0R1R1	Serine/threonine-protein kinase PAK 4	PAK4	33,472,000	0	0	33,472,000	0	1
A0A1C7CYZ1	Mitogen-activated protein kinase 15	MAPK15	33,062,000	6,944,400	14,185,000	7,347,000	4,586,000	1
A0A0C4DGL8	Haptoglobin;Haptoglobin alpha chain;Haptoglobi	HP	32,080,000	0	0	0	32,080,000	2
P05109	Protein S100-A8;Protein S100-A8, N-terminally p	S100A8	29,241,000	14,931,000	0	10,002,000	4,308,000	2
Q03135	Caveolin-1;Caveolin	CAV1	28,128,000	0	0	0	28,128,000	2
P01714	Ig lambda chain V-III region SH	IGLV3-19	26,041,000	4,373,400	0	0	21,668,000	1
P19474	E3 ubiquitin-protein ligase TRIM21	TRIM21	25,255,000	18,886,000	4,813,800	1,555,300	0	4
P62979	Ubiquitin-40S ribosomal protein S27a;Ubiquitin;4	RPS27A	25,055,000	1,656,300	2,801,700	7,174,300	13,423,000	2
P81605	Dermcidin;Survival-promoting peptide;DCD-1	DCD	22,842,000	12,716,000	3,502,900	0	6,623,700	2
P52594-2	Arf-GAP domain and FG repeat-containing protei	AGFG1	22,167,000	16,991,000	2,315,700	2,860,400	0	1
A0A0C4DH35	Probable non-functional immunoglobulin	IGHV3-35	20,964,000	12,648,000	3,344,000	2,850,000	2,122,100	1
Q86VF2-5	Isoform 5 of Immunoglobulin-like	IGFN1	20,453,000	0	0	0	20,453,000	1
K7EJT5	60S ribosomal protein L22	RPL22	18,553,000	4,268,800	0	0	14,284,000	2
A0A0A0MSV6	Complement C1q subcomponent subunit B	C1QB	18,258,000	0	6,523,400	0	11,734,000	2
A0A075B6K0	Ig lambda chain V-IV region Hil;Ig lambda chain \	IGLV3-16	18,172,000	0	4,095,500	3,407,600	10,669,000	1
P06702	Protein S100-A9	S100A9	17,656,000	10,525,000	0	7,131,300	0	2
F8W0I9	Microspherule protein 1	MCRS1	16,973,000	16,973,000	0	0	0	1
P48741	Putative heat shock 70 kDa protein 7;Heat shock	HSPA7	15,835,000	7,272,600	1,230,000	4,196,900	3,135,800	2

P04430	Ig kappa chain V-I region BAN	IGKV1-16	15,155,000	0	1,349,600	3,349,700	10,456,000	1
O75594	Peptidoglycan recognition protein 1	PGLYRP1	14,595,000	2,156,900	2,885,000	0	9,552,700	1
P01599	Ig kappa chain V-I region Gal	IGKV1-17	14,133,000	1,638,200	1,801,900	5,586,300	5,106,400	1
A0A6Q8PHQ9	Prelamin-A/C;Lamin-A/C	LMNA	13,477,000	10,473,000	0	990,760	2,014,100	3
F8WCU1	Coiled-coil domain-containing protein 150	CCDC150	13,165,000	13,165,000	0	0	0	1
P11021	78 kDa glucose-regulated protein	HSPA5	12,097,000	12,097,000	0	0	0	3
P10515	Dihydrolipoyllysine-residue acetyltransferase cor	DLAT	11,577,000	0	0	0	11,577,000	2
A0A0C4DH73	Ig kappa chain V-I region Daudi;Ig kappa chain V	IGKV1-12	11,157,000	4,228,600	3,358,000	0	3,570,100	1
Q02413	Desmoglein-1	DSG1	11,044,000	6,539,700	4,504,100	0	0	4
A0A2R8Y851	40S ribosomal protein S29	RPS29	10,819,000	0	0	0	10,819,000	1
E9PHT9	Annexin;Annexin A5	ANXA5	10,757,000	0	0	0	10,757,000	2
P01766	Ig heavy chain V-III region BRO	IGHV3-13	9,742,100	6,872,500	2,869,600	0	0	3
I3L0Q1	CREB-binding protein;Histone acetyltransferase	CREBBP	9,408,100	9,408,100	0	0	0	2
A0A0A0MT36	Immunoglobulin kappa variable 6D-21	IGKV6D-21	9,327,900	0	0	0	9,327,900	1
P35030-5	Trypsin-3	PRSS3	8,538,700	4,010,200	0	0	4,528,500	1
P02747	Complement C1q subcomponent subunit C	C1QC	8,466,800	0	6,587,500	1,879,200	0	2
A0A0B4J1V0	Immunoglobulin heavy variable 3-15	IGHV3-15	8,461,900	2,460,400	6,001,500	0	0	2
C9JD14	Guanine nucleotide-binding protein G(I)/G(S)/G(T	GNB4	8,022,200	0	0	0	8,022,200	1
A0A0C4DH68	Immunoglobulin kappa variable 2-24	IGKV2-24	7,515,800	7,515,800	0	0	0	2
Q5T3N1	Annexin;Annexin A1	ANXA1	7,426,700	1,331,300	0	803,800	5,291,600	2
A0A0A0MRA5	Heterogeneous nuclear ribonucleoprotein U-like	HNRNPUL1	6,653,000	6,653,000	0	0	0	3
P0DP04	Ig heavy chain V-III region DOB	IGHV3-43D	6,600,800	0	3,028,100	3,572,700	0	3
P02675	Fibrinogen beta chain;Fibrinopeptide B;Fibrinoge	FGB	6,128,300	6,128,300	0	0	0	2
Q9NZT1	Calmodulin-like protein 5	CALML5	6,023,300	1,202,800	0	4,408,400	412,040	3
A0A0C4DH67	Immunoglobulin kappa variable 1-8	IGKV1-8	5,877,100	2,421,000	3,456,100	0	0	1
A0A2R8YD12	Serpin B6	SERPINB6	5,710,400	5,710,400	0	0	0	1
A0A0A0MRQ5	Peroxiredoxin-2;Peroxiredoxin-1	PRDX1	5,706,700	0	0	2,361,100	3,345,600	1
Q5VVL7	Lipoamide acyltransferase component of branche	DBT	5,612,200	3,395,200	0	2,217,000	0	1
P06310	Ig kappa chain V-II region RPMI 6410	IGKV2-30	5,336,000	0	0	2,017,100	3,318,900	2
P50991	T-complex protein 1 subunit delta	CCT4	4,474,800	0	0	0	4,474,800	1
A0A0C4DH36	Probable non-functional immunoglobulin heavy v	IGHV3-38	4,238,600	0	4,238,600	0	0	2
P47929	Galectin-7	LGALS7	4,195,800	0	0	1,755,800	2,440,000	3
B4E1S2	Annexin;Annexin A4	ANXA4	4,022,500	0	0	0	4,022,500	1
E7ETU5	RNA-binding motif, single-stranded-interacting pr	RBMS1	3,858,200	2,150,500	0	1,707,700	0	2
I3L1P8	Mitochondrial 2-oxoglutarate/malate carrier prote	SLC25A11	3,820,000	0	0	0	3,820,000	1
Q71U36-2	Tubulin alpha-1A chain;Tubulin alpha-1B chain;T	TUBA1A	3,782,000	3,782,000	0	0	0	2
D6R9P3	Heterogeneous nuclear ribonucleoprotein A/B	HNRNPAB	3,571,200	3,120,400	0	450,800	0	2
E9PJT1	Phosphatidylinositol-binding clathrin assembly pr	PICALM	3,561,800	3,561,800	0	0	0	1
A0A0B4J1V6	Immunoglobulin heavy variable 3-73	IGHV3-73	3,460,100	0	1,501,600	1,958,600	0	3
P14923	Junction plakoglobin	JUP	3,261,700	2,178,900	0	0	1,082,900	3
Q5T749	Keratinocyte proline-rich protein	KPRP	3,196,400	3,196,400	0	0	0	2
P15924	Desmoplakin	DSP	2,976,300	0	2,479,300	0	497,000	3
E9PKD2	Nuclear pore complex protein Nup214	NUP214	2,854,500	1,488,400	1,366,100	0	0	1
B3KV94	Lysine-specific demethylase 5B	KDM5B	2,598,600	0	2,598,600	0	0	1
P78406	mRNA export factor	RAE1	2,408,100	2,408,100	0	0	0	1
P17661	Desmin	DES	2,140,500	0	0	1,047,300	1,093,200	4
P31994-5	Low affinity immunoglobulin gamma Fc	FCGR2B	2,042,300	0	2,042,300	0	0	1
A0A087WT15	N-acetylglucosaminyldiphosphodolichol	ALG13	1,878,000	0	1,878,000	0	0	1
P31944	Caspase-14;Caspase-14 subunit p17, mature for	CASP14	880,720	0	880,720	0	0	1
A0A3B3ISA6	Complement C4-A;Complement C4 beta chain;C	C4B	664,880	0	0	0	664,880	1

Table 3
Proteins identified in MDMX immunoprecipitations (IP).
Protein extracts O1, O4, O6, Q1, Q4, and R4 were immunoprecipitated in one experiment.

Unique to MDMX IP	Common to all IP	Majority protein ID	Protein	Gene	Total Intensity	Intensity MDMX 01	Intensity MDMX 04	Intensity MDMX 06	Intensity MDMX Q1	Intensity MDMX Q4	Intensity MDMX R4	Peptides
		P01857	Ig gamma-1 chain C region	IGHG1	172,120,000,000	22,238,000,000	2,879,300,000	4,953,400,000	85,828,000,000	8,388,500,000	47,830,000,000	17
	Yes	P68871	Hemoglobin subunit beta	HBB	49,360,000,000	2,016,400,000	36,158,000,000	924,450,000	902,880,000	6,065,100,000	3,293,300,000	14
	Yes	P69905	Hemoglobin subunit alpha	HBA1	46,601,000,000	3,529,000,000	26,425,000,000	1,616,500,000	1,416,300,000	6,485,900,000	7,128,000,000	15
		P20073-2	Annexin A7	ANXA7	25,375,000,000	5,386,800,000	1,897,400,000	6,836,600,000	2,658,100,000	3,368,800,000	5,226,900,000	31
	Yes	Q9Y6R7	IgGFc-binding protein	FCGBP	19,471,000,000	6,976,500,000	5,284,100,000	2,450,000,000	1,183,900,000	470,780,000	3,105,900,000	75
		P81605	Dermcidin;Survival-promoting peptide;DCD-1	DCD	11,575,000,000	2,289,500,000	1,337,700,000	2,158,100,000	2,832,500,000	985,260,000	1,971,800,000	9
Yes		P50995	Annexin A11	ANXA11	11,312,000,000	478,090,000	1,687,700,000	1,675,600,000	1,407,600,000	3,235,200,000	2,827,400,000	22
	Yes	P01871	Ig mu chain C region	IGHM	10,253,000,000	2,115,600,000	3,548,100,000	788,140,000	926,840,000	1,253,200,000	1,620,700,000	18
		P63261	Actin, cytoplasmic 2	ACTG1	7,787,800,000	669,640,000	2,068,500,000	955,900,000	645,430,000	2,563,700,000	884,630,000	16
	Yes	P69892	Hemoglobin subunit gamma-2	HBG2	7,148,400,000	1,386,800,000	780,010,000	795,220,000	661,950,000	460,580,000	3,063,800,000	12
Yes		P55072	Transitional endoplasmic reticulum ATPase	VCP	4,620,000,000	185,550,000	758,330,000	1,565,000,000	411,970,000	553,090,000	1,146,000,000	39
	Yes	P07355	Annexin A2;Annexin;Putative annexin A2-like	ANXA2	4,497,800,000	586,000,000	417,330,000	1,170,600,000	722,980,000	573,440,000	1,027,400,000	24
Yes		P15924	Desmoplakin	DSP	4,032,200,000	470,760,000	397,430,000	777,640,000	503,940,000	1,011,000,000	871,340,000	71
	Yes	Q02413	Desmoglein-1	DSG1	3,842,500,000	671,480,000	532,380,000	484,300,000	578,340,000	684,390,000	891,590,000	23
	Yes	P01834	Ig kappa chain C region	IGKC	3,261,700,000	842,260,000	1,005,100,000	115,500,000	198,480,000	706,400,000	393,970,000	8
		P08670	Vimentin	VIM	3,157,700,000	489,550,000	337,990,000	734,410,000	251,720,000	392,940,000	951,130,000	25
Yes		A0A0C4DH90	Ig kappa chain V-III region POM	IGKV3OR2-268	2,570,200,000	1,897,100,000	0	13,227,000	0	225,870,000	434,010,000	1
Yes		V9HW50	Alcohol dehydrogenase 1B	HEL-S-117	2,525,500,000	0	2,445,000,000	0	0	80,447,000	0	17
	Yes	P17931	Galectin-3;Galectin	LGALS3	2,429,700,000	1,214,100,000	169,570,000	378,710,000	177,170,000	77,588,000	412,490,000	8
Yes		Q08554-2	Desmocollin-1	DSC1	2,289,200,000	409,040,000	260,520,000	496,130,000	269,620,000	267,980,000	585,960,000	11
	Yes	P0DOY3	Ig lambda-1 chain C regions	IGLC1	2,060,500,000	902,940,000	302,390,000	106,470,000	55,564,000	332,740,000	360,390,000	6
	Yes	P14923	Junction plakoglobin	JUP	1,729,100,000	212,940,000	113,640,000	343,050,000	269,710,000	404,730,000	385,000,000	15
Yes		Q8N5G2-2	Macoilin	MACO1	1,581,700,000	99,294,000	476,890,000	430,010,000	308,790,000	0	266,730,000	2
		Q5T749	Keratinocyte proline-rich protein	KPRP	1,575,500,000	330,330,000	141,660,000	226,220,000	285,640,000	313,090,000	278,590,000	12
	Yes	P19474	E3 ubiquitin-protein ligase TRIM21	TRIM21	1,493,600,000	373,480,000	221,830,000	137,660,000	252,360,000	260,040,000	248,270,000	10
	Yes	Q9NZT1	Calmodulin-like protein 5	CALML5	1,415,300,000	243,820,000	182,070,000	222,180,000	153,060,000	70,118,000	544,030,000	5
		P04083	Annexin A1;Annexin	ANXA1	1,402,800,000	51,347,000	99,256,000	209,080,000	80,360,000	733,430,000	229,300,000	12
Yes		P02647	Apolipoprotein A-I;Proapolipoprotein A-I	APOA1	1,331,000,000	11,399,000	117,700,000	5,319,000	16,475,000	1,162,800,000	17,217,000	15
Yes		A0A3B3IS80	Fructose-bisphosphate aldolase B	ALDOB	1,149,700,000	0	1,053,900,000	0	0	95,806,000	0	15
		P04406	Glyceraldehyde-3-phosphate dehydrogenase	GAPDH	1,024,600,000	45,228,000	381,510,000	144,970,000	70,343,000	219,600,000	162,960,000	13
	Yes	A0A286YES1	Ig gamma-3 chain C region	IGHG3	1,009,000,000	138,810,000	318,110,000	154,420,000	99,280,000	160,810,000	137,620,000	15
	Yes	P02675	Fibrinogen beta chain	FGB	987,840,000	3,484,400	109,660,000	9,669,900	0	843,190,000	21,839,000	8
		A0A5F9ZH78	Arginase-1	ARG1	985,040,000	29,882,000	296,130,000	165,080,000	133,750,000	191,750,000	168,450,000	7
		P04040	Catalase	CAT	883,310,000	55,685,000	377,410,000	124,610,000	80,278,000	132,340,000	112,980,000	10
		A0A286YEY1	Ig alpha-1 chain C region	IGHA1	816,250,000	19,070,000	323,900,000	34,146,000	95,177,000	136,490,000	207,470,000	11
	Yes	P01023	Alpha-2-macroglobulin	A2M	764,980,000	22,095,000	427,860,000	9,797,400	18,372,000	162,150,000	124,700,000	19
Yes		Q2L6G8	Corneodesmosin	CDSN	755,530,000	85,379,000	142,160,000	258,560,000	81,346,000	84,291,000	103,800,000	5
	Yes	P11021	78 kDa glucose-regulated protein	HSPA5	754,080,000	73,659,000	267,450,000	111,330,000	14,914,000	122,090,000	164,640,000	19
Yes		Q14103-3	Heterogeneous nuclear ribonucleoprotein D0	HNRNPD	743,760,000	190,940,000	159,680,000	172,750,000	62,051,000	75,439,000	82,904,000	7
	Yes	S4R460	Ig heavy chain V-III region BRO	IGHV3OR16-9	737,650,000	77,631,000	167,330,000	68,300,000	164,380,000	145,600,000	114,400,000	2
Yes		Q8N257	Histone H2B type 3-B	HIST3H2BB	735,150,000	68,866,000	97,720,000	133,440,000	90,551,000	222,990,000	121,590,000	4
		P02671	Fibrinogen alpha chain;Fibrinopeptide A	FGA	727,500,000	0	39,906,000	0	0	687,600,000	0	20
Yes		H0Y9N0	Alcohol dehydrogenase 4	ADH4	720,950,000	0	690,910,000	0	0	30,039,000	0	13
		A0A6Q8PFJ0	Prelamin-A/C;Lamin-A/C	LMNA	692,900,000	124,240,000	137,300,000	102,670,000	16,496,000	157,450,000	154,750,000	15
Yes		P31327	Carbamoyl-phosphate synthase [ammonia], mitochondrial	CPS1	684,130,000	0	639,470,000	0	0	44,655,000	0	22
		P02787	Serotransferrin	TF	652,910,000	0	470,270,000	0	0	146,010,000	36,628,000	17
	Yes	Q01469	Fatty acid-binding protein, epidermal	FABP5	620,650,000	95,889,000	59,613,000	208,230,000	97,652,000	68,443,000	90,819,000	6
Yes		Q9BTM1	Histone H2A.J	H2AFJ	616,220,000	134,230,000	164,340,000	41,711,000	94,091,000	86,576,000	95,268,000	3
Yes		P02042	Hemoglobin subunit delta	HBD	608,730,000	5,412,700	569,100,000	0	0	34,217,000	0	11
	Yes	P31943	Heterogeneous nuclear ribonucleoprotein H	HNRNPH1	586,320,000	235,200,000	40,807,000	91,509,000	52,962,000	116,480,000	49,360,000	10
Yes		Q15007	Pre-mRNA-splicing regulator WTAP	WTAP	583,670,000	146,160,000	79,564,000	83,145,000	52,450,000	83,328,000	139,020,000	11
		E7ETU5	RNA-binding motif, single-stranded-interacting protein 1	RBMS1	582,990,000	101,720,000	109,470,000	87,943,000	47,975,000	117,990,000	117,880,000	4
		F8VZY9	Keratin, type I cytoskeletal 18	KRT18	508,470,000	182,680,000	57,886,000	98,079,000	48,183,000	67,435,000	54,210,000	11
Yes		P01024	Complement C3;Complement C3 beta chain	C3	484,020,000	0	112,750,000	0	0	371,270,000	0	18
Yes		F5H5D3	Tubulin alpha-1C chain;Tubulin alpha-1B chain	TUBA1C	478,170,000	54,611,000	141,340,000	66,825,000	35,734,000	118,870,000	60,793,000	7
Yes		C9JEU5	Fibrinogen gamma chain	FGG	455,740,000	0	79,865,000	2,023,400	0	368,680,000	5,169,500	8
Yes		P31942-2	Heterogeneous nuclear ribonucleoprotein H3	HNRNPH3	453,350,000	48,222,000	34,002,000	131,920,000	77,527,000	103,460,000	58,216,000	7
	Yes	A0A286YEY4	Ig gamma-2 chain C region	IGHG2	432,350,000	114,780,000	109,100,000	83,334,000	18,798,000	68,437,000	37,904,000	10
Yes		P06733	Alpha-enolase	ENO1	410,010,000	29,654,000	202,800,000	42,689,000	15,683,000	119,190,000	0	12
		E9PGY2	Dynein assembly factor 5, axonemal	DNAAF5	404,800,000	19,772,000	183,310,000	67,144,000	0	69,246,000	65,333,000	1
Yes		E5RHP7	Carbonic anhydrase 1	CA1	401,260,000	0	391,980,000	0	0	9,284,600	0	8
		O43866	CD5 antigen-like	CD5L	377,830,000	69,239,000	55,821,000	96,818,000	44,043,000	63,341,000	48,571,000	7
		O14979-3	Heterogeneous nuclear ribonucleoprotein D-like	HNRNPDL	365,710,000	19,376,000	5,685,600	198,730,000	94,806,000	32,417,000	14,696,000	8
Yes		Q9UNZ2	NSFL1 cofactor p47	NSFL1C	347,920,000	35,893,000	47,043,000	106,430,000	50,500,000	26,935,000	81,121,000	8
		P01767	Ig heavy chain V-III region BUT	IGHV3-66	341,860,000	194,310,000	62,905,000	0	45,120,000	39,526,000	0	3
		P06702	Protein S100-A9	S100A9	328,250,000	18,939,000	0	0	0	309,310,000	0	5
		E7EQB2	Lactotransferrin;Lactoferricin-H	LTF	327,250,000	38,827,000	139,660,000	27,766,000	5,594,100	60,142,000	55,260,000	7
		J3QSA3	Ubiquitin-40S ribosomal protein S27a	UBB	324,440,000	21,637,000	77,494,000	57,113,000	32,248,000	60,277,000	75,668,000	2
Yes		P35579	Myosin-9	MYH9	312,240,000	3,676,700	19,015,000	0	0	289,550,000	0	14
Yes		P00488	Coagulation factor XIII A chain	F13A1	309,550,000	38,304,000	144,670,000	49,351,000	0	12,444,000	64,783,000	11
		P16403	Histone H1.2	HIST1H1C	308,980,000	26,941,000	14,080,000	6,953,300	0	29,397,000	231,610,000	8
Yes		P05091	Aldehyde dehydrogenase, mitochondrial	ALDH2	295,420,000	0	295,420,000	0	0	0	0	13
	Yes	P31944	Caspase-14;Caspase-14 subunit p17, mature form	CASP14	292,460,000	41,450,000	20,154,000	92,287,000	47,890,000	24,225,000	66,452,000	5
Yes		P23141-3	Liver carboxylesterase 1	CES1	287,760,000	0	275,240,000	0	0	12,513,000	0	8
		Q13492-3	Phosphatidylinositol-binding clathrin assembly protein	PICALM	280,250,000	0	13,085,000	54,721,000	40,016,000	68,106,000	104,330,000	2
Yes		P08263	Glutathione S-transferase A1	GSTA1	276,080,000	0	276,080,000	0	0	0	0	6
		P01709	Ig lambda chain V-II region MGC		272,320,000	194,040,000	27,482,000	0	0	20,496,000	30,296,000	1
Yes		K7EMS3	Keratin, type I cytoskeletal 19	KRT19	271,550,000	43,143,000	35,179,000	52,355,000	28,751,000	3,693,300	108,430,000	8
Yes		P32119	Peroxiredoxin-2	PRDX2	264,970,000	10,440,000	193,050,000	17,114,000	0	28,665,000	15,708,000	7
		P11142	Heat shock cognate 71 kDa protein	HSPA8	256,440,000	21,135,000	64,536,000	39,021,000	0	87,034,000	44,712,000	12
Yes		H3BQ34	Pyruvate kinase;Pyruvate kinase PKM	PKM	253,600,000	157,610,000	12,316,000	26,633,000	7,716,200	41,154,000	8,175,000	4
Yes		M0QZK8	Gamma-glutamylcyclotransferase	GGCT	252,790,000	23,067,000	23,773,000	53,047,000	57,290,000	26,710,000	68,899,000	3
		P62805	Histone H4	HIST1H4A	247,550,000	32,165,000	44,025,000	57,166,000	32,274,000	24,152,000	57,770,000	3
		F8VV32	Lysozyme;Lysozyme C	LYZ	237,840,000	25,942,000	54,297,000	24,124,000	46,944,000	38,336,000	48,197,000	3
Yes		A0A2R8YGD1	Tripeptidyl-peptidase 1	TPP1	228,720,000	59,580,000	36,930,000	40,003,000	12,722,000	48,382,000	31,107,000	2
		A0A286YFJ8	Ig gamma-4 chain C region	IGHG4	221,300,000	21,901,000	25,795,000	0	48,084,000	94,876,000	30,645,000	9
Yes		P30086	Phosphatidylethanolamine-binding protein 1	PEBP1	220,410,000	0	220,410,000	0	0	0	0	6
		Q8NDC0	MAPK-interacting and spindle-stabilizing protein-like	MAPK1IP1L	219,790,000	0	0	74,677,000	0	55,083,000	90,029,000	1
Yes		E9PSB3	Eukaryotic translation initiation factor 3 Sub M	EIF3M	204,390,000	0	0	204,390,000	0	0	0	1
Yes		P00367	Glutamate dehydrogenase 1, mitochondrial	GLUD1	202,320,000	0	194,820,000	0	0	7,505,800	0	8
Yes		P01040	Cystatin-A;Cystatin-A, N-terminally processed	CSTA	200,650,000	31,866,000	28,575,000	24,874,000	17,883,000	0	97,455,000	3
Yes		H0Y755	Low affinity immunoglobulin gamma Fc region receptor III-A	FCGR3A	200,010,000	96,729,000	0	76,577,000	15,235,000	0	11,468,000	2
Yes		Q6UWP8	Suprabasin	SBSN	199,090,000	23,686,000	5,567,100	53,784,000	11,163,000	9,392,600	95,502,000	7
Yes		H0YH81	ATP synthase subunit beta,mitochondrial	ATP5B	192,440,000	0	150,240,000	11,186,000	0	26,174,000	4,835,000	3
Yes		P00738	Haptoglobin;Haptoglobin alpha chain	HP	191,600,000	0	83,217,000	0	0	105,830,000	2,547,800	8
	Yes	P05109	Protein S100-A8;Protein S100-A8, N-terminally processed	S100A8	188,970,000	15,112,000	51,461,000	6,955,600	7,752,500	102,410,000	5,286,800	4
		P10412	Histone H1.4	HIST1H1E	188,770,000	0	51,503,000	19,340,000	0	38,303,000	79,622,000	7
		P30101	Protein disulfide-isomerase A3	PDIA3	184,850,000	27,987,000	81,404,000	9,267,600	0	52,967,000	13,224,000	7
Yes		Q60FE5	Filamin-A	FLNA	176,900,000	17,314,000	62,222,000	4,156,600	0	93,211,000	0	14
	Yes	P59666	Neutrophil defensin 3;HP 3-56;Neutrophil defensin 2	DEFA3	175,940,000	12,525,000	147,180,000	0	0	0	16,235,000	4
		A0A7I2V4I6	Heterogeneous nuclear ribonucleoproteins A2/B1	HNRNPA2B1	175,770,000	10,611,000	33,709,000	28,025,000	3,763,900	47,208,000	52,448,000	8
		C9JZN1	Guanine nucleotide-binding protein G(I)/G(S)/G(T) subunit 2	GNB2	167,230,000	0	32,409,000	0	114,540,000	0	20,285,000	3
Yes		E9PJX3	DC-STAMP domain-containing protein 1	DCST1	165,830,000	165,830,000	0	0	0	0	0	1
Yes		Q93088	Betaine--homocysteine S-methyltransferase 1	BHMT	156,930,000	0	156,930,000	0	0	0	0	5
Yes		Q08188	Protein-glutamine gamma-glutamyltransferase E	TGM3	151,040,000	19,454,000	14,749,000	30,930,000	27,901,000	11,456,000	46,554,000	6
		Q5JP53	Tubulin beta chain;Tubulin beta-2B chain	TUBB	148,810,000	0	39,759,000	10,457,000	5,418,600	93,172,000	0	3
Yes		P00352	Retinal dehydrogenase 1	ALDH1A1	147,820,000	0	143,910,000	0	0	3,905,500	0	7
		A0A7I2V3H3	Putative elongation factor 1-alpha-like 3	EEF1A1	146,880,000	10,829,000	56,560,000	10,460,000	7,325,300	52,315,000	9,388,600	1
Yes		P29508-2	Serpin B3	SERPINB3	144,360,000	34,074,000	0	63,249,000	7,558,700	7,745,700	31,729,000	3
		P47929	Galectin-7	LGALS7	142,190,000	14,374,000	0	53,808,000	19,822,000	41,851,000	12,331,000	4
Yes		P02730	Band 3 anion transport protein	SLC4A1	137,560,000	0	122,820,000	6,434,500	0	0	8,304,400	6
Yes		P25705-2	ATP synthase subunit alpha, mitochondrial	ATP5A1	135,600,000	25,045,000	92,411,000	4,146,300	0	14,002,000	0	9
Yes		P09467	Fructose-1,6-bisphosphatase 1	FBP1	134,090,000	0	112,310,000	0	0	21,781,000	0	4
Yes		A0A6Q8PFK8	Heat shock protein beta-1	HSPB1	129,770,000	6,293,600	23,017,000	23,662,000	14,009,000	27,850,000	34,937,000	3
		P14625	Endoplasmin	HSP90B1	128,220,000	0	87,804,000	12,003,000	1,880,000	22,276,000	4,253,300	6
		A0A5F9ZHX5	Chromodomain-helicase-DNA-binding protein 3	CHD3	126,410,000	72,151,000	0	0	0	0	54,262,000	1
		D3YTK1	B-cell lymphoma/leukemia 11B	BCL11B	124,710,000	76,098,000	14,068,000	16,701,000	0	0	17,845,000	1
Yes		P07476	Involucrin	IVL	120,360,000	0	0	0	0	120,360,000	0	6
Yes		P00558-2	Phosphoglycerate kinase 1	PGK1	119,430,000	0	106,620,000	0	0	12,816,000	0	5
		A0A0G2JRN3	Alpha-1-antitrypsin;Short peptide from AAT	SERPINA1	119,420,000	0	0	0	0	119,420,000	0	2
Yes		P10599-2	Thioredoxin	TXN	119,320,000	32,992,000	7,421,500	15,014,000	6,942,900	38,357,000	18,590,000	3
		A0A087WVQ6	Clathrin heavy chain;Clathrin heavy chain 1	CLTC	118,860,000	7,694,400	39,319,000	4,351,100	5,094,400	27,799,000	34,607,000	5

		P11166	Solute carrier family 2, facilitated glucose transporter member 1	SLC2A1	117,840,000	27,594,000	20,800,000	27,638,000	17,045,000	17,769,000	6,991,000	1
Yes		A0A0A0MSI0	Peroxiredoxin-1	PRDX1	117,410,000	0	23,434,000	24,158,000	0	50,913,000	18,908,000	6
		P04843	Dolichyl-diphosphooligosaccharide--protein glycosyltransferase subunit 1	RPN1	114,750,000	14,069,000	19,291,000	38,305,000	0	5,918,100	37,166,000	5
		Q9BS26	Endoplasmic reticulum resident protein 44	ERP44	114,410,000	0	19,792,000	0	57,777,000	15,611,000	21,226,000	2
Yes		P31040	Succinate dehydrogenase [ubiquinone] flavoprotein subunit, mitochondrial	SDHA	110,870,000	21,023,000	29,762,000	5,004,900	6,511,700	7,760,200	40,805,000	5
		E9PS23	Cofilin-1	CFL1	105,680,000	0	47,412,000	6,922,800	6,769,200	42,374,000	2,206,100	2
Yes		P00918	Carbonic anhydrase 2	CA2	103,530,000	0	103,530,000	0	0	0	0	6
Yes		P40926	Malate dehydrogenase, mitochondrial;Malate dehydrogenase	MDH2	102,110,000	0	102,110,000	0	0	0	0	6
Yes		P09210	Glutathione S-transferase A2	GSTA2	101,640,000	0	101,640,000	0	0	0	0	6
Yes		P09211	Glutathione S-transferase P	GSTP1	101,360,000	0	24,528,000	0	0	76,833,000	0	2
Yes		P00338-3	L-lactate dehydrogenase A chain	LDHA	101,020,000	0	67,486,000	0	0	33,536,000	0	4
Yes		P30084	Enoyl-CoA hydratase, mitochondrial	ECHS1	100,510,000	0	100,510,000	0	0	0	0	5
Yes		P00326	Alcohol dehydrogenase 1C	ADH1C	99,362,000	0	99,362,000	0	0	0	0	12
Yes		P11182	Lipoamide acyltransferase component of branched-chain α-keto acid	DBT	98,020,000	2,429,500	0	88,425,000	7,165,200	0	0	6
Yes		P60174	Triosephosphate isomerase	TPI1	96,410,000	0	96,410,000	0	0	0	0	6
Yes		P31995-4	Low affinity immunoglobulin gamma Fc region receptor II-c	FCGR2C	95,150,000	0	0	21,613,000	16,029,000	0	57,508,000	2
Yes		P81605-2	Dermcidin;Survival-promoting peptide;DCD-1	DCD	94,948,000	0	17,310,000	24,755,000	14,705,000	27,485,000	10,693,000	8
		A0A7I2V2R3	Heterogeneous nuclear ribonucleoprotein A3	HNRNPA3	94,476,000	0	0	40,480,000	18,442,000	11,950,000	23,604,000	5
Yes		Q15828	Cystatin-M	CST6	90,006,000	23,842,000	0	12,469,000	11,616,000	14,124,000	27,955,000	1
Yes		P04259	Keratin, type II cytoskeletal 6B	KRT6B	89,853,000	0	3,936,600	12,262,000	4,134,500	69,520,000	0	56
		K7EQ02	DAZ-associated protein 1	DAZAP1	88,043,000	0	4,283,400	36,199,000	21,232,000	26,328,000	0	2
Yes		P08238	Heat shock protein HSP 90-beta	HSP90AB1	87,486,000	9,004,500	43,177,000	0	0	26,031,000	9,274,000	8
Yes		Q13835-2	Plakophilin-1	PKP1	87,271,000	14,367,000	4,843,200	0	14,614,000	47,376,000	6,070,300	3
		P16401	Histone H1.5	HIST1H1B	86,334,000	0	0	0	0	33,838,000	52,496,000	5
Yes		P21549	Serine--pyruvate aminotransferase	AGXT	84,253,000	0	84,253,000	0	0	0	0	3
Yes		E7EQR4	Ezrin	EZR	83,177,000	11,616,000	57,174,000	0	0	0	14,386,000	6
Yes		A8MW49	Fatty acid-binding protein, liver	FABP1	80,281,000	0	80,281,000	0	0	0	0	3
Yes		Q09666	Neuroblast differentiation-associated protein AHNAK	AHNAK	79,609,000	4,552,900	0	0	0	75,056,000	0	8
Yes		P06396-2	Gelsolin	GSN	77,391,000	0	0	0	0	77,391,000	0	5
Yes		P08311	Cathepsin G	CTSG	75,345,000	0	64,752,000	0	0	10,593,000	0	3
Yes		P07737	Profilin-1	PFN1	73,460,000	0	45,606,000	0	0	27,854,000	0	2
Yes		Q13867	Bleomycin hydrolase	BLMH	71,299,000	15,720,000	8,186,000	22,679,000	0	9,475,800	15,237,000	2
Yes		A0A0G2JIW1	Heat shock 70 kDa protein 1A;Heat shock 70 kDa protein 1B	HSPA1A	70,838,000	0	40,124,000	9,828,700	0	14,307,000	6,577,900	7
Yes		P25311	Zinc-alpha-2-glycoprotein	AZGP1	70,437,000	17,679,000	10,057,000	36,466,000	0	0	6,235,100	6
		A0A7I2YQK6	60 kDa heat shock protein, mitochondrial	HSPD1	70,230,000	0	41,023,000	0	0	29,206,000	0	3
Yes		P30041	Peroxiredoxin-6	PRDX6	70,214,000	0	70,214,000	0	0	0	0	2
Yes		P17066	Heat shock 70 kDa protein 6;Putative heat shock 70 kDa protein 7	HSPA6	69,823,000	0	31,296,000	5,901,700	4,534,000	18,897,000	9,194,300	4
	Yes	E9PHT9	Annexin;Annexin A5	ANXA5	69,705,000	7,186,600	4,930,200	11,971,000	16,361,000	5,489,900	23,766,000	4
		P31025	Lipocalin-1;Putative lipocalin 1-like protein 1	LCN1	68,579,000	17,246,000	0	8,715,500	19,543,000	9,898,400	13,176,000	2
		P31930	Cytochrome b-c1 complex subunit 1, mitochondrial	UQCRC1	66,759,000	0	7,055,500	32,142,000	9,727,500	17,834,000	0	2
Yes		P22735	Protein-glutamine gamma-glutamyltransferase K	TGM1	66,068,000	9,145,000	8,097,100	11,141,000	12,123,000	8,823,300	16,739,000	2
Yes		Q6ZVX7	F-box only protein 50	NCCRP1	65,548,000	18,299,000	1,627,800	13,871,000	10,069,000	9,179,600	12,502,000	2
Yes		Q92637	High affinity immunoglobulin gamma Fc receptor IB	FCGR1B	65,085,000	14,808,000	24,911,000	0	0	0	25,367,000	2
		P31947-2	14-3-3 protein sigma	SFN	65,014,000	0	0	0	0	65,014,000	0	4
		M0R3F1	Heterogeneous nuclear ribonucleoprotein U-like protein 1	HNRNPUL1	64,921,000	7,997,300	41,310,000	15,614,000	0	0	0	3
		Q9HAU0-6	Pleckstrin homology domain-6	PLEKHA6	64,712,000	0	0	0	35,710,000	13,996,000	15,006,000	1
Yes		Q16822	Phosphoenolpyruvate carboxykinase [GTP], mitochondrial	PCK2	63,356,000	0	63,356,000	0	0	0	0	6
Yes		P42765	3-ketoacyl-CoA thiolase, mitochondrial	ACAA2	63,130,000	0	63,130,000	0	0	0	0	3
Yes		V9GYC1	Apolipoprotein A-II;Proapolipoprotein A-II;Truncated apolipoprotein A-II	APOA2	63,025,000	0	0	0	0	63,025,000	0	3
Yes		O95954	Formimidoyltransferase-cyclodeaminase	FTCD	62,955,000	0	62,955,000	0	0	0	0	3
		P01833	Polymeric immunoglobulin receptor;Secretory component	PIGR	62,780,000	55,565,000	0	7,215,700	0	0	0	2
Yes		H3BUH7	Fructose-bisphosphate aldolase;Fructose-bisphosphate aldolase A	ALDOA	61,547,000	0	30,590,000	0	0	30,957,000	0	2
Yes		I3NI03	Protein disulfide-isomerase	P4HB	61,057,000	5,594,500	24,393,000	6,481,000	4,107,900	14,479,000	6,001,800	1
Yes		P04899-4	Guanine nucleotide-binding protein G(i) subunit alpha-2	GNAI2	60,628,000	0	5,045,200	17,245,000	6,652,900	12,318,000	19,367,000	3
Yes		J3QS36	L-xylulose reductase	DCXR	58,887,000	0	58,887,000	0	0	0	0	4
Yes		D6REM4	Casein kinase I isoform alpha;Casein kinase I isoform alpha-like	CSNK1A1	58,574,000	58,574,000	0	0	0	0	0	1
		P01594	Ig kappa chain V-I region AU;Ig kappa chain V-I region AG	IGKV1D-33	58,512,000	35,985,000	4,295,800	2,809,900	3,517,000	4,290,800	7,612,700	1
		A0A0A0MSV6	Complement C1q subcomponent subunit B	C1QB	58,010,000	0	0	58,010,000	0	0	0	2
Yes		P69891	Hemoglobin subunit gamma-1	HBG1	57,351,000	0	0	20,525,000	11,885,000	0	24,940,000	11
Yes		Q5T6W2	Heterogeneous nuclear ribonucleoprotein K	HNRNPK	56,797,000	0	9,694,800	10,343,000	0	20,754,000	16,006,000	1
Yes		Q6P0N6	Dystonin	DST	55,054,000	0	0	0	55,054,000	0	0	1
Yes		P08559-3	Pyruvate dehydrogenase E1 component subunit alpha, mitochondrial	PDHA1	54,649,000	0	0	36,915,000	17,733,000	0	0	2
Yes		P54868	Hydroxymethylglutaryl-CoA synthase, mitochondrial	HMGCS2	54,294,000	0	54,294,000	0	0	0	0	3
Yes		K7EP41	Glucose-6-phosphate isomerase	GPI	51,787,000	0	28,093,000	0	0	23,693,000	0	1
		A0A7I2V5R8	Dipeptidyl peptidase 4 soluble form	DPP4	49,250,000	16,947,000	0	6,971,900	0	0	25,332,000	3
Yes		P02745	Complement C1q subcomponent subunit A	C1QA	49,029,000	0	0	26,241,000	7,260,800	0	15,527,000	1
Yes		H7C131	3-ketoacyl-CoA thiolase, peroxisomal	ACAA1	49,012,000	0	39,040,000	0	0	9,971,800	0	2
Yes		P14550	Alcohol dehydrogenase [NADP(+)]	AKR1A1	48,970,000	0	48,970,000	0	0	0	0	3
Yes		H7BYH4	Superoxide dismutase [Cu-Zn]	SOD1	48,641,000	0	36,536,000	0	0	12,105,000	0	1
Yes		O75891-2	Cytosolic 10-formyltetrahydrofolate dehydrogenase	ALDH1L1	47,334,000	0	47,334,000	0	0	0	0	4
Yes		P16152	Carbonyl reductase [NADPH] 1	CBR1	46,537,000	0	46,537,000	0	0	0	0	3
Yes		Q16762	Thiosulfate sulfurtransferase	TST	46,314,000	0	46,314,000	0	0	0	0	3
		P98082-2	Disabled homolog 2	DAB2	46,020,000	7,661,800	4,233,100	4,780,500	11,910,000	4,537,100	12,898,000	1
Yes		A0A2R8Y7L2	Peroxisomal multifunctional enzyme type 2;Enoyl-CoA hydratase 2	HSD17B4	44,462,000	0	44,462,000	0	0	0	0	3
Yes		F5H5P2	2-oxoisovalerate dehydrogenase subunit alpha, mitochondrial	BCKDHA	44,336,000	0	0	27,748,000	6,992,100	9,596,700	0	2
		P07910	Heterogeneous nuclear ribonucleoproteins C1/C2	HNRNPC	44,199,000	0	0	19,282,000	0	24,917,000	0	2
		P01701	Ig lambda chain V-I region NEW	IGLV1-51	43,260,000	43,260,000	0	0	0	0	0	1
Yes		Q16610-2	Extracellular matrix protein 1	ECM1	43,164,000	16,073,000	0	4,679,200	16,017,000	0	6,394,400	3
Yes		P80748	Ig lambda chain V-III region LOI	IGLV3-9	39,938,000	39,938,000	0	0	0	0	0	2
Yes		P00480	Ornithine carbamoyltransferase, mitochondrial	OTC	38,811,000	0	38,811,000	0	0	0	0	3
Yes		P06727	Apolipoprotein A-IV	APOA4	38,730,000	0	0	0	0	38,730,000	0	4
	Yes	A0A3B3ISA6	Complement C4-A;Complement C4 beta chain	C4B	37,477,000	0	0	0	0	37,477,000	0	3
		C9J2I0	Arf-GAP domain and FG repeat-containing protein 1	AGFG1	37,463,000	0	19,993,000	0	17,470,000	0	0	1
Yes		P62081	40S ribosomal protein S7	RPS7	36,563,000	0	0	0	0	36,563,000	0	1
Yes		P00505	Aspartate aminotransferase, mitochondrial	GOT2	36,173,000	0	36,173,000	0	0	0	0	1
Yes		Q14669	E3 ubiquitin-protein ligase TRIP12	TRIP12	35,387,000	5,063,600	0	0	1,274,500	7,478,400	21,571,000	2
Yes		P00747	Plasminogen;Plasmin heavy chain A;Activation peptide;Angiostatin	PLG	35,204,000	0	18,546,000	0	0	16,658,000	0	2
Yes		A0A5F9ZHD4	Acetyl-CoA acetyltransferase, mitochondrial	ACAT1	34,864,000	0	34,864,000	0	0	0	0	1
Yes		P42357	Histidine ammonia-lyase	HAL	34,798,000	3,023,300	5,789,400	4,315,200	4,655,100	3,693,900	13,321,000	4
Yes		P08574	Cytochrome c1, heme protein, mitochondrial	CYC1	34,705,000	17,970,000	0	0	3,321,100	6,646,500	6,767,300	1
Yes		A0A7I2V2G2	Stress-70 protein, mitochondrial	HSPA9	34,422,000	3,644,700	30,777,000	0	0	0	0	5
		Q13151	Heterogeneous nuclear ribonucleoprotein A0	HNRNPA0	34,332,000	9,337,700	8,802,000	6,967,600	9,225,100	0	0	1
Yes		Q00266	S-adenosylmethionine synthase isoform type-1	MAT1A	34,266,000	0	34,266,000	0	0	0	0	3
		B4E1S2	Annexin;Annexin A4	ANXA4	34,107,000	0	23,248,000	7,248,900	0	0	3,610,400	2
Yes		E7EN95	Filamin-B	FLNB	33,248,000	0	0	0	0	33,248,000	0	4
Yes		Q15149-7	Plectin	PLEC	32,622,000	0	0	0	0	32,622,000	0	5
Yes		Q5T750	Skin-specific protein 32	XP32	32,441,000	14,229,000	12,308,000	0	5,905,100	0	0	1
		P29401	Transketolase	TKT	32,236,000	0	25,916,000	0	0	6,320,100	0	4
Yes		R4GN49	Protein S100-A2	S100A2	32,039,000	0	0	0	0	32,039,000	0	2
Yes		Q14574-2	Desmocollin-3	DSC3	31,820,000	0	0	11,287,000	9,170,400	0	11,362,000	2
Yes		P07900	Heat shock protein HSP 90-alpha	HSP90AA1	31,748,000	0	0	18,987,000	0	12,762,000	0	7
Yes		K7ESE1	Keratin, type I cytoskeletal 17	KRT17	31,444,000	0	0	0	0	31,444,000	0	6
		H7BZJ3	Protein disulfide-isomerase A3	PDIA3	31,218,000	10,969,000	0	0	0	12,027,000	8,221,900	2
Yes		A0A2R8YGX3	Tropomyosin alpha-4 chain	TPM4	30,416,000	0	0	0	0	30,416,000	0	4
		A0A1X7SBZ2	Probable ATP-dependent RNA helicase DDX17	DDX17	30,189,000	11,040,000	12,105,000	0	0	7,044,500	0	1
Yes		P68133	Actin, alpha skeletal muscle; Actin, aortic smooth muscle	ACTA1	28,542,000	0	0	22,625,000	0	5,916,600	0	11
Yes		P31151	Protein S100-A7	S100A7	28,377,000	16,068,000	0	0	3,923,400	5,362,900	3,022,700	1
Yes		O75874	Isocitrate dehydrogenase [NADP] cytoplasmic	IDH1	27,456,000	0	27,456,000	0	0	0	0	3
Yes		P63104	14-3-3 protein zeta/delta	YWHAZ	26,529,000	0	0	3,983,100	0	11,736,000	10,810,000	3
Yes		A0A7I2V3U0	Aconitate hydratase, mitochondrial	ACO2	26,341,000	0	7,668,600	3,421,200	0	7,748,000	7,503,500	2
Yes		C9JEH7	40S ribosomal protein S4, X isoform	RPS4Y1	26,072,000	26,072,000	0	0	0	0	0	3
Yes		D6RHJ7	Dihydropteridine reductase	QDPR	25,964,000	0	22,627,000	0	0	3,337,100	0	2
Yes		P21980	Protein-glutamine gamma-glutamyltransferase 2	TGM2	25,527,000	0	25,527,000	0	0	0	0	3
	Yes	I3L1P8	Mitochondrial 2-oxoglutarate/malate carrier protein	SLC25A11	25,396,000	0	0	9,416,800	0	5,550,200	10,429,000	1
Yes		E9PP21	Cysteine and glycine-rich protein 1	CSRP1	25,181,000	0	19,963,000	5,218,000	0	0	0	1
Yes		P26641	Elongation factor 1-gamma	EEF1G	25,062,000	8,120,000	0	0	0	16,942,000	0	2
Yes		Q99497	Protein deglycase DJ-1	PARK7	24,469,000	0	24,469,000	0	0	0	0	2
		B4DK69	Aldo-keto reductase family 1 member C2	AKR1C2	23,775,000	0	23,775,000	0	0	0	0	3
Yes		H3BTX9	Acyl-coenzyme A synthetase ACSM2B, mitochondrial	ACSM2B	23,403,000	0	23,403,000	0	0	0	0	2
		P17096	High mobility group protein HMG-I/HMG-Y	HMGA1	23,239,000	0	0	0	0	0	23,239,000	1
Yes		O43548	Protein-glutamine gamma-glutamyltransferase 5	TGM5	22,931,000	0	0	5,106,200	3,459,400	5,197,500	9,168,100	1
Yes		A0A6E1W9L1	Zinc finger and BTB domain-containing protein 3	ZBTB3	22,345,000	5,533,200	0	7,473,000	0	9,338,700	0	2
Yes		P07099	Epoxide hydrolase 1	EPHX1	21,730,000	0	21,730,000	0	0	0	0	2
Yes		A0A7I2YQ74	UTP--glucose-1-phosphate uridylyltransferase	UGP2	21,651,000	0	21,651,000	0	0	0	0	3
Yes		P34896-3	Serine hydroxymethyltransferase, cytosolic	SHMT1	21,544,000	0	21,544,000	0	0	0	0	2
Yes		P51857-2	3-oxo-5-beta-steroid 4-dehydrogenase	AKR1D1	21,175,000	0	21,175,000	0	0	0	0	2
Yes		H0YCY6	Bifunctional ATP-dependent dihydroxyacetone kinase; ATP-dependent	TKFC	20,829,000	0	20,829,000	0	0	0	0	3
Yes		F8VPF3	Myosin light polypeptide 6;Myosin light chain 6B	MYL6	20,561,000	0	0	0	0	20,561,000	0	1
Yes		P01019	Angiotensinogen;Angiotensin-1;Angiotensin-2;Angiotensin-3;Angiotensin-4	AGT	20,374,000	0	0	0	0	20,374,000	0	2

Yes		P25325-2	3-mercaptopyruvate sulfurtransferase;Sulfurtransferase	MPST	19,789,000	0	19,789,000	0	0	0	0	2
Yes		A0A3B3ISY1	Tissue factor pathway inhibitor 2	TFPI2	19,686,000	8,176,900	0	0	8,803,000	2,706,500	0	2
Yes		Q16698-2	2,4-dienoyl-CoA reductase, mitochondrial	DECR1	19,661,000	0	19,661,000	0	0	0	0	2
Yes		C9JV37	Prothrombin;Activation peptide fragment 1	F2	19,349,000	0	0	0	0	19,349,000	0	1
Yes		A0A6Q8PFC6	Glycine amidinotransferase, mitochondrial	GATM	18,900,000	0	18,900,000	0	0	0	0	1
Yes		A0A075B6H9	Immunoglobulin lambda variable 4-69	IGLV4-69	18,184,000	18,184,000	0	0	0	0	0	1
Yes		V9GYG0	ADP/ATP translocase 3;ADP/ATP translocase 3, N-terminally processed	SLC25A4	17,956,000	0	0	6,886,600	4,931,600	0	6,137,900	1
Yes		A0A1W2PP35	Heterogeneous nuclear ribonucleoprotein U	HNRNPU	17,783,000	0	0	17,783,000	0	0	0	3
Yes		E5RGW4	Nucleophosmin	NPM1	17,763,000	0	0	0	0	17,763,000	0	1
Yes		J3QRN2	Beta-2-glycoprotein 1	APOH	17,755,000	0	8,891,500	0	0	0	8,863,300	1
		E9PRN7	3 beta-hydroxysteroid dehydrogenase/Delta 5-->4-isomerase type 2	HSD3B1	17,661,000	0	0	4,061,200	6,881,400	0	6,718,400	1
Yes		P52758	Ribonuclease UK114	HRSP12	16,603,000	0	16,603,000	0	0	0	0	1
Yes		Q15084-3	Protein disulfide-isomerase A6	PDIA6	16,371,000	0	10,683,000	0	0	5,687,900	0	1
Yes		Q5TF55	Delta-1-pyrroline-5-carboxylate dehydrogenase, mitochondrial	ALDH4A1	16,343,000	0	16,343,000	0	0	0	0	1
Yes		H0Y4K8	Fibronectin;Anastellin;Ugl-Y1;Ugl-Y2;Ugl-Y3	FN1	16,129,000	2,290,000	0	7,354,100	0	0	6,485,400	1
Yes		A0A494C1T2	C-1-tetrahydrofolate synthase, cytoplasmic	MTHFD1	15,674,000	0	15,674,000	0	0	0	0	3
		E7EPM6	Long-chain-fatty-acid--CoA ligase 1	ACSL1	15,503,000	0	15,503,000	0	0	0	0	2
Yes		H0YJF9	Dihydrolipoyllysine-residue succinyltransferase/2-oxoglutarate dehydrogen	DLST	14,869,000	0	0	11,035,000	0	3,833,400	0	2
Yes		Q14134-2	Tripartite motif-containing protein 29	TRIM29	14,797,000	0	0	0	0	14,797,000	0	2
Yes		P18206-2	Vinculin	VCL	14,766,000	0	0	0	0	0	14,766,000	1
	Yes	D6R9P3	Heterogeneous nuclear ribonucleoprotein A/B	HNRNPAB	14,544,000	0	0	14,544,000	0	0	0	3
Yes		P10696	Alkaline phosphatase, placental-like;Alkaline phosphatase, placental type	ALPPL2	14,464,000	14,464,000	0	0	0	0	0	1
Yes		H3BRG4	Cytochrome b-c1 complex subunit 2, mitochondrial	UQCRC2	14,346,000	0	14,346,000	0	0	0	0	2
Yes		C9JRL4	Malate dehydrogenase;Malate dehydrogenase, cytoplasmic	MDH1	14,124,000	0	14,124,000	0	0	0	0	1
Yes		P62258	14-3-3 protein epsilon	YWHAE	14,037,000	0	5,850,000	0	0	0	8,187,500	2
Yes		D6RFG5	Annexin;Annexin A3	ANXA3	13,723,000	0	0	0	0	13,723,000	0	1
Yes		O60701-3	UDP-glucose 6-dehydrogenase	UGDH	13,415,000	0	13,415,000	0	0	0	0	2
Yes		B0YIW2	Apolipoprotein C-III	APOC3	13,244,000	0	0	0	0	13,244,000	0	1
Yes		A0A0G2JQH2	40S ribosomal protein S18	RPS18	13,172,000	0	0	0	0	13,172,000	0	1
Yes		P49189	4-trimethylaminobutyraldehyde dehydrogenase	ALDH9A1	13,161,000	0	13,161,000	0	0	0	0	1
Yes		P11277-3	Spectrin beta chain, erythrocytic	SPTB	13,077,000	0	13,077,000	0	0	0	0	3
Yes		Q9HC84	Mucin-5B	MUC5B	12,990,000	0	12,990,000	0	0	0	0	2
Yes		P46783	40S ribosomal protein S10;Putative 40S ribosomal protein S10-like	RPS10	12,790,000	0	6,330,400	0	0	6,459,400	0	1
Yes		P04080	Cystatin-B	CSTB	12,717,000	7,164,000	0	5,552,700	0	0	0	1
Yes		F6RFD5	Destrin	DSTN	12,619,000	0	12,619,000	0	0	0	0	1
Yes		P25786	Proteasome subunit alpha type-1;Proteasome subunit alpha type	PSMA1	12,242,000	0	8,949,000	3,292,900	0	0	0	2
Yes		P16157-14	Ankyrin-1	ANK1	12,173,000	0	12,173,000	0	0	0	0	2
Yes		A0A087WT59	Transthyretin	TTR	11,910,000	0	0	0	0	11,910,000	0	2
Yes		E9PK47	Alpha-1,4 glucan phosphorylase;Glycogen phosphorylase, liver form	PYGL	11,862,000	0	11,862,000	0	0	0	0	2
		P02808	Statherin	STATH	11,823,000	11,823,000	0	0	0	0	0	1
Yes		P08246	Neutrophil elastase	ELANE	11,630,000	0	11,630,000	0	0	0	0	1
		P52907	F-actin-capping protein subunit alpha-1	CAPZA1	11,591,000	0	0	0	0	11,591,000	0	1
		C9JA05	Immunoglobulin J chain	JCHAIN	11,558,000	0	0	0	0	11,558,000	0	1
Yes		Q9UG54	Mitogen-activated protein kinase kinase kinase 7	DKFZp586F0420	11,510,000	11,510,000	0	0	0	0	0	1
Yes		P45954-2	Short/branched chain specific acyl-CoA dehydrogenase, mitochondrial	ACADSB	11,392,000	0	11,392,000	0	0	0	0	1
Yes		B5MD38	Trifunctional enzyme subunit beta, mitochondrial;3-ketoacyl-CoA thiolase	HADHB	11,328,000	0	11,328,000	0	0	0	0	1
Yes		P25815	Protein S100-P	S100P	11,215,000	0	0	0	0	0	11,215,000	1
Yes		P02549-2	Spectrin alpha chain, erythrocytic 1	SPTA1	10,654,000	0	10,654,000	0	0	0	0	2
Yes		H0YAG8	Alcohol dehydrogenase class-3	ADH5	10,551,000	0	10,551,000	0	0	0	0	1
		A0A087WW87	Ig kappa chain V-II region FR;Ig kappa chain V-II region Cum	IGKV2-40	10,538,000	0	0	0	0	10,538,000	0	1
Yes		B1AKI5	Muscleblind-like protein 3;Muscleblind-like protein 2	MBNL3	10,394,000	0	10,394,000	0	0	0	0	2
Yes		B1AKQ8	Guanine nucleotide-binding protein G(I)/G(S)/G(T) subunit beta-1	GNB1	10,354,000	0	0	0	0	0	10,354,000	1
Yes		A0A0J9YXZ5	Ras GTPase-activating-like protein IQGAP1	IQGAP1	10,328,000	0	0	0	0	10,328,000	0	2
Yes		P13716-2	Delta-aminolevulinic acid dehydratase	ALAD	10,259,000	0	10,259,000	0	0	0	0	2
Yes		Q13404-8	Ubiquitin-conjugating enzyme E2 variant 1	UBE2V1	9,964,900	0	9,964,900	0	0	0	0	1
Yes		M0R0Y6	Heterogeneous nuclear ribonucleoprotein M	HNRNPM	9,627,300	0	0	0	0	9,627,300	0	1
		A0A7I2V699	Nucleolin	NCL	9,473,600	0	0	0	0	9,473,600	0	1
		P05387	60S acidic ribosomal protein P2	RPLP2	9,359,400	3,670,500	0	0	0	5,688,900	0	2
Yes		Q06520	Bile salt sulfotransferase	SULT2A1	9,347,800	0	9,347,800	0	0	0	0	1
Yes		P21399	Cytoplasmic aconitate hydratase	ACO1	9,273,300	0	9,273,300	0	0	0	0	1
		P27824-3	Calnexin	CANX	9,232,100	0	0	0	0	9,232,100	0	2
Yes		A0A0C4DGA2	Enoyl-CoA delta isomerase 2, mitochondrial	ECI2	9,217,600	0	9,217,600	0	0	0	0	1
		A0A140TA58	Keratin-associated protein 9-9	KRTAP9-9	9,046,100	0	9,046,100	0	0	0	0	2
Yes		J3KRG2	Gasdermin-A	GSDMA	8,582,300	0	3,803,000	0	0	0	4,779,300	2
Yes		F5GZP6	Liprin-beta-1	PPFIBP1	8,376,800	8,376,800	0	0	0	0	0	1
Yes		P32926	Desmoglein-3	DSG3	8,254,400	0	0	0	0	8,254,400	0	2
Yes		A0A0G2JMB2	Ig alpha-2 chain C region	IGHA2	7,976,600	0	7,976,600	0	0	0	0	5
Yes		M0QY85	Tubulin beta-4A chain;Tubulin beta-4B chain	TUBB4A	7,933,700	0	7,933,700	0	0	0	0	2
Yes		Q14117	Dihydropyrimidinase	DPYS	7,893,100	0	7,893,100	0	0	0	0	3
		E9PE82	Short-chain specific acyl-CoA dehydrogenase, mitochondrial	ACADS	7,313,700	0	7,313,700	0	0	0	0	1
		F2Z2W8	Selenium-binding protein 1	SELENBP1	6,229,500	0	6,229,500	0	0	0	0	2
Yes		Q13011	Delta(3,5)-Delta(2,4)-dienoyl-CoA isomerase, mitochondrial	ECH1	5,760,800	0	5,760,800	0	0	0	0	1
		Q9UBG3	Cornulin	CRNN	5,651,400	0	0	5,651,400	0	0	0	1
		Q08257-2	Quinone oxidoreductase	CRYZ	5,461,300	0	5,461,300	0	0	0	0	1
Yes		P28838-2	Cytosol aminopeptidase	LAP3	5,135,200	0	5,135,200	0	0	0	0	1
Yes		A8MUD9	60S ribosomal protein L7	RPL7	4,984,000	4,984,000	0	0	0	0	0	1
		E9PEB5	Far upstream element-binding protein 1	FUBP1	4,190,600	0	0	4,190,600	0	0	0	2
Yes		P09651	Heterogeneous nuclear ribonucleoprotein A1	HNRNPA1	3,752,800	3,752,800	0	0	0	0	0	2
		P22314-2	Ubiquitin-like modifier-activating enzyme 1	UBA1	3,748,100	0	3,748,100	0	0	0	0	1
Yes		Q14032	Bile acid-CoA:amino acid N-acyltransferase	BAAT	3,451,500	0	3,451,500	0	0	0	0	1
Yes		G3V5K1	Protein transport protein Sec23A	SEC23A	2,912,600	0	0	0	0	2,912,600	0	1
		H7C4C8	T-complex protein 1 subunit theta	CCT8	2,848,600	0	2,848,600	0	0	0	0	1
		E9PBS1	Multifunctional protein ADE2;Phosphoribosylaminoimidazole carboxylase	PAICS	2,615,600	0	2,615,600	0	0	0	0	1

Table 4
Proteins identified in PICALM immunoprecipitations.
Placental extracts U1, R4, Q1, Q4, O1, and N3 were immunoprecipitated in one experiment.

Majority protein ID	Protein	Gene	Total Intensity	Intensity PICALM U1	Intensity PICALM R4	Intensity PICALM Q1	Intensity PICALM Q4	Intensity PICALM O1	Intensity PICALM N3	Peptides
P01857	Ig gamma-1 chain C region	IGHG1	48,398,000,000	197,890,000	13,091,000,000	789,180,000	14,626,000,000	12,977,000,000	6,715,700,000	23
Q13492	Phosphatidylinositol-binding clathrin assembly prote	PICALM	18,858,000,000	901,110,000	5,271,000,000	657,650,000	3,743,800,000	4,066,800,000	4,217,400,000	35
P50995-2	Annexin A11	ANXA11	15,851,000,000	139,870,000	4,529,400,000	433,220,000	3,795,300,000	3,270,300,000	3,682,800,000	37
P20073-2	Annexin A7	ANXA7	9,130,600,000	666,020,000	2,765,200,000	238,940,000	1,535,100,000	2,049,900,000	1,875,500,000	32
A0A286YES1	Ig gamma-3 chain C region	IGHG3	4,336,300,000	33,112,000	1,106,600,000	53,173,000	927,810,000	812,970,000	1,402,600,000	20
A0A7I2V378	Laminin subunit beta-1	LAMB1	3,056,100,000	0	3,056,100,000	0	0	0	0	1
E7EVS6	Actin, cytoplasmic 1;Actin, cytoplasmic 1, N-termina	ACTB	2,600,000,000	74,816,000	1,747,800,000	140,870,000	230,680,000	217,870,000	187,980,000	19
P01834	Ig kappa chain C region	IGKC	2,165,500,000	19,359,000	221,050,000	1,391,900,000	195,150,000	232,100,000	105,920,000	9
A0A286YFJ8	Ig gamma-4 chain C region	IGHG4	1,609,600,000	0	218,830,000	22,468,000	138,990,000	428,050,000	801,270,000	17
P0DOY3	Immunoglobulin lambda constant 3	IGLC3	1,591,000,000	2,681,900	60,706,000	741,050,000	302,850,000	240,510,000	243,250,000	9
A0A286YEY1	Ig alpha-1 chain C region	IGHA1	1,335,500,000	23,359,000	584,930,000	130,660,000	252,550,000	139,020,000	204,990,000	14
Q9Y6R7	IgGFc-binding protein	FCGBP	1,098,700,000	9,162,000	128,730,000	9,654,400	38,684,000	824,150,000	88,293,000	30
P01624	Ig kappa chain V-III region POM	IGKV3D-15	1,060,200,000	0	124,770,000	613,850,000	116,590,000	205,020,000	0	2
P31943	Heterogeneous nuclear ribonucleoprotein H;Heteroc	HNRNPH1	1,047,700,000	10,293,000	217,040,000	24,254,000	289,540,000	295,340,000	211,190,000	11
P08670	Vimentin	VIM	951,490,000	6,378,400	298,510,000	5,089,400	72,211,000	358,520,000	210,780,000	26
H0YEF7	Phosphatidylinositol-binding clathrin assembly prote	PICALM	874,480,000	16,602,000	212,520,000	57,324,000	467,540,000	68,277,000	52,211,000	14
E9PQV5	Coiled-coil domain-containing protein 37	CCDC37	870,490,000	0	0	870,490,000	0	0	0	1
A0A4W8ZXM2	Immunoglobulin heavy variable 3-72	IGHV3-72	808,240,000	44,918,000	282,930,000	12,296,000	137,660,000	204,230,000	126,190,000	3
P05783	Keratin, type I cytoskeletal 18	KRT18	760,020,000	0	231,740,000	8,635,500	185,390,000	187,570,000	146,680,000	17
P07355	Annexin A2;Annexin;Putative annexin A2-like protei	ANXA2	742,370,000	6,496,700	256,760,000	55,166,000	54,726,000	196,500,000	172,720,000	15
P01871	Ig mu chain C region	IGHM	722,270,000	105,950,000	12,770,000	0	95,422,000	155,950,000	352,180,000	18
P31942-2	Heterogeneous nuclear ribonucleoprotein H3	HNRNPH3	681,640,000	0	133,900,000	68,508,000	133,680,000	231,950,000	113,610,000	9
Q8NDC0	MAPK-interacting and spindle-stabilizing protein-like	MAPK1IP1L	497,400,000	15,599,000	39,220,000	243,740,000	59,063,000	32,791,000	106,990,000	1
P51512-2	Matrix metalloproteinase-16	MMP16	429,540,000	0	178,440,000	27,390,000	0	223,720,000	0	1
H0Y8G5	Heterogeneous nuclear ribonucleoprotein D0	HNRNPD	409,120,000	0	31,290,000	27,715,000	95,052,000	151,740,000	103,320,000	5
E7ETU5	RNA-binding motif, single-stranded-interacting prote	RBMS1	391,920,000	5,970,500	68,667,000	17,784,000	143,760,000	44,979,000	110,760,000	7
Q8WZ42	Titin	TTN	387,820,000	0	0	0	75,928,000	210,050,000	101,840,000	1
P02675	Fibrinogen beta chain;Fibrinopeptide B;Fibrinogen b	FGB	348,580,000	0	343,520,000	2,249,600	0	0	2,806,500	16
A0A0D9SF16	Methyl-CpG-binding domain protein 5	MBD5	346,080,000	0	0	0	346,080,000	0	0	1
O14979-3	Heterogeneous nuclear ribonucleoprotein D-like	HNRNPDL	334,140,000	4,097,000	84,425,000	6,682,100	92,722,000	38,095,000	108,120,000	6
P98082	Disabled homolog 2	DAB2	308,620,000	30,904,000	53,571,000	22,044,000	29,573,000	79,395,000	93,129,000	8
A0A286YEY4	Ig gamma-2 chain C region	IGHG2	295,690,000	3,630,700	140,820,000	13,340,000	30,486,000	32,731,000	74,683,000	15
P68871	Hemoglobin subunit beta;LVV-hemorphin-7;Spinorp	HBB	289,630,000	17,601,000	25,216,000	58,392,000	73,808,000	70,816,000	43,798,000	4
P11021	78 kDa glucose-regulated protein	HSPA5	278,720,000	66,634,000	8,224,700	0	44,577,000	12,509,000	146,770,000	14
P04083	Annexin A1;Annexin	ANXA1	264,550,000	7,343,100	128,430,000	38,085,000	12,426,000	24,473,000	53,792,000	13
P01594	Ig kappa variable 1-33	IGKV1-33	258,450,000	2,181,900	6,309,800	167,650,000	34,900,000	29,177,000	18,233,000	2
O43866	CD5 antigen-like	CD5L	258,210,000	0	64,662,000	0	27,301,000	135,430,000	30,812,000	5
F8VV32	Lysozyme;Lysozyme C	LYZ	201,490,000	13,865,000	0	33,772,000	58,974,000	48,689,000	46,193,000	3
P21980-2	Protein-glutamine gamma-glutamyltransferase 2	TGM2	182,780,000	21,051,000	6,206,000	155,520,000	0	0	0	4
P01615	Immunoglobulin kappa varibable 2D-28	IGKV2D-28	157,840,000	0	0	56,727,000	2,124,500	1,244,100	97,746,000	1
Q5T749	Keratinocyte proline-rich protein	KPRP	156,670,000	0	14,536,000	42,583,000	12,523,000	41,980,000	45,045,000	8
Q5T7N2	LINE-1 type transposase domain-containing protein	L1TD1	147,570,000	0	33,515,000	51,668,000	0	0	62,386,000	2
A0A6Q8PGK1	Heat shock protein beta-1	HSPB1	140,170,000	5,102,400	5,175,100	116,740,000	0	9,140,400	4,009,100	4
Q02413	Desmoglein-1	DSG1	139,520,000	4,467,600	13,159,000	21,449,000	21,775,000	52,035,000	26,635,000	9
F8VVB9	Tubulin alpha-1B chain;Tubulin alpha-1A chain;Tubu	TUBA1B	130,470,000	4,960,800	53,076,000	11,800,000	10,998,000	17,150,000	32,482,000	4
A0A6Q8PFJ0	Prelamin-A/C;Lamin-A/C	LMNA	126,810,000	51,770,000	36,048,000	0	9,173,200	5,398,800	24,420,000	7
P69905	Hemoglobin subunit alpha	HBA1	120,580,000	8,819,100	32,928,000	0	19,697,000	31,037,000	28,103,000	3
P02671	Fibrinogen alpha chain;Fibrinopeptide A;Fibrinogen	FGA	119,010,000	5,765,800	89,186,000	13,712,000	0	1,589,500	8,753,800	6
A0A0B4J231	Immunoglobulin lambda-like polypeptide 5;Ig lambd	IGLL5	113,780,000	0	823,960	0	51,884,000	45,566,000	15,503,000	7
Q9HAU0-6	Pleckstrin homology domain-6	PLEKHA6	100,890,000	0	9,826,200	91,063,000	0	0	0	1
Q92945	Far upstream element-binding protein 2	KHSRP	96,813,000	25,823,000	0	0	5,257,900	16,437,000	49,295,000	8
R4GNB1	Acyl-CoA synthetase family member 4	AASDH	94,959,000	0	6,802,400	6,567,300	14,507,000	47,725,000	19,358,000	1
C9JEU5	Fibrinogen gamma chain	FGG	90,470,000	63,046,000	15,905,000	0	10,380,000	0	1,139,700	7
P04406	Glyceraldehyde-3-phosphate dehydrogenase	GAPDH	89,398,000	4,504,400	74,117,000	3,593,000	1,898,700	5,284,800	0	6
K7ERX7	ATP synthase subunit alpha, mitochondrial	ATP5A1	87,648,000	0	49,222,000	0	0	20,992,000	17,434,000	5
E9PPG9	mRNA export factor	RAE1	87,447,000	0	0	0	58,237,000	2,416,200	26,794,000	4
P30101	Protein disulfide-isomerase A3	PDIA3	86,682,000	0	34,607,000	0	0	17,446,000	34,628,000	8
K7EQ02	DAZ-associated protein 1	DAZAP1	83,974,000	0	11,234,000	0	42,826,000	23,140,000	6,774,000	2
Q01469	Fatty acid-binding protein, epidermal	FABP5	79,112,000	0	8,010,100	12,771,000	28,053,000	0	30,278,000	1
Q01085	Nucleolysin TIAR;Nucleolysin TIA-1 isoform p40	TIAL1	77,006,000	0	15,592,000	0	14,334,000	18,441,000	28,639,000	4
P21397-2	Amine oxidase [flavin-containing] A;Amine oxidase	MAOA	76,723,000	0	33,332,000	0	16,437,000	0	26,954,000	4
A6NHN2	Roquin-2	RC3H2	74,367,000	0	0	50,159,000	0	8,880,000	15,328,000	1
P14866	Heterogeneous nuclear ribonucleoprotein L	HNRNPL	68,836,000	0	0	0	0	0	68,836,000	7
Q5JPU3	Pyruvate dehydrogenase E1 component subunit alp	PDHA1	66,908,000	0	12,367,000	0	31,262,000	13,254,000	10,024,000	3
Q8IUC1	Keratin-associated protein 11-1	KRTAP11-1	65,493,000	0	18,492,000	28,950,000	0	18,051,000	0	3
Q5JP53	Tubulin beta chain	TUBB	64,164,000	3,856,400	37,532,000	2,310,200	7,223,200	4,449,300	8,792,800	3
C9J2I0	Arf-GAP domain and FG repeat-containing protein 1	AGFG1	59,976,000	4,759,100	12,457,000	0	0	18,719,000	24,041,000	1
P19474	E3 ubiquitin-protein ligase TRIM21	TRIM21	58,811,000	0	6,681,800	0	0	29,267,000	22,862,000	5
D6R9P3	Heterogeneous nuclear ribonucleoprotein A/B	HNRNPAB	58,548,000	0	7,571,700	2,186,500	9,640,700	28,004,000	11,145,000	4
Q5T1M5	FK506-binding protein 15	FKBP15	58,396,000	11,484,000	0	0	14,598,000	0	32,314,000	4
E9PGY2	Dynein assembly factor 5, axonemal	DNAAF5	56,016,000	0	0	0	20,626,000	25,326,000	10,064,000	1
P63261	Actin, cytoplasmic 2;Actin, cytoplasmic 2, N-termina	ACTG1	55,103,000	0	29,965,000	6,910,800	6,077,800	5,127,100	7,022,400	19
Q9NZT1	Calmodulin-like protein 5	CALML5	54,136,000	0	7,928,200	10,694,000	0	27,905,000	7,608,500	1
C9JZN1	Guanine nucleotide-binding protein G(I)/G(S)/G(T) s	GNB2	53,184,000	0	0	45,048,000	8,135,900	0	0	4
A0A7I2YQK6	60 kDa heat shock protein, mitochondrial	HSPD1	50,218,000	1,514,400	15,195,000	0	15,571,000	6,895,200	11,042,000	3
P31040-2	Succinate dehydrogenase [ubiquinone] flavoprotein	SDHA	49,094,000	0	23,561,000	0	3,205,300	15,958,000	6,369,600	5
A0A7I2V2R3	Heterogeneous nuclear ribonucleoprotein A3	HNRNPA3	48,903,000	0	15,655,000	0	7,296,200	11,237,000	14,714,000	2
Q8IWB6-3	Inactive serine/threonine-protein kinase TEX14	TEX14	48,249,000	0	0	0	0	21,743,000	26,507,000	1
P68371	Tubulin beta-4B chain;Tubulin beta-4A chain	TUBB4B	48,032,000	0	39,150,000	0	4,137,600	0	4,744,800	3
H0YFX9	Histone H2A;Histone H2A type 1-J;Histone H2A type	H2AFJ	45,901,000	12,453,000	7,861,100	20,288,000	0	0	5,298,900	1
Q8IUC0	Keratin-associated protein 13-1;Keratin-associated p	KRTAP13-1	44,512,000	0	7,315,500	7,365,500	0	29,831,000	0	1
A0A087WVQ6	Clathrin heavy chain;Clathrin heavy chain 1	CLTC	44,504,000	21,103,000	0	0	0	0	23,400,000	3
P63267	Actin, gamma-enteric smooth muscle;Actin, alpha s	ACTG2	44,025,000	0	23,112,000	0	0	8,310,000	12,603,000	12
H7BZJ3	Protein disulfide-isomerase A3	PDIA3	43,257,000	4,680,500	27,448,000	0	0	11,128,000	0	3
A0A0B4J1V1	Ig heavy chain V-III region JON;Ig heavy chain V-III	IGHV3-21	43,147,000	0	9,064,600	2,411,600	0	22,858,000	8,812,900	2
H7C582	Integrator complex subunit 1	INTS1	42,661,000	0	0	42,661,000	0	0	0	1
Q9BYR6	Keratin-associated protein 3-3	KRTAP3-3	40,458,000	0	40,458,000	0	0	0	0	2
Q13151	Heterogeneous nuclear ribonucleoprotein A0	HNRNPA0	39,870,000	0	0	5,577,800	21,067,000	9,442,300	3,783,300	1
H0Y6B2	Sushi domain-containing protein 1	SUSD1	38,095,000	0	0	22,678,000	8,950,800	6,466,400	0	1
A0A1B0GVP4	Ligand-dependent nuclear receptor corepressor	LCORL	36,335,000	0	16,645,000	0	9,411,000	0	10,278,000	1
P14923	Junction plakoglobin	JUP	35,503,000	0	0	4,915,000	0	21,240,000	9,347,600	6
P01023	Alpha-2-macroglobulin	A2M	35,281,000	0	0	0	18,291,000	0	16,990,000	2
A0A7I2V3H3	Putative elongation factor 1-alpha-like 3;Elongation	EEF1A1	34,691,000	0	20,615,000	0	0	6,899,500	7,176,500	3
I3L0W5	14-3-3 protein epsilon	YWHAE	34,151,000	0	4,124,200	16,649,000	3,202,500	4,882,900	5,292,400	1
P02787	Serotransferrin	TF	33,379,000	5,509,000	0	4,698,000	8,538,800	1,682,500	12,951,000	3
Q08554-2	Desmocollin-1	DSC1	31,458,000	0	0	2,709,100	0	22,304,000	6,444,900	2
E5RGE1	14-3-3 protein zeta/delta	YWHAZ	31,118,000	0	0	31,118,000	0	0	0	2
P06576	ATP synthase subunit beta, mitochondrial;ATP synt	ATP5B	31,113,000	0	31,113,000	0	0	0	0	3
P17931	Galectin-3;Galectin	LGALS3	30,883,000	0	0	30,883,000	0	0	0	3
C9JA05	Immunoglobulin J chain	JCHAIN	29,005,000	6,597,900	8,495,000	8,405,600	0	0	5,506,600	1

A0A0G2JRN3	Alpha-1-antitrypsin;Short peptide from AAT	SERPINA1	28,649,000	1,644,400	2,510,900	10,667,000	8,084,300	1,831,300	3,911,300	2
P31025	Lipocalin-1;Putative lipocalin 1-like protein 1	LCN1	28,552,000	0	0	2,845,200	0	6,027,100	19,679,000	2
P07237	Protein disulfide-isomerase	P4HB	28,383,000	0	18,574,000	0	0	4,970,100	4,837,900	3
H0Y5H6	Ubiquitin-associated protein 2-like	UBAP2L	25,709,000	0	0	0	0	8,179,400	17,530,000	1
Q96CBB	Integrator complex subunit 12	INTS12	25,627,000	0	0	0	0	25,627,000	0	1
S4R460	Ig heavy chain V-III region BRO region DOB	IGHV3OR16-9	24,932,000	0	13,396,000	0	0	6,415,600	5,120,200	3
Q5JTQ6	Alpha-catulin	CTNNAL1	23,896,000	0	0	17,301,000	0	6,594,900	0	1
P07910	Heterogeneous nuclear ribonucleoproteins C1/C2	HNRNPC	23,699,000	0	15,502,000	0	8,197,000	0	0	2
E9PEB5	Far upstream element-binding protein 1	FUBP1	23,687,000	0	0	0	0	20,589,000	3,098,200	3
Q07065	Cytoskeleton-associated protein 4	CKAP4	23,211,000	0	10,484,000	0	0	7,232,200	5,495,600	5
Q9UBG3	Cornulin	CRNN	23,063,000	0	0	23,063,000	0	0	0	3
A0A0C4DH31	Ig heavy chain V-I region V35	IGHV1-18	22,114,000	0	7,494,400	0	0	8,305,200	6,314,800	2
P04843	Dolichyl-diphosphooligosaccharide--protein glycosyl	RPN1	21,647,000	0	6,872,300	0	2,481,300	3,898,300	8,395,600	3
A0A0G2JIW1	Heat shock 70 kDa protein 1A;Heat shock 70 kDa pr	HSPA1A	21,113,000	1,946,300	16,283,000	0	0	2,883,300	0	4
P11142-2	Heat shock cognate 71 kDa protein	HSPA8	20,977,000	14,054,000	0	1,367,200	1,373,400	4,182,300	0	6
Q15365	Poly(rC)-binding protein 1;Poly(rC)-binding protein 3	PCBP1	19,851,000	0	8,243,700	0	0	7,620,100	3,987,300	4
P29401	Transketolase	TKT	19,791,000	2,617,800	17,173,000	0	0	0	0	3
P11166	Solute carrier family 2, facilitated glucose transporte	SLC2A1	19,512,000	0	19,512,000	0	0	0	0	1
M0R3F1	Heterogeneous nuclear ribonucleoprotein U-like pro	HNRNPUL1	19,055,000	0	0	0	0	0	19,055,000	4
P69892	Hemoglobin subunit gamma-2;Hemoglobin subunit g	HBG2	18,869,000	8,500,000	10,370,000	0	0	0	0	4
A0A7I2V4I6	Heterogeneous nuclear ribonucleoproteins A2/B1	HNRNPA2B1	18,704,000	0	0	0	0	12,162,000	6,541,300	4
A0A5F9ZH78	Arginase-1	ARG1	17,366,000	0	4,850,200	0	0	5,206,700	7,309,200	2
J3KPS3	Fructose-bisphosphate aldolase;Fructose-bisphosph	ALDOA	16,868,000	0	16,868,000	0	0	0	0	3
A0A7I2YQY2	Heterogeneous nuclear ribonucleoprotein A1;Heterc	HNRNPA1	16,360,000	2,149,600	2,573,000	0	7,993,500	3,644,300	0	1
Q9BYQ3	Keratin-associated protein 9-3	KRTAP9-3	16,191,000	0	16,191,000	0	0	0	0	2
Q9BS26	Endoplasmic reticulum resident protein 44	ERP44	16,007,000	0	7,136,300	0	0	7,435,300	1,435,800	3
P15924-2	Desmoplakin	DSP	15,924,000	0	0	6,126,800	0	9,797,400	0	5
P05109	Protein S100-A8;Protein S100-A8, N-terminally proc	S100A8	15,760,000	828,670	4,227,300	10,704,000	0	0	0	1
E9PMZ8	T-lymphoma invasion and metastasis-inducing prote	TIAM2	15,463,000	0	0	15,463,000	0	0	0	1
P01833	Polymeric immunoglobulin receptor;Secretory comp	PIGR	15,458,000	0	11,036,000	0	0	3,208,000	1,214,700	3
H3BQZ7	Heterogeneous nuclear ribonucleoprotein U-like pro	HNRNPUL2-BSCL2	15,173,000	1,669,300	0	0	0	0	13,503,000	1
P55795	Heterogeneous nuclear ribonucleoprotein H2	HNRNPH2	14,987,000	0	4,489,200	0	1,825,300	5,079,900	3,592,900	5
A0A0G2JPP1	Keratin-associated protein 4-8	KRTAP4-8	14,521,000	0	14,521,000	0	0	0	0	1
E9PHT9	Annexin;Annexin A5	ANXA5	12,946,000	0	0	12,946,000	0	0	0	2
A0A6Q8PF87	Apoptosis-inducing factor 1, mitochondrial	AIFM1	12,539,000	0	12,539,000	0	0	0	0	1
M0R1R1	Serine/threonine-protein kinase PAK 4	PAK4	12,509,000	0	0	0	0	0	12,509,000	1
P04040	Catalase	CAT	12,392,000	0	3,717,800	1,498,500	0	3,932,900	3,243,300	1
A0A140TA58	Keratin-associated protein 9-9;Keratin-associated pr	KRTAP9-9	12,125,000	0	12,125,000	0	0	0	0	2
A0A0A0MS98	Band 3 anion transport protein	SLC4A1	12,063,000	2,108,100	0	0	3,363,800	0	6,591,400	1
P0DP03	Ig heavy chain V-III region CAM;Ig heavy chain V-II	IGHV3-23	11,962,000	0	0	0	0	7,237,200	4,724,800	1
P81605	Dermcidin;Survival-promoting peptide;DCD-1	DCD	11,727,000	0	0	7,387,600	0	4,338,900	0	2
H0YFA4	Cysteine-rich protein 2	CRIP2	11,648,000	0	0	7,587,800	4,060,200	0	0	2
A0A3B3ITD8	Nuclear pore complex protein Nup98-Nup96;Nuclea	NUP98	11,301,000	0	0	0	11,301,000	0	0	2
P14625	Endoplasmin	HSP90B1	11,207,000	11,207,000	0	0	0	0	0	4
Q96PK6	RNA-binding protein 14	RBM14	11,150,000	0	0	0	7,074,900	0	4,075,400	1
E7ENL6	Collagen alpha-3(VI) chain	COL6A3	10,671,000	10,671,000	0	0	0	0	0	3
F8WBE5	Transferrin receptor protein 1;Transferrin receptor p	TFRC	10,642,000	3,853,100	0	0	0	0	6,788,600	1
A0A0G2JMB2	Ig alpha-2 chain C region	IGHA2	10,360,000	0	5,177,500	0	0	2,870,900	2,311,700	9
A0A7I2YQJ0	Transitional endoplasmic reticulum ATPase	VCP	10,078,000	10,078,000	0	0	0	0	0	2
B3KVK2	Guanine nucleotide-binding protein G(I)/G(S)/G(T) s	GNB1	9,941,900	0	0	6,870,800	0	3,071,100	0	1
Q9BYR3	Keratin-associated protein 4-4	KRTAP4-4	9,925,900	0	9,925,900	0	0	0	0	1
P52597	Heterogeneous nuclear ribonucleoprotein F;Heterog	HNRNPF	9,850,000	0	3,857,200	0	0	0	5,992,800	3
P01024	Complement C3;Complement C3 beta chain;C3-bet	C3	9,848,400	0	9,848,400	0	0	0	0	2
P80723-2	Brain acid soluble protein 1	BASP1	9,527,100	0	0	0	0	0	9,527,100	2
F8W1T6	RNA-binding motif, single-stranded-interacting prote	RBMS2	9,438,700	0	0	0	0	0	9,438,700	4
P31944	Caspase-14;Caspase-14 subunit p17, mature form;(	CASP14	9,239,700	0	0	5,161,200	0	0	4,078,600	1
P0DP08	Ig heavy chain V-II region NEWM;Ig heavy chain V-	IGHV4-4	9,180,400	0	0	0	0	5,589,100	3,591,300	1
H3BU13	Pyruvate kinase;Pyruvate kinase PKM	PKM	9,106,300	0	9,106,300	0	0	0	0	1
F8WEU2	ATP-dependent 6-phosphofructokinase, liver type	PFKL	9,083,300	9,083,300	0	0	0	0	0	1
A0A0C4DH25	Immunoglobulin kappa variable 3D-20	IGKV3D-20	8,934,800	0	0	0	0	0	8,934,800	1
P52907	F-actin-capping protein subunit alpha-1	CAPZA1	8,912,600	0	8,912,600	0	0	0	0	1
I3L1P8	Mitochondrial 2-oxoglutarate/malate carrier protein	SLC25A11	8,767,800	0	0	8,767,800	0	0	0	1
B4E3S0	Coronin;Coronin-1C	CORO1C	8,702,200	0	4,567,500	0	0	4,134,700	0	1
F8W6D9	Sentrin-specific protease 6	SENP6	8,679,600	0	0	0	0	0	8,679,600	2
P36957-2	Dihydrolipoyllysine-residue succinyltransferase com	DLST	8,276,700	0	5,934,900	0	0	0	2,341,800	1
P31930	Cytochrome b-c1 complex subunit 1, mitochondrial	UQCRC1	8,234,200	0	3,957,100	0	0	0	4,277,000	2
P02808	Statherin	STATH	8,064,100	0	0	8,064,100	0	0	0	1
P16403	Histone H1.2;Histone H1.3	HIST1H1C	7,889,100	0	2,483,600	5,405,500	0	0	0	3
K7EMF8	Very long-chain specific acyl-CoA dehydrogenase, r	ACADVL	7,844,000	0	7,844,000	0	0	0	0	1
C9JP00	Muscleblind-like protein 1	MBNL1	7,830,800	0	0	0	0	2,369,000	5,461,800	1
A0A6I8PIN8	F-actin-capping protein subunit beta	CAPZB	7,662,300	0	0	6,785,600	0	876,710	0	1
O95205	Muscleblind-like protein 2	MBLL	7,485,300	0	0	0	0	1,647,200	5,838,000	1
A0A590UK99	Deleted in malignant brain tumors 1 protein	DMBT1	7,481,500	1,749,100	0	0	3,277,000	0	2,455,300	1
P01766	Ig heavy chain V-III region BRO	IGHV3-13	6,767,800	0	0	0	0	4,376,000	2,391,900	2
J3KSH9	Integrin beta-4	ITGB4	6,700,000	0	0	0	0	0	6,700,000	1
P55268	Laminin subunit beta-2	LAMB2	6,456,200	6,456,200	0	0	0	0	0	2
P47929	Galectin-7	LGALS7	6,362,600	0	0	1,822,500	0	0	4,540,100	1
E9PFG7	2-oxoglutarate dehydrogenase, mitochondrial	OGDH	6,288,400	6,288,400	0	0	0	0	0	1
E5RK69	Annexin;Annexin A6	ANXA6	6,072,900	0	0	0	0	0	6,072,900	2
E7EQB2	Lactotransferrin;Lactoferricin-H;Kaliocin-1;Lactoferr	LTF	6,032,800	0	3,762,400	2,270,400	0	0	0	3
E9PRN7	3 beta-hydroxysteroid dehydrogenase/Delta 5-->4-is	HSD3B1	5,960,500	0	5,960,500	0	0	0	0	1
P17661	Desmin	DES	5,939,400	0	5,939,400	0	0	0	0	5
A0A087X0S5	Collagen alpha-1(VI) chain	COL6A1	5,903,600	5,903,600	0	0	0	0	0	2
P0DP09	Immunoglobulin kappa variable 1-13	IGKV1D-13	5,730,000	0	0	5,730,000	0	0	0	1
P62805	Histone H4	HIST1H4A	5,728,200	0	2,222,200	0	0	3,506,000	0	2
Q8WVV4	Protein POF1B	POF1B	5,534,300	0	0	0	0	5,534,300	0	1
A0A1W2PP22	Heterogeneous nuclear ribonucleoprotein U	HNRNPU	5,391,800	0	0	0	0	0	5,391,800	1
Q9BW30	Tubulin polymerization-promoting protein family me	TPPP3	5,092,600	5,092,600	0	0	0	0	0	1
P08572	Collagen alpha-2(IV) chain;Canstatin	COL4A2	5,034,400	5,034,400	0	0	0	0	0	1
A0A075B6K5	Ig lambda chain V-III region LOI	IGLV3-9	5,025,200	0	0	2,660,600	0	0	2,364,600	1
H0YJL6	Ena/VASP-like protein	EVL	4,998,300	0	0	4,998,300	0	0	0	1
P59666	Neutrophil defensin 3;HP 3-56;Neutrophil defensin 2	DEFA3	4,545,800	0	0	0	0	4,545,800	0	1
Q9NQP5	Coagulation factor XIII A chain	F13A1	4,473,400	4,473,400	0	0	0	0	0	2
E9PS23	Cofilin-1	CFL1	4,289,600	0	2,251,300	0	2,038,300	0	0	2
B4DU11	Estradiol 17-beta-dehydrogenase 1	HSD17B1	4,274,500	0	2,367,500	1,907,000	0	0	0	1
C9J9S3	Serine/threonine-protein phosphatase;Serine/threon	PPP1CB	4,214,000	0	0	1,916,400	0	0	2,297,500	1
C9JHS9	Vigilin	HDLBP	4,198,300	0	0	0	1,536,900	0	2,661,400	1
P05187	Alkaline phosphatase, placental type;Alkaline phosp	ALPP	4,169,700	0	0	0	0	0	4,169,700	2
F8WEW2	Actin-related protein 3	ACTR3	4,132,700	0	4,132,700	0	0	0	0	1
Q9ULV0	Unconventional myosin-Vb	MYO5B	4,073,000	2,220,100	0	0	1,853,000	0	0	2
J3QSA3	Ubiquitin-40S ribosomal protein S27a;Ubiquitin;40S	UBB	4,045,100	1,288,700	0	0	0	0	2,756,400	1
B8ZZ51	Malate dehydrogenase, cytoplasmic	MDH1	4,029,700	0	0	4,029,700	0	0	0	1
E9PQ34	Serpin H1	SERPINH1	4,018,600	0	4,018,600	0	0	0	0	1
I3L245	Nuclear pore complex protein Nup88	NUP88	3,921,000	0	0	0	0	0	3,921,000	1
Q13263-2	Transcription intermediary factor 1-beta	TRIM28	3,569,200	3,569,200	0	0	0	0	0	1
Q9HD89	Resistin	RETN	3,487,400	0	0	2,254,600	0	1,232,800	0	1
Q9GZM7-3	Tubulointerstitial nephritis antigen-like	TINAGL1	3,481,600	0	3,481,600	0	0	0	0	1

P27824-3	Calnexin	CANX	3,444,400	0	0	0	0	0	3,444,400	1
A0A3B3ISA6	Complement C4-A;Complement C4 beta chain;Com	C4B	3,381,500	0	0	0	0	0	3,381,500	1
A6NCI4-3	von Willebrand factor A domain-containing protein 3	VWA3A	3,185,200	0	0	0	3,185,200	0	0	1
Q8WV48-5	Coiled-coil domain-containing protein 107	CCDC107	3,057,000	0	0	3,057,000	0	0	0	1
Q00013-2	55 kDa erythrocyte membrane protein	MPP1	2,911,300	0	2,911,300	0	0	0	0	1
Q14677	Clathrin interactor 1	CLINT1	2,901,400	0	0	0	0	2,901,400	0	1
A6NHR2	39S ribosomal protein L37, mitochondrial	MRPL37	2,898,500	0	0	0	0	2,898,500	0	1
P82663-3	8S ribosomal protein S25, mitochondrial	MRPS25	2,580,800	0	0	0	0	0	2,580,800	1
H7C4C8	T-complex protein 1 subunit theta	CCT8	2,560,000	0	2,560,000	0	0	0	0	1
P16401	Histone H1.5	HIST1H1B	2,527,600	0	0	2,527,600	0	0	0	1
A0A3B3ITI4	Stress-70 protein, mitochondrial	HSPA9	2,413,000	2,413,000	0	0	0	0	0	1
Q8TE68	Epidermal growth factor receptor kinase substrate 8	EPS8L1	2,165,700	2,165,700	0	0	0	0	0	1
Q8TDL5	BPI fold-containing family B member 1	BPIFB1	2,146,600	0	0	0	0	1,170,700	975,880	1
P31146	Coronin-1A	CORO1A	2,123,800	0	0	0	0	2,123,800	0	1
E9PSE0	MAP kinase-interacting S/T-protein kinase 1	MKNK1	1,976,500	0	0	0	1,976,500	0	0	1
A0A1X7SBZ2	Probable ATP-dependent RNA helicase DDX17	DDX17	1,903,300	0	0	0	1,903,300	0	0	1
M0R1B5	Acetolactate synthase-like protein	ILVBL	1,702,000	0	1,702,000	0	0	0	0	1
M0QX10	Nuclear pore glycoprotein p62	NUP62	1,380,100	0	0	0	0	0	1,380,100	1
P09525-2	Annexin A4	ANXA4	1,341,500	0	0	1,341,500	0	0	0	1
O15400-2	Syntaxin-7	STX7	1,329,200	1,329,200	0	0	0	0	0	1
H3BS21	Haptoglobin;Haptoglobin alpha chain;Haptoglobin b	HP	1,311,500	0	1,311,500	0	0	0	0	2
U3KQK0	Histone H2B;Histone H2B type 1-L;Histone H2B typ	HIST1H2BN	1,266,700	0	1,266,700	0	0	0	0	1
K7EJ44	Profilin-1	PFN1	1,249,400	0	0	0	0	1,249,400	0	1
K7EK06	Phenylalanine--tRNA ligase alpha subunit	FARSA	1,246,700	0	1,246,700	0	0	0	0	1
P10412	Histone H1.4	HIST1H1E	1,033,200	0	0	1,033,200	0	0	0	3
A0A087WUX6	Proteasomal ubiquitin receptor ADRM1	ADRM1	993,900	0	993,900	0	0	0	0	1
B1AUU8	Epidermal growth factor receptor substrate 15	EPS15	797,470	797,470	0	0	0	0	0	1
O76041	Nebulette	NEBL	651,720	0	0	0	0	0	651,720	1

Table 5
Protein levels of MDMX (A), PICALM (B), OT-R (C) and V1aR (D) in 44 placental extracts.
MDMX and PICALM values are relative to extract Q1, and OT-R and V1aR values relative to sample V1. Replicate and mean values are shown.

A

MDMX % of Q1								
Patient								MEAN
H1		128.4	116.9	116.5	78.2	116.9	141.1	116.3
H2			19.1	60.8	32.5	18.9	16.0	29.5
H3			8.3	9.0	26.3	17.4	4.2	13.0
I-1		128.8	209.0	114.6	222.2	102.8	146.1	153.9
I-2				57.1	75.4	106.7	51.6	72.7
I-3		123.6	72.5	77.1	84.1	37.8	71.7	77.8
I-4	136.6	88.3	135.7	81.5	58.8	133.1	103.0	94.1
J-1					118.1	130.2	119.1	122.5
J-2					92.9	56.5	58.9	69.5
J-3					84.0	60.8	66.2	70.3
L1			46.6	61.1	72.0	35.8	41.9	51.5
L2					46.3	55.2	31.0	44.2
L3					72.1	69.1	47.5	62.9
L4				11.9	23.9	16.2	8.9	16.3
M1				57.2	57.5	29.7	62.4	51.7
M3						76.8	37.2	57.0
M4			60.1	40.8	42.1	68.7	52.9	
N1		60.1	40.8	42.1	68.7	101.6	101.6	115.5
N2		10.2	31.0	45.5	58.0	58.2	6.6	34.9
N3			75.3	167.8	85.8	80.4	68.0	95.5
N4				55.9	52.5	60.4	48.7	54.4
O1			57.5	34.5	46.1	101.6	49.8	57.9
O2				78.4	82.8	34.4	85.6	70.3
O3		77.3	58.3	22.3	42.5	11.0	8.6	36.7
O4			72.9	24.9	34.5	25.4	111.4	53.8
O5					244.4	229.0	145.1	206.1
O7					167.2	179.6	163.3	170.0
Q1	100.0	100.0	100.0	100.0	100.0	100.0	100.0	100.0
Q2		199.7	169.8	211.0	205.4	156.5	144.9	181.2
Q3		90.9	90.1	76.0	75.8	74.2	88.5	82.6
Q4		50.5	86.2	28.6	45.5	62.7	31.5	50.8
R3		28.2	99.6	57.5	20.0	60.2	77.0	54.5
R4			126.7	116.9	93.8	58.6	109.0	101.3
R5					33.6	79.8	48.8	54.1
S1					207.4	128.9	151.4	162.6
S2					202.5	107.1	110.4	140.0
T1				124.8	161.9	155.5	124.5	141.7
T2					115.0	91.3	82.9	96.4
U1					119.7	87.7	103.7	103.7
U2					163.0	175.0	122.9	153.6
V1					75.4	71.1	21.0	55.9
V2					92.8	72.9	99.0	88.2
W1					99.2	72.4	84.0	85.2
W2					261.5	197.7	173.8	211.0

B

PICALM % of Q1								
Patient								MEAN
H1					21.3	31.8	34.7	29.3
H2					32.8	31.2	55.6	39.9
H3				126.3	114.0	164.0	120.6	131.2
I-1						59.9	77.3	68.6
I-2						64.9	78.8	71.8
I-3					31.5	28.4	10.5	23.4
I-4			15.7	14.2	2.0	7.1	2.9	8.4
J-1	85.4	122.8	105.8	72.0	126.2	127.1	103.0	106.0
J-2				30.9	21.9	21.6	41.0	28.8
J-3			93.6	118.5	113.6	166.7	101.5	118.8
L1				95.2	122.6	227.4	127.2	143.1
L2					60.2	58.9	91.8	70.3
L3				100.2	102.2	142.1	94.5	109.7
L4					77.4	92.1	115.4	95.0
M1				167.9	156.1	131.4	159.8	153.8
M3					4.6	4.3	4.2	4.4
M4					106.1	78.3	104.0	96.1
N1					42.5	34.5	80.1	52.4
N2				50.7	49.6	87.1	62.5	62.5
N3					72.7	69.7	77.3	73.2
N4				45.2	42.4	43.5	51.3	45.6
O1				41.5	43.8	35.3	11.4	33.0
O2				96.6	42.9	109.5	117.3	91.6
O3				53.7	66.5	45.6	151.3	79.3
O4				157.1	63.8	54.9	188.3	116.0
O5						153.7	134.3	144.0
O7						142.0	216.5	179.2
Q1	100.0	100.0	100.0	100.0	100.0	100.0	100.0	100.0
Q2			166.3	186.0	176.6	138.0	140.5	161.5
Q3					115.3	138.5	138.3	130.7
Q4						198.8	188.6	193.7
R3					95.8	208.0	244.3	182.7
R4					83.7	64.9	42.0	63.5
R5						205.3	274.9	240.1
S1				150.9	115.3	97.3	186.9	137.6
S2				192.9	181.9	233.0	216.2	206.0
T1						173.3	169.2	171.3
T2				226.5	181.1	130.8	219.4	189.5
U1					104.2	165.3	217.6	162.3
U2					119.8	122.6	218.0	153.5
V1					147.0	207.3	288.0	214.1
V2					225.3	215.0	251.0	230.4
W1				129.3	200.6	263.6	152.0	186.4
W2					125.9	125.7	184.5	145.4

C

OT-R % of V1						
Patient						MEAN
H1			31.9	32.6	34.9	33.1
H2			44.6	47.5	*54.3*	48.8
H3		52.7	53.5	66.5	64.1	59.2
I-1			45.9	44.5	43.4	44.6
I-2	56.0	64.8	43.0	40.5	*51.5*	*35.1*	48.5
I-3			43.3	42.7	29.3	32.2	36.9
I-4				24.3	24.4	18.2	22.3
J-1			78.0	66.2	80.9	*83.8*	77.2
J-2				64.8	55.1	*44.8*	54.9
J-3		74.2	64.0	62.4	73.1	*87.1*	72.2
L1					85.6	*77.4*	81.5
L2			84.2	80.5	86.5	93.2	86.1
L3			77.8	72.1	61.6	81.6	73.3
L4			79.0	70.5	82.2	*82.3*	78.5
M1				43.2	37.9	41.8	41.0
M3			22.0	22.3	21.1	18.9	21.1
M4				57.8	42.3	45.7	48.6
N1			73.6	61.4	84.1	88.0	76.8
N2				75.7	80.6	78.6	78.3
N3				102.2	95.9	108.0	102.0
N4			56.3	55.7	*76.5*	55.9	61.1
O1			40.0	61.6	46.1	43.1	47.7
O2				81.7	85.7	90.1	85.8
O3			67.0	77.0	90.8	93.7	82.1
O4		80.5	81.2	84.9	93.8	97.9	87.7
O5			100.2	85.9	89.7	95.0	92.7
O7				67.1	71.1	*79.1*	72.4
Q1			83.6	76.2	85.0	99.4	86.1
Q2			93.4	102.4	103.9	119.0	104.7
Q3	69.1	65.4	91.4	67.6	71.4	74.1	73.2
Q4				77.3	*70.4*	*82.6*	76.8
R3				117.8	101.2	*107.9*	109.0
R4			87.2	75.4	84.6	97.8	86.2
R5			80.3	79.4	83.4	*122.1*	91.3
S1			106.7	99.1	116.1	*118.3*	110.6
S2		102.9	89.2	116.9	119.2	116.5	108.9
T1		120.1	104.1	*113.7*	129.4	119.7	117.4
T2			118.7	*112.9*	*127.8*	122.0	120.4
U1		84.5	66.8	*75.1*	126.9	103.6	91.4
U2			107.0	101.2	*117.9*	112.0	109.5
V1	100.0	100.0	100.0	100.0	100.0	100.0	100.0
V2		111.0	100.6	104.7	*117.9*	114.4	109.7
W1			102.0	113.8	121.5	*118.2*	113.9
W2		92.1	107.5	101.6	*115.0*	96.9	102.6

D

V1aR % of V1						
Patient						MEAN
H1				27.0	46.7	36.9
H2			51.5	62.7	70.4	61.5
H3				73.0	73.8	73.4
I-1			77.8	61.7	72.6	70.7
I-2				51.4	56.5	53.9
I-3				58.5	69.7	64.1
I-4				56.4	67.2	61.8
J-1		41.2	43.3	54.9	67.6	51.7
J-2				55.3	42.6	48.9
J-3			56.8	61.7	75.2	64.5
L1		43.6	57.5	63.6	67.0	57.9
L2			80.4	76.0	91.4	82.6
L3			87.9	87.8	98.6	91.5
L4			87.2	68.3	75.9	77.1
M1			76.4	90.0	87.7	84.7
M3			118.5	80.7	108.1	102.4
M4		43.9	60.7	66.4	63.1	58.5
N1			67.4	79.6	76.5	74.5
N2		65.5	58.4	72.5	81.7	69.5
N3			71.8	70.9	85.2	75.9
N4	30.3	16.9	46.6	46.1	31.8	34.3
O1			83.8	60.3	76.4	73.5
O2			75.0	72.3	77.4	74.9
O3			74.5	72.2	79.3	75.3
O4			69.9	51.4	70.2	63.8
O5	49.8	93.2	68.2	85.9	73.6	74.2
O7			83.8	73.3	88.3	81.8
Q1		98.8	62.7	98.3	79.8	84.9
Q2	91.1	77.3	102.2	99.7	100.8	94.2
Q3			71.5	62.4	66.2	66.7
Q4	68.5	60.6	96.9	78.0	73.7	82.9	76.7
R3	33.1	64.9	74.7	51.4	74.6	59.7
R4		98.1	81.9	92.3	103.7	94.0
R5		66.6	42.8	72.9	68.6	62.7
S1			95.2	105.6	93.2	98.0
S2			78.4	86.0	99.7	88.0
T1	129.5	91.3	102.2	77.7	100.1	100.2
T2	69.6	73.3	93.1	84.7	95.1	83.2
U1		63.1	51.1	77.3	65.0	64.1
U2			78.1	79.5	87.6	81.7
V1	100.0	100.0	100.0	100.0	100.0	100.0	100.0
V2			93.0	98.1	107.1	99.4
W1		105.0	94.9	91.2	92.2	95.8
W2	111.0	62.2	103.1	99.2	75.4	90.2

Table 6

Regression coefficients from univariable analysis of MDMX protein band intensity (relative to internal reference individual Q1)

Covariate	Regression Coefficient (95% CI)	P-value
Age	1.94 (-0.79, 4.67)	0.17
Gravidity	9.66 (3.59, 15.70)	$3x10^{-3}$
Gestational Age	-1.79 (-12.40, 8.86)	0.74
Body Mass Index in Labor and Delivery Suite	0.97 (-0.18, 2.13)	0.11
Race		
White	(REF)	
Black	22.20 (-14.85, 59.26)	0.24
Asian	-32.49 (-133.62, 68.64)	0.53
Unknown	-3.74 (-77.21, 69.73)	0.92
Hispanic	-0.66 (-37.72, 36.39)	0.97
Preeclampsia		
No	(REF)	
Yes	-44.13 (-71.63, -16.64)	$3x10^{-3}$
Diabetes		
No	(REF)	
Type II	47.63 (14.27, 90.00)	$8x10^{-3}$
GDM	47.91 (5.51, 90.32)	0.03
Mode of Delivery		
SVD	(REF)	
CD prior to onset of Labor	56.16 (24.13, 88.18)	$1x10^{-3}$
CD after onset of Labor	34.80 (-4.46, 74.07)	0.09
VBAC	5.55 (-85.70, 96.79)	0.91
Neonate Sex		
Female	(REF)	
Male	5.04 (-24.35, 34.43)	0.74
Neonatal Weight (g)	0.03 (0.01, 0.06)	$3x10^{-3}$

Table 7

Regression coefficients from univariable analysis of PICALM protein band intensity (relative to internal reference individual Q1)

Covariate	Regression Coefficient (95% CI)	P-value
Age	3.68 (0.28, 7.08)	0.04
Gravidity	7.64 (-0.68, 15.95)	0.08
Gestational Age	6.88 (-6.62, 20.37)	0.32
Body Mass Index in Labor and Delivery Suite	2.06 (0.66, 3.45)	$6x10^{-3}$
Race		
White	(REF)	
Black	17.33 (-24.11, 60.77)	0.44
Asian	17.49 (-101.07, 136.05)	0.77
Unknown	-75.81 (-161.94, 10.32)	0.09
Hispanic	-46.39 (-89.82, -2.95)	0.04
Preeclampsia		
No	(REF)	
Yes	-35.60 (-73.25, 2.04)	0.07
Diabetes		
No	(REF)	
Type II	23.28 (-23.57, 70.13)	0.34
GDM	38.05 (-21.50, 97.60)	0.22
Mode of Delivery		
SVD	(REF)	
CD prior to onset of Labor	59.96 (19.24, 100.68)	$6x10^{-3}$
CD after onset of Labor	5.69 (-44.23, 55.62)	0.82
VBAC	-50.27 (-166.29, 65.75)	0.40
Neonate Sex		
Female	(REF)	
Male	19.10 (-18.16, 56.37)	0.32
Neonatal Weight (g)	0.03 ($7x10^{-7}$, 0.06)	0.06

Table 8

Regression coefficients from univariable analysis of OT-R protein band intensity (relative to internal reference individual T1)

Covariate	Regression Coefficient (95% CI)	P-value
Age	1.56 (0.13, 2.99)	0.04
Gravidity	1.02 (-2.60, 4.64)	0.58
Gestational Age	1.73 (-4.00, 7.45)	0.56
Body Mass Index in Labor and Delivery Suite	0.55 (-0.07, 1.17)	0.09
Race		
White	REF	REF
Black	-10.77 (-30.15, 8.61)	0.28
Asian	-6.04 (-58.92, 46.85)	0.82
Unknown	-27.94 (-66.36, 10.49)	0.16
Hispanic	-19.53 (-38.90, -0.15)	0.06
Preeclampsia		
No	REF	REF
Yes	-15.28 (-31.12, 0.54)	0.07
Diabetes		
No	REF	REF
Type 2	24.16 (5.47, 42.85)	0.02
GDM	15.32 (-8.44, 39.07)	0.21
Mode of Delivery		
SVD	REF	REF
CD prior to onset of Labor	21.82 (4.09, 39.55)	0.02
CD after onset of Labor	0.55 (-21.19, 22.29)	0.96
VBAC	-19.308 (-69.60, 31.44)	0.46
Neonatal Sex		
Female	REF	REF
Male	8.56 (-7.11, 24.23)	0.29
Neonatal Weight (g)	0.01 (8.36×10^{-4}, 0.03)	0.04

Table 9

Regression coefficients from univariable analysis of V1aR protein band intensity (relative to internal reference individual T1)

Covariate	Regression Coefficient (95% CI)	P-value
Age	0.63 (-0.30, 1.56)	0.19
Gravidity	1.84 (-0.38, 4.07)	0.11
Gestational Age	-0.72 (-4.34, 2.90)	0.70
Body Mass Index in Labor and Delivery Suite	0.20 (-0.20, 0.60)	0.34
Race		
White	REF	REF
Black	7.77 (-4.51, 20.04)	0.22
Asian	-15.55 (-49.05, 17.94)	0.37
Unknown	-13.74 (-38.07, 10.60)	0.28
Hispanic	-0.24 (-12.52, 12.03)	0.97
Preeclampsia		
No	REF	REF
Yes	-5.17 (-15.46, 5.12)	0.33
Diabetes		
No	REF	REF
Type 2	11.84 (-0.34, 24.03)	0.06
GDM	7.67 (-7.82, 23.16)	0.34
Mode of Delivery		
SVD	REF	REF
CD prior to onset of Labor	20.36 (10.58, 30.13)	$6x10^{-3}$
CD after onset of Labor	-1.05 (-13.04, 10.93)	0.86
VBAC	-9.60 (-18.26, 37.44)	0.50
Neonatal Sex		
Female	REF	REF
Male	-4.53 (-14.46, 5.40)	0.38
Neonatal Weight (g)	$5x10^{-3}$ ($-3.00x\ 10^{-3}$, 0.013)	0.23

Table 10

Regression coefficients from multivariable analysis of MDMX protein band intensity (relative to internal reference individual Q1)

Covariate	Regression Coefficient (95% CI)	P-value
Gravidity	7.19 (1.24, 13.14)	0.02
Preeclampsia		
No	(REF)	
Yes	-40.61 (-66.18, -15.04)	$3x10^{-3}$
Diabetes		
No	(REF)	
Type II	20.10 (-16.80, 57.00)	0.29
GDM	31.20 (-8.81, 71.22)	0.14
Mode of Delivery		
SVD	(REF)	
CD prior to onset of Labor	9.05 (-26.72, 44.83)	0.62
CD after onset of Labor	27.22 (-8.08, 62.52)	0.14
VBAC	-15.92 (-93.98, 62.13)	0.69
Neonatal Weight (g)	0.01 (-0.01, 0.04)	0.37

Table 11

Regression coefficients from multivariable analysis of PICALM protein band intensity (relative to internal reference individual Q1)

Covariate	Regression Coefficient (95% CI)	P-value
Age	1.73 (-1.64, 5.09)	0.32
Body Mass Index in Labor and Delivery Suite	1.35 (-0.07, 2.77)	0.07
Mode of Delivery		
SVD	(REF)	
CD prior to onset of Labor	40.00 (-3.85, 83.85)	0.08
CD after onset of Labor	0.82 (-48.29, 49.93)	0.97
VBAC	-37.87 (-151.23, 75.48)	0.52

Table 12

Regression coefficients from multivariable analysis of OT-R protein band intensity (relative to internal reference individual T1)

Covariate	Regression Coefficient (95% CI)	P-value
Age	0.71 (-0.83, 2.35)	0.39
Diabetes		
No	REF	REF
Type 2	14.0 (-11.14, 37.70)	0.27
GDM	5.64 (-21.43, 32.00)	0.68
Mode of Delivery		
SVD	REF	REF
CD prior to onset of Labor	13.25 (-7.83, 34.33)	0.23
CD after onset of Labor	-1.04 (-23.92, 21.84)	0.93
VBAC	-0.17 (-68.44, 34.32)	0.52
Neonatal Weight (g)	4.05×10^{-4} (-0.02, 0.02)	0.96

Table 13

Regression coefficients from bootstrapped replicates of univariable analysis of MDMX protein band intensity (relative to internal reference individual Q1)

Covariate	(95% quantiles of point estimate from bootstrapped replicates)	Percentage of replicates <0.05 (95% quantiles of P-value)
Age	(0.43, 2.90)	1.7% (0.05, 0.77)
Gravidity	(6.82, 12.15)	95.5% ($8x10^{-4}$, 0.06)
Gestational Age	(-6.88, 1.78)	0% (0.25, 0.97)
Body Mass Index in Labor and Delivery Suite	(0.60, 1.50)	12.6% (0.03, 0.34)
Race		
White	(REF)	
Black	(5.10, 39.4)	0.9% (0.07, 0.80)
Asian	(-53.55, -6.43)	0% (0.33, 0.91)
Unknown	(-30.86, 17.09)	0% (0.46, 0.99)
Hispanic	(-19.69, 13.18)	0% (0.32, 0.99)
Preeclampsia		
No	(REF)	
Yes	(-54.91, -28.15)	91.2% ($9x10^{-4}$, 0.08)
Diabetes		
No	(REF)	
Type II	(24.47, 60.41)	60% ($2x10^{-3}$, 0.23)
GDM	(24.83, 67.47)	44.8% ($7x10^{-3}$,0.30)
Mode of Delivery		
SVD	(REF)	
CD prior to onset of Labor	(38.96, 67.36)	98.6% ($5x10^{-4}$, 0.04)
CD after onset of Labor	(17.16, 55.75)	15.5% (0.18, 0.46)
VBAC	(-25.22, 55.19)	0% (0.28, 0.99)
Neonate Sex		
Female	(REF)	
Male	(-10.62, 15.81)	0% (0.32, 0.99)
Neonatal Weight (g)	(0.02, 0.05)	85.8% ($3x10^{-4}$, 0.14)

Table 14

Regression coefficients from bootstrapped replicates of univariable analysis of PICALM protein band intensity (relative to internal reference individual Q1)

Covariate	(95% quantiles of point estimate from bootstrapped replicates)	Percentage of replicates <0.05 (95% quantiles of P-value)
Age	(2.19, 5.17)	41% ($7.1x10^{-3}$, 0.27)
Gravidity	(3.42, 11.80)	22% (0.01, 0.46)
Gestational Age	(1.82, 11.72)	0.1% (0.11, 0.82)
Body Mass Index in Labor and Delivery Suite	(1.41, 2.66)	90% ($8x10^{-4}$, 0.09)
Race		
White	(REF)	
Black	(-7.10, 40.07)	0% (0.12, 0.97)
Asian	(-40.69,111.00)	0% (0.9, 0.99)
Unknown	(-96.07, -53.30)	2% (0.05, 0.28)
Hispanic	(-64.85, -29.39)	40% (0.01, 0.24)
Preeclampsia		
No	(REF)	
Yes	(-52.30, -18.88)	20.3% (0.01, 0.37)
Diabetes		
No	(REF)	
Type II	(2.82, 45.52)	0.6% (0.08, 0.91)
GDM	(23.35, 56.54)	0.6% (0.08, 0.51)
Mode of Delivery		
SVD	(REF)	
CD prior to onset of Labor	(41.39, 79.89)	88.5% ($9x10^{-4}$, 0.08)
CD after onset of Labor	(-17.08, 31.02)	0% (0.26, 0.99)
VBAC	(-82.60, -27.18)	0% (0.22, 0.67)
Neonate Sex		
Female	(REF)	
Male	(3.42, 35.19)	0.3% (0.10, 0.84)
Neonatal Weight (g)	(0.01, 0.05)	35.1% (3x10-3, 0.40)

Table 15

Regression coefficients from bootstrapped replicates of univariable analysis of OT-R protein band intensity (relative to internal reference individual T1)

Covariate	(95% quantiles of point estimate from bootstrapped replicates)	Percentage of replicates <0.05 (95% quantiles of P-value)
Age	(1.17, 2.01)	54.7% (0.01, 0.14)
Gravidity	(0.15, 2.08)	0% (0.29, 0.93)
Gestational Age	(-0.00, 3.40)	0% (0.26, 0.96)
Body Mass Index in Labor and Delivery Suite	(0.34, 0.77)	15% (0.02, 0.30)
Race		
White	REF	REF
Black	(-17.36, -3.71)	0% (0.09, 0.74)
Asian	(-13.48, 1.09)	0% (0.62, 0.99)
Unknown	(-33.74, -21.97)	0% (0.10, 0.30)
Hispanic	(-24.88, -14.18)	32% (0.02, 0.18)
Preeclampsia		
No	REF	REF
Yes	(-20.16, -10.62)	24% (0.02, 0.22)
Diabetes		
No	REF	REF
Type 2	(17.21, 31.63)	84% (0.00, 0.10)
GDM	(8.96, 22.63)	1% (0.07, 0.48)
Mode of Delivery		
SVD	REF	REF
CD prior to onset of Labor	(16.54, 27.71)	83% (0.01, 0.09)
CD after onset of Labor	(-5.28, 6.19)	0% (0.57, 0.99)
VBAC	(-29.34, -2.46)	0% (0.27, 0.93)
Neonatal Sex		
Female	REF	REF
Male	(4.20, 13.13)	0% (0.11, 0.62)
Neonatal Weight (g)	(0.01, 0.02)	49% (0.01, 0.17)

Table 16

Regression coefficients from bootstrapped replicates of univariable analysis of V1aR protein band intensity (relative to internal reference individual T1)

Covariate	(95% quantiles of point estimate from bootstrapped replicates)	Percentage of replicates <0.05 (95% quantiles of P-value)
Age	(0.17, 1.12)	6% (0.03, 0.74)
Gravidity	(0.48, 3.04)	14% (0.02, 0.71)
Gestational Age	(-2.20, 0.98)	0% (0.30, 0.98)
Body Mass Index in Labor and Delivery Suite	(-0.03, 0.43)	2% (0.07, 0.93)
Race		
White	REF	REF
Black	(1.07, 14.58)	3% (0.04, 0.88)
Asian	(-32.74, -3.26)	0% (0.09, 0.87)
Unknown	(-24.28, -1.85)	0% (0.09, 0.89)
Hispanic	(-7.10, 7.06)	0% (0.26, 0.99)
Preeclampsia		
No	REF	REF
Yes	(-11.01, 0.40)	2% (0.07, 0.94)
Diabetes		
No	REF	REF
Type 2	(5.78, 19.09)	23% ($9x10^{-3}$, 0.41)
GDM	(-4.01, 18.40)	4% (0.04, 0.95)
Mode of Delivery		
SVD	REF	REF
CD prior to onset of Labor	(14.50, 26.60)	100% ($4x10^{-5}$, $2x10^{-2}$)
CD after onset of Labor	(-7.93, 5.70)	0% (0.26, 0.99)
VBAC	(-7.09, 23.62)	0% (0.16, 0.97)
Neonatal Sex		
Female	REF	REF
Male	(-9.92, 0.86)	0% (0.11, 0.93)
Neonatal Weight (g)	($1.0x\ 10^{-3}$, $9.0x\ 10^{-3}$)	2% (0.05, 0.82)

Table 17

Regression coefficients from bootstrapped replicates of multivariable analysis of MDMX protein band intensity (relative to internal reference individual Q1)

Covariate	(95% quantiles of point estimate from bootstrapped replicates)	Percentage of replicates <0.05 (95% quantiles of P-value)
Gravidity	(4.17, 9.81)	44% (0.01, 0.28)
Preeclampsia		
No	REF	
Yes	(-54.42, -22.05)	80% ($1x10^{-3}$, 0.17)
Diabetes		
No	(REF)	
Type II	(-7.15, 35.26)	1% (0.10, 0.97)
GDM	(7.02, 50.01)	5% (0.04, 0.78)
Mode of Delivery		
SVD	(REF)	
CD prior to onset of Labor	(-7.87, 27.66)	0% (0.22, 0.98)
CD after onset of Labor	(7.62, 49.52)	8% (0.03, 0.69)
VBAC	(-45.98, 36.55)	0% (0.32, 0.86)
Neonatal Weight (g)	(-0.002, 0.03)	2% (0.07, 0.96)

Table 18

Regression coefficients from bootstrapped replicates of multivariable analysis of PICALM protein band intensity (relative to internal reference individual Q1)

Covariate	(95% quantiles of point estimate from bootstrapped replicates)	Percentage of replicates <0.05 (95% quantiles of P-value)
Age	(0.09, 3.35)	1% (0.07, 0.93)
Body Mass Index in Labor and Delivery Suite	(0.55, 2.11)	26% (0.008, 0.54)
Mode of Delivery		
SVD	REF	
CD prior to onset of Labor	(17.36, 62.80)	20% (0.02, 0.48)
CD after onset of Labor	(-23.42, 26.23)	0% (0.31, 0.99)
VBAC	(-70.17, -12.72)	0% (0.29, 0.84)

Table 19

Regression coefficients from bootstrapped replicates of multivariable analysis of OT-R protein band intensity (relative to internal reference individual T1)

Covariate	(95% quantiles of point estimate from bootstrapped replicates)	Percentage of replicates <0.05 (95% quantiles of P-value)
Age	(0.27, 1.17)	0% (0.17, 0.76)
Diabetes		
No	REF	REF
Type 2	(6.09, 21.30)	0% (0.10, 0.65)
GDM	(-1.66, 14.21)	0% (0.32, 0.99)
Mode of Delivery		
SVD	REF	REF
CD prior to onset of Labor	(7.33, 19.97)	0% (0.09, 0.51)
CD after onset of Labor	(-6.97, 4.89)	0% (0.55, 0.99)
VBAC	(-27.20, -0.44)	0% (0.32, 0.98)
Neonatal Weight (g)	(-4×10^{-3}, 5×10^{-3})	0% (0.52, 0.99)

Table 20

Autoantigens listed by Neiman et al. among the proteins in VEGFR2, MDMX, and PICALM immunoprecipitations (IP).

	Uniprot	Gene	Protein name	Autoimmune disease
VEGFR2 IP	P01023	A2M	Alpha-2-macroglobulin (Alpha-2-M)	Sjögren's syndrome
	E7EVS6	ACTB	Actin, cytoplasmic 1 (Beta-actin)	Autoimmune hemolytic anemia
	P07355	ANXA2	Annexin A2 (Annexin II) (Annexin-2)	Antiphospholipid syndrome
	P08758	ANXA5	Annexin A5 (Anchorin CII)	Antiphospholipid syndrome
	P11182	DBT	Lipoamide acyltransferase BCOADC-E2	Primary biliary cholangitis
	P17661	DES	Desmin	Sjögren's syndrome
	P10515	DLAT	PDC-E2	Primary biliary cirrhosis
	Q02413	DSG1	Desmoglein-1	Pemphigus foliaceus
	P19474	TRIM21	E3 ubiquitin-protein ligase TRIM21	Sjögren's syndrome; Systemic Lupus Erythematosus
	Q8WZ42	TTN	Titin	Myasthenia gravis
	P08670	VIM	Vimentin	Rheumatoid arthritis
MDMX IP	P01023	A2M	Alpha-2-macroglobulin (Alpha-2-M)	Sjögren's syndrome
	P68133	ACTA1	Actin, alpha skeletal muscle	Autoimmune hemolytic anemia; myashenia gravis
	P07355	ANXA2	Annexin A2 (Annexin II) (Annexin-2)	Antiphospholipid syndrome
	P08758	ANXA5	Annexin 5	Antiphospholipid syndrome
	P11182	DBT	Lipoamide acyltransferase BCOADC-E2	Primary biliary cirrhosis
	Q6P0N6	DST	Dystonin	Bollous pemphigoid
	P06733	ENO1	α-Enolase	Multiple sclerosis
	P35579	MYH9	Myosin-9	Multiple sclerosis
	P08559	PDHA1	Pyruvate dehydrogenase E1-A type 1	Primary biliary cholangitis
	P21980	TGM2	Isopeptidase TGM2	Celiac's disease
	Q08188	TGM3	Transglutaminase-3	Dermatitis herpetiformis
	P29401	TKT	Transketolase	Multiple sclerosis
	P19474	TRIM21	E3 ubiquitin-protein ligase TRIM21	Sjögren's syndrome; Systemic Lupus Erythematosus
	P18206	VCL	Vinculin	Myasthenia gravis
PICALM IP	P01023	A2M	Alpha-2-macroglobulin (Alpha-2-M)	Sjögren's syndrome
	E7EVS6	ACTB	Actin, cytoplasmic 1 (Beta-actin)	Autoimmune hemolytic anemia
	P63261	ACTG1	Actin, cytoplasmic 2/γ-actin	Autoimmune hemolytic anemia; myashenia gravis
	P63267	ACTG2	Alpha-actin-2	Autoimmune hemolytic anemia; myashenia gravis
	P07355	ANXA2	Annexin A2 (Annexin II) (Annexin-2)	Antiphospholipid syndrome
	P08758	ANXA5	Annexin A5 (Anchorin CII)	Antiphospholipid syndrome
	P17661	DES	Desmin	Sjögren's syndrome
	P36957	DLST	2-oxoglutarate dehydrogenase E2	Pernicuous anemia
	Q08554	DSC1	Desmocollin-1	IgA pemphigus
	Q02413	DSG1	Desmoglein-1	Pemphigus foliaceus
	Q9Y285	FARSA	Phenylalanyl-tRNA synthetase α-subunit	Schizophrenia
	Q02218	OGDH	2-oxoglutarate dehydrogenase E1	Pernicuous anemia
	Q5JPU3	PDHA1	Pyruvate dehydrogenase E1-A type 1	Primary biliary cholangitis
	P21980	TGM2	Isopeptidase TGM2	Celiac's disease
	P29401	TKT	Transketolase	Multiple sclerosis
	P19474	TRIM21	E3 ubiquitin-protein ligase TRIM21	Sjögren's syndrome; Systemic Lupus Erythematosus
	Q13263	TRIM28	E3 SUMO-protein ligase TRIM28	Myositis
	Q8WZ42	TTN	Titin	Myasthenia gravis
	P08670	VIM	Vimentin	Rheumatoid arthritis

Table 21

Patient demographics

Clinical characteristics	Study subjects (n=44)	% of n
Maternal Age		
18-34	40	91%
≥35	4	9%
BMI		
Underweight (<18.5)	0	0%
Normal (18.5-24.9)	3	7%
Overweight (25-29.9)	9	20%
Obesity I (30-34.9)	12	27%
Obesity II (35-35.9)	5	11%
Extreme Obesity (≥40)	15	34%
Parity		
Nulliparous	11	25%
Multiparous	33	75%
Gestational Age at Delivery		
< 37 weeks	4	9%
≥ 37 weeks	40	91%
Race		
White	17	39%
African American	12	27%
Hispanic	12	27%
Other	3	7%
Diabetes	14	32%
Type 1	0	0%
Type 2	9	20%
Gestational	5	11%
Chronic Hypertension	6	14%
Normotensive	28	64%
Preeclampsia	16	36%
Preeclampsia and Diabetes	4	9%